



**Università  
degli Studi  
di Ferrara**

**DOTTORATO DI RICERCA IN FISICA  
CICLO XXXIII**

Coordinatore: Prof. Elenora Luppi

**Advanced Human Hemodynamic  
Modelling and Valuation using MRI  
imaging**

Settore Scientifico Disciplinare FIS/07

**Dottoranda:**

Dott. Mohammadyari Parvin

**Tutore:**

Prof. Taibi Angelo

**Co-tutor:**

Dott. Gadda Giacomo

Anni 2017-2020



*To me*

*To my lovely Family*

*To my supportive fiancée*



# Abstract

Proper functioning of brain critically depends on cerebral blood inflow and outflow. Moreover, the venous contribution in auto-regulation function and maintaining pressure and blood flow balance in body organs such as brain has been highlighted. Auto-regulating mechanism and cerebral circulation are influenced by many biophysical factors such as aging, posture and gravitational pressure change, and vessel stenosis. Therefore, it is important to gain a satisfactory understanding of physiological and biomechanical properties of the venous system and the interaction between intra- and extracranial compartments under different physiological conditions. For what concerns congenital vascular disease is one of the known leading causes of death in paediatric age. Despite the importance of paediatric haemodynamics, large investigations have been devoted to the evaluation of circulation in adults. The novelties of this study consist in the development of a well calibrated mathematical model of cardiovascular circulation in paediatric subjects as well as adults, simulating the full range posture change effects on hemodynamic physiology from head down tilt to supine and upright, predicting the flow rate change in main neck arteries and veins in microgravity environment, and the IJV asymmetric stenosis (followed by head rotation) effects on the head and neck hemodynamic alteration. The model consists of two parts that simulates the arterial (1D) and brain and venous (0D) vascular tree. The cardiovascular system is built as a network of hydraulic resistances and capacitances to properly model physiological parameters like total peripheral resistance, and to calculate vascular pressure and the related flow rate at any branch of the tree.

This dissertation presents the results of the scientific work developed in collaboration with the paediatric hospital of Sant Joan de Déu, Spain. A data set was provided including information about human vessels network anatomy, blood rheology (blood velocity and flow), vessel status, venous biomechanics factors (inner pressure and wall shear stress) and volunteers characteristics (age, respiratory rate, blood pressure and clinical reason of their MRI scan). The model presented here was tuned by using two different MRI datasets. We benefited from the use of 2D and 4D PC-MRI techniques.

Results show that the model is able to reproduce the physiological behavior of IJVs and other collateral veins, with average values in good agreement with experimental data of supine paediatric and adult subjects. Physiological age-related parameters were used to adjust left ventricle pressure

---

pulse and cerebral blood flow for paediatrics. Every simulated data fell inside the standard error from the corresponding average experimental value. The model outcomes indicated about 88% correlation with MRI data.

Concerning the head rotation effects simulation, the conductance of left IJV was decreased to model the imposed stenosis influenced by torsion-compression force. MR image acquisition and numerical simulation were performed in two situations: the neutral and 80° left head rotation. Flow rate and wall shear stress analysis within IJVs demonstrated a strong interindividual dependency. Concerning the posture change and microgravity study, the model in line with literature confirmed the role of peripheral veins in regional blood redistribution during posture change from supine to upright and microgravity environment as hypothesized in literature. Therefore, model outcomes are in excellent agreement with experimental average flows and literature.

The methods presented can be used to predict the response of the hemodynamic system in many other physiological and pathological conditions in both paediatric and adult cases. It also provides a virtual laboratory to examine the consequence of a wide range of orthostatic stresses on haemodynamics.

# Contents

<b>1</b>	<b>Introduction</b>	<b>1</b>
<b>2</b>	<b>Mathematical model of cerebral and extracerebral blood circulation</b>	<b>9</b>
2.1	Background . . . . .	10
2.2	Anatomy and physiology of the cerebral drainage system . . . . .	12
2.3	Mathematical Modelling Description . . . . .	13
2.3.1	Description of the 0D Brain and venous submodel . . . . .	13
2.3.2	Description of the 1D arterial submodel . . . . .	18
2.4	Mathematical Modelling Advancement . . . . .	21
2.4.1	Extending the vessels anatomy map of the model . . . . .	21
2.4.2	Modelling Physiology Advancements . . . . .	25
2.4.3	Flow Analysis . . . . .	30
<b>3</b>	<b>Experimental validation by Real Medical data</b>	<b>35</b>
3.1	Patients Selection Procedures . . . . .	36
3.1.1	Study group I . . . . .	36
3.1.2	Study group II . . . . .	36
3.2	MRI protocols . . . . .	38
3.2.1	2D-Flow PC-MRI technique . . . . .	39
3.2.2	4D-Flow PC-MRI technique . . . . .	39
3.3	MRI data processing . . . . .	42
3.3.1	2D-flow PC-MRI data . . . . .	42
3.3.2	4D-flow PC-MRI data . . . . .	43
<b>4</b>	<b>Results and discussion</b>	<b>45</b>
4.1	Paediatric Hemodynamic Model: Aging study . . . . .	45
4.1.1	Arterial adjustments results . . . . .	46

---

4.1.2	Venous adjustments results . . . . .	47
4.2	Asymmetric IJV stenosis study: Head Rotation . . . . .	51
4.3	Modelling microgravity and orthostatic stress effects . . . . .	57
4.4	Study Limitations . . . . .	65
<b>5</b>	<b>Conclusions</b>	<b>67</b>
	<b>Bibliography</b>	<b>71</b>

# List of Figures

2.1	Schematic representation of the main vessels of the neck drainage system. . . .	12
2.2	Previously published model for the study of the cerebral and extracerebral circulation. Box on the top part is the scheme of the intracranial 0D submodel. Right part is the representation of the 0D submodel for the cerebral drainage system, while in the left part the 1D submodel for the human arterial tree is depicted. [20] . . . . .	20
2.3	Scheme of the advance haemodynamic model with all the new anatomical update.	22
2.4	Flowchart of all the contributions used to build the paediatric model. . . . .	25
2.5	The simulated cardiac pressure waveform. a Comparison of the aortic and ventricle pressure wave in paediatric. b Comparison of the ventricle pressure wave in paediatric and adult. The inset shows the physiological pattern . . . .	26
2.6	Illustration of the three modelled segments of IJV heights from the $H_{IPCSF}$ .	30
2.7	Simulated hydraulic map to model human circulation. Red boxes are the anatomy (left) and scheme (right) of the arterial tree. Green boxes are the anatomy (left) and scheme (middle) of the Willis circle tree, and the scheme of the intracranial 0D submodel (right). Blue box is the scheme (left) and anatomy (right) of the venouscompartment . . . . .	31
3.1	2D-flow PC-MRI of the neck vessels at the vertebral level C5/C6 (J2) in neutral (left) and rotated (right) position. . . . .	40
3.2	The 2D PC-MR Images acquired from one of the volunteers. . . . .	41
3.3	The 4D PC-MR Images acquired from one of the volunteers. . . . .	42
4.1	Cardiac and arterial pressure waveforms. The inset shows the zoom of one cardiac cycle. AAo Ascending aorta, ECA Extracranial artery, ICA Intracranial artery, FA Facial artery, VA Vertebral artery . . . . .	46

4.2	Comparison between intracranial (Pic) and venous sinus (Pvs) pulse in paediatric (dashed line) and adult (solid line) . . . . .	48
4.3	Comparison of simulated paediatric and adult flow rates, and paediatric experimental data. Q Cerebral blood flow, dcv Deep cervical vein, ejl Left external jugular vein, ejr Right external jugular vein, Qex Extracerebral blood flow, jl1 Lower segment of the left jugular vein, jl2 Middle segment of the left jugular vein, jl3 Upper segment of the left jugular vein, jr1 Lower segment of the right jugular vein, jr2 Middle segment of the right jugular vein, jr3 Upper segment of the right jugular vein, Qtot Blood flow to the head, vp Venous plexus, vs Venous sinus, vv Vertebral vein . . . . .	49
4.4	Comparison between intracranial (Pic) and venous sinus (Pvs) pulse in paediatric (dashed line) and adult (solid line) . . . . .	50
4.5	a) CSA Comparison for both neutral and rotated head position including the standard deviation in error bars on the MRI extracted data. b) Comparison of measured and simulated cycle-averaged flow rates for both neutral and rotated orientation. . . . .	52
4.6	Measured flow rate change over the length of left and right IJV for both neutral (black line) and rotated (red dashed line) head position for all of the 4D PC-MRI cases. Flow in Case#2 IJV-L and Case#3 IJV-R subplots are not reported because the IJV is fully collapsed and absent in the MRI measurement platform. 53	53
4.7	Contour plots of WSS for neutral and rotated head position at the level of neck for three different drainage cases and brain images of the case #1 and #2, the two most visualized intracranial blood redistribution. . . . .	56
4.8	Comparison of the simulated pressure of (a) intracranial (Pic), (b) venous sinus (Pvs). . . . .	57
4.9	Simulated pressure difference caused by hydraulic pressure change and weightlessness at the level of a) aorta, b) braincase, c) SVC, d) upper, middle, and lower left IJV segments (Jl3, Jl2, Jl1) . . . . .	59
4.10	Comparison of simulated flow rates for a) different posture condition on Earth (1g) and a) supine and HDT on Earth (1g), and weightlessness (uG). . . . .	61

# List of Tables

2.1	Glossary of terms related to the 0D part of the model. . . . .	14
2.2	Parameters of the arterial model. $No.$ is the vessel number in the model, $L$ is the length of the vessel, $c$ is the mean velocity, $Z_0$ is the characteristic impedance, $t_d$ is the time delay, and $R_f$ is the reflection coefficient of the peripherals [53]. . . . .	19
2.3	Parameters of the arterial model. $No.$ is the vessel number in the model, $L$ is the length of the vessel, $c$ is the mean velocity, $Z_0$ is the characteristic impedance, $t_d$ is the time delay, and $R_f$ is the reflection coefficient of the peripherals. . . . .	23
3.1	Characteristic of the enrolled subjects . . . . .	37
3.2	Volunteers demographic characteristic . . . . .	37
3.3	2D-MR imaging parameters. . . . .	39
3.4	4D-MR imaging parameters. . . . .	40
4.1	Comparing the computed pressure values (mmHg) (value $\pm$ standard deviation) of my model with measurement and modelling in literature. . . . .	58
4.2	Comparing the computed flow rates (ml/s) of my model with measurement in literature. . . . .	63
4.3	Simulated mean pressure and literature pressure values (mean $\pm$ standard deviation) considered in this study. All values are reported in mmHg. . . . .	64



# Chapter 1

## Introduction

The circulation system is known as one of the most important systems in human body. The function of the circulation is to service the needs of the body tissues. The heart and blood vessels, in turn, are controlled to provide the necessary cardiac output and arterial pressure to cause the needed tissue blood flow [1]. Brain as the most critical body organ has a precise cerebral blood flow (CBF) and cerebrospinal fluid (CSF) circulation which play a key role in the autoregulation of brain physiology [2,3].

The mechanisms for controlling blood volume and flow are related to all the other functions of the circulation system [1]. Moreover, many biophysical factors affect cerebral circulation such as **aging, posture and gravitational force change**, and **vessel stenosis** that they are known as the biological and mechanical factors in both physiological and pathological conditions [5,6,41]. Since the cardiovascular system works to maintain blood flow to each organ quite constant at the requested rate, the compensatory acts and adaptation attempts by the system requires some physiology changes [4]. Therefore, it is important to gain a satisfactory understanding of the circulation mechanism under different physiological conditions.

Mathematical modelling and computer simulation have been developing rapidly to study blood circulation [7]. Their benefits are not only limited to the understanding of the fluid behaviour in vessels but also for surgical planning and intervention [9]. Most of the numerical studies were dedicated to computational fluid dynamics investigation in modelling the cardiovascular and pulmonary vessels diseases while less attention has been paid to study of the neck and brain vascular diseases [13,14]. Models are regulated based on physics and mechanics rules to understand the influences of the involved biological factors [15,16]. Moreover, pathological cases can be simulated starting from a model previously calibrated to mimic

healthy subjects [19, 21]. Indeed, such modelling must carry on a comprehensive information about the morphology of the human vessels tree, that is crucial to understand how a given change of the physiological parameters can affect the results. This thesis consists of three sub projects that in each project one physiological response of head and neck hemodynamic to aforementioned biophysical factors were investigated, as following:

- Pediatric hemodynamic modelling: development and experimental validation using quantitative flow MR Imaging. [22]
- Head rotation Effects on youth Head and Neck hemodynamic using PC MR Imaging and Mathematical Modelling. [23]
- Modelling physiology of haemodynamic adaptation in short-term Microgravity exposure and orthostatic stress on Earth. [24]

An important advantage of computational modelling is that it provides a virtual laboratory and allows the exploration of a wide range of possibilities in age related bio factors or orthostatic stresses and their complex physiological chain of events on the intra- and extracranial compartments at a low medical and computational cost [25, 26]. Many valuable models of the cerebral circulation (like the works of Gisolf et al. [16] and Buckey et al. [28]) focused on intracranial segments and related control mechanisms, by providing a simplified description of the main arterial inflow and extracranial venous return. Whole body models such as the one developed by Zhang et al. [27] and Gallo et al [29] do not include brain compartments, and only the main outflow routes (IJV and VV) are included in the vascular network. The comprehensive model as the one introduced by Muller et al [80] includes only the main vascular network and does not include the peripheral and collateral's vessels. While, in literature the important role peripheral vessels in the brain and head drainage are highlighted [16, 59], so that the choice to not account for them in order to simplify the model is not reasonable. Hence, the need of a comprehensive model that considers both extracranial and intracranial compartments with their interactions to adapt the whole hemodynamic system to changing environmental conditions is still not satisfied. Therefore, our overall goal is to make a hemodynamic model able to simulate the main and most reported physiological parameters. Noteworthy, the lack of knowledge, discordant literature and measured data is a challenge in such study filed.

The cardiovascular modelling is a challenging subject of study due to the complex geometry and the high number of enrolled physiological parameters which they are highly related to

each other [13]. In the case of paediatric studies, the difficulty is higher because of the substantial limitations such as lack of standardizing data due to patient intolerance to the clinical examinations, different physiology, and higher tissue sensitivity in comparison with adults. These barriers limit the options for choosing proper diagnostic methods [30]. Thereby, the need for more paediatric cardiovascular studies is frequently highlighted [5, 30]. The importance is emphasized by the claim: “children are not small adults” [31]. Consequently, it is inappropriate to generalize or extrapolate data from adult to calculate the parameters and build a paediatric model [30, 31].

In terms of clinical needs, a large group of diseases which are known as different types of stenosis interrupting the brain blood flow or CSF circulation (like Moyamoya disease [32] and Chiari malformation [33]) and vascular malfunction diseases can be studied by using a comprehensive mathematical model. Moreover, the common clinical procedures such as sideward head rotation during internal jugular vein (IJV) catheterization and Valsalva Maneuver, as a diagnostic aid, are affecting the head and neck blood circulation in a possible way to model. Therefore, computational modelling can be considered as a powerful tool for clinical applications while experimental access to cerebral circulation dynamics is limited.

Recent literature has mentioned the role of external cranial venous drainage on the intracranial drainage and physiology [6, 10, 59, 60]. As an example, the head elevation and rotation are known as external reasons of intracranial pressure (ICP) increase [6]. The medical care guidelines highlighted the consistent monitoring and prevent the secondary injury due to high ICP [6, 100]. However, the physiological effects of head rotation on the intracranial and extracranial hemodynamic requires further studies and standardization [85, 111, 112].

Head rotation is a common clinical method used in diagnostic and therapy. Haemodialysis in chronically dialyzed patients, fluid management in traumatic brain injury cases are the frequently mentioned examples of using head rotation method in therapy [45, 85]. In diagnostic, head is being rotated during ultrasound assessment of carotid artery distensibility [98]. In occasional situations like brain trauma or cardiac surgical patients who needs central venous cannulation, right IJV is used for catheterization [85, 96, 98]. By turning head to the left, the distance between right IJV and carotid artery increases [85, 112]. Therefore, the risk of puncturing the carotid artery and hematoma is minimized [113]. Percutaneous cannulation of IJV is an extremely common and risky procedure in paediatric cases and more difficult than in adults due to the small range of vessels size [6, 45, 85]. Noteworthy, few literature explored

the internal and external cranial haemodynamics through mathematical models of the whole body circulation, and none of them relates to paediatrics.

Head rotation has been an ongoing research subject since last decades to understand the displacement in the relative position of vessels and variation in the physiological parameters [6, 85, 93]. While head has a sideward rotation, the sternomastoid muscle and surrounding tissues compress the same side IJV and decreases significantly the vessel cross-section area (CSA) [85, 93, 112]. To study the effects of vessel compression, the four dimensional flow measurement techniques provide the mechanical bio-factors such as WSS and pressure gradient. WSS by definition is the frictional shearing force on the vessel walls [90].

In the term of other research activities, since gravity fundamentally affects the blood circulation by altering the vessels pressure, flow rate and volume [34] this kind of research is also very important considering the arising projects about long term space missions, to ensure safety of astronauts. Physiological effects of microgravity on cardiovascular function has been known since the first data from Soviet and American space flight were studied [35, 37]. It is reported that about 50% of astronauts after their space mission suffer from orthostatic pressure intolerance in the upright posture [35, 38]. The physiological effects of hydrostatics pressure change on different parameters of cardiovascular system have mostly been studied on human and animal [39, 40]. For instance, studying hydrostatic stress mechanism in living on Earth by posture change from head down tilt angle (HDT) to head up tilt (HUT) up to 90°, and microgravity environment by exposing the subjects into the weightlessness condition [16, 41, 44, 46]. However, the mechanisms of cardiovascular adaptation to microgravity and posture changes are poorly understood [28, 34, 47].

In response to the question: “When there is no gravity pulling back the blood to heart, how the human body changes the venous drain strategy?” there is one hypothesis that due to microgravity venous congestion causing a syndrome in which fluid shifts away from legs towards upper limbs and head. These head-ward fluid shift leads to an augmentation in venous volume and CSF which brings facial puffiness and bird legs [48]. Previous studies have demonstrated increase in cardiac output [35], cerebral blood volume and inflow [49, 50] and cerebral blood flow velocity (up to 30 % ) [51]. Internal cranial pressure (ICP) change and the underlying physiological mechanisms have been remained a topic of debate.

To experimentally simulate the effect of microgravity on Earth and study the cardiovascular functional adaptation, the Earth-based model that causes fluid shift are widely used such as

HDT. The other way is using parabolic flights in which 20-30s weightlessness prepares an opportunity to perform some measurements in such a short time [34]. However, the results vary depending on the study situations, accuracy of the measurement and the duration of space mission [52]. Regards to these limitations, there is not a unique protocol to measure the physiological parameters in astronauts. Also, the explanation provide by Earth-based simulation might not be expandable to understand the microgravity situation. By that, the necessity of having computed simulation tool is highlighted [28]. The intracranial and venous part of the model (i.e. the 0-D part) has been built in collaboration with the Department of Electrical, Electronic and Information Engineering of the University of Bologna (Bologna, Italy), while the arterial 1-D part in collaboration with the Institute of Nuclear Physics, Polish Academy of Sciences (Kraków, Poland). These features make it an useful tool for the study of the correlations between extracranial blood redistributions and changes in the intracranial environment.

The model consists of an anatomically informed 1-D arterial network and two 0-D networks of the brain and venous drainage, respectively. The arterial network is designed by a compartmental method in which the vessels are treated as mono mode 1-D wave guides. The parameters such as vessels length, mean blood velocity, topology of the arterial segments and the characteristic impedance of each segment are used to simulate the arterial hemodynamic characteristics [53]. In the 0-D networks, vasculature is considered as an electric circuit, and the veins are electric elements with given values of capacitance and conductance. The model equations satisfy the momentum and mass conservation laws and describe the pressure-area relationship in accordance with literature and experimental data . The contribution to venous pressure due to respiration is also added to simulate the effect of the thoracic pump on the drainage system [15, 20, 21, 54].

The arterial model consists of a compartmental network of transmission lines developed to simulate propagation of the pulse waves in human arteries [53]. Through a system of differential equations, it takes into account the pulse-wave transmission properties of the 55 main arteries, together with the principal hydraulic mechanisms that ensure the proper blood supply of the brain and other organs. Results from the arterial 1D model are used as input to the 0D models to simulate several pressure variations due to periodic perturbations like heartbeat, movements such as cycling, or to the occurrence of vascular diseases like tachycardia.

The basic idea is to obtain a simple tool for improving the understanding of a complex system. The main features of the model are that:

- It includes a validated submodel for the simulation of the intracranial circulation and the related autoregulation mechanisms [15, 22, 54];
- It includes a submodel of the cerebral venous outflow system that accounts for the dependence of the hydraulic properties of the IJVs with respect to the strength of gravity field [20, 21, 24];
- It includes a detailed submodel of the main arteries of the human arterial system; [53].

This dissertation presents the results of the scientific work developed in collaboration with paediatric hospital of Sant Joan de Déu, (Barcelona, Spain). The research is dedicated to studying the human neck and brain circulation considering the biophysical factors such as aging, posture change and head rotation. In this regard, the basic need is to perform some measurement and provide a proper data set including information about human vessels network anatomy, blood rheology (e.g., blood velocity and flow), and vessel status (hydraulic resistance and capacitance, inner pressure and cross section area). At the next step, I expended, adjusted and validated the mathematical model developed by the Medical Physics group at the University of Ferrara that were calibrated by using limited experimental data only in supine and upright positions [21]. In this work, new ideas were followed to fulfil the purposes listed below:

- to simulate a the effects of aging on the hemodynamic physiological parameters and provide a pediatric model as the first attempt;
- to simulate the circle of Willis to include a brain 1D compartment;
- to investigate the role of collateral veins in carrying out blood in case of IJV collapse (HUT) or expansion (HDT and microgravity);
- to simulate a full range of posture changes from HDT to supine and HUT, other than microgravity;
- to introduce new indexes useful for future investigations.
- to calculate flow rate and pressure changes after in different study condition;

- to investigate the asymmetric IJV stenosis in a non-invasive way by head rotation and simulate the hemodynamic variation as the first attempt;
- to measure the flow rate and wall shear stress (WSS) over IJV length before and after head rotation as the first attempt;
- to compare the simulation results with measured data and literature;

To validate the model advancement, a proper magnetic resonance imaging (MRI) data sets were used to extract information about blood flow rate from both healthy and stenotic subjects. Then, the model has been tuned by the data sets to reproduce the known parameters. The model has the potential to predict important clinical parameters before and after physiological and pathological changes with focus on head and neck circulation, such as posture changes, vessel occlusions, venous thrombosis, and congenital diseases. That is the motivation of performing this research work to produce an advance model which is able to use the maximum capacity of its own.

An advanced mathematical model for the simulation the cerebral and extracerebral blood circulation is the subject of Chapter 2. In the chapter, the explanation of how the model is able to be upgraded and simulate variations of the human circulatory system in different physiological and pathological conditions are presented, such as age, IJV stenosis imposed by the non-invasive head rotation method, gravitational force value and environment such as the full range posture change from head down up to standing position and microgravity. Chapter 3 focuses on explaining the MRI experimental data acquiring and processing.

In chapter 4 the results are explained in three different sections in which clinical or research applications for the model are discussed. The section 4.1 refers the built paediatric model results. In the section 4.2, the head rotation effects on head and neck hemodynamic in imposing the asymmetric non-invasive IJV stenosis were explained. The results of the MRI study were compared with simulation. In the section 4.3, the results of imposing human body to different gravity field including short-term microgravity on hemodynamic system were discussed. At the last chapter 5, the thesis outcomes are concluded.



## Chapter 2

# Mathematical model of cerebral and extracerebral blood circulation

The purpose of this chapter is to describe the mathematical model and its advancement process to study the intracranial and extracranial blood flow and pressure change [22]. Such model was developed in collaboration with several scientific groups and research centers. The main idea of the project, arises from the collaboration with the Vascular Diseases Center of the University of Ferrara (Ferrara, Italy). The intracranial and venous part of the model (i.e. the 0D part) has been built in collaboration with the Department of Electrical, Electronic and Information Engineering of the University of Bologna (Bologna, Italy), while the arterial 1D part in collaboration with the Institute of Nuclear Physics, Polish Academy of Sciences (Krak´ow, Poland). The model was advanced in collaboration with Sant Juan de Deu university hospital (Barcelona, Spain) to improve the anatomy map of the model together with MRI data for experimental validation.

Details including a background information about computer simulations and mathematical modelling, anatomy and physiology of the cerebral drainage system is provided at the sections of 2.1 and 2.2. In the following sections of 2.3 and 2.4 mathematics of our basic model and the improvements of the current version were explained to provide information about the differences between the advanced version and the base model. Anatomical improvements (including 21 arterial blocks and 9 peripheral veins) in line with necessary physiological improvements (at arterial, brain and venous compartments) and literature were performed to achieve a reliable model with ability to simulate physiological and pathological cases [22–24].

## 2.1 Background

Mathematical modelling is recently known as a non-invasive alternative method of blood hemodynamic analysis [7, 21, 28]. Therefore, new research direction has focused on simulation to have a reliable tool that quantitatively investigate the impact of vessels disorder on human hemodynamic, and also to be used for treatment planning purpose [8, 9]. Due to the inter-individual differences and complexity in the anatomy and physiology of hemodynamic circulation mechanism the large variety of parameters are involved. Therefore, it is extremely difficult to understand the effect of one parameter alteration on the rest of system, for instance, the extracranial circulation changes on brain.

Cardiovascular mathematical modelling is a common tool that the design is according to the human physiology and anatomy [28]. The pivotal goal of such model is to largely benefit from the use of computational method describing a complex behavior using a system of equations by providing a simplified descriptions of hemodynamic system. In general, to create the most close model to reality like cerebral circulation and of its implications in healthy and pathological conditions, the model has to be validated with the real medical data. In current study, the simulation results are validated by using magnetic resonance imaging (MRI) experimental blood flow, cross-section area, pressure, and wall shear stress were measured in humans (see Chapter 3 Section 3.3).

In general, most models of the cerebral circulation only focused on intracranial segments and related control mechanisms, by providing just a very simplified description of arterial inflow and extracranial venous return. The current model allows simulation of the blood flows and pressures in the main vessels and collateral routes of the cerebral and extracerebral circulation. With this model it is possible to study how blood flow changes from head down to supine and upright position and correlation among posture variations, microgravity, vessel stenosis, muscle movement, heartbeat, aging and the consequent pressure changes. This may have a great impact toward a deeper understanding of pathological disorders involving abnormalities of the cerebral inflow and outflow. For example, it can be used to easily assess which alterations in the extracranial venous outflow may be in relation with central nervous system disorders [11, 12, 57].

The present model includes accurate submodels of the neck venous network(Section 2.3.1), whole body arterial tree (Section 2.3.2) and the intracranial circulation (Section 2.3.1) which

incorporates the autoregulation of cerebral blood flow (CBF) [15, 54]. They provide a correct value of CBF to the venous part of the model, allowing a quantitative analysis of the effect of alterations in the venous pathways on intracranial quantities, such as intracranial pressure, venous sinuses pressure, capillary pressure, and cerebrospinal fluid (CSF) circulation. A sophisticated description of the collateral pathways, including the most important venous network such as the vertebral plexus, external jugular veins and frontal and occipital anastomosis is included in the model which leading blood to the downstream sections of the jugular veins [11, 57, 59]. It is known that the physical and biomechanical parameters such as cross-sectional area and wall shear stress of veins depend on pressure changes inside the vessel [10]. Moreover, head rotation is a common non-invasive way to cause pressure changes by posture change [10, 85]. Since, at this time, there is no established invasive or noninvasive diagnostic imaging modality capable to assess intracranial and/or parenchymal circulatory parameters in relation to extracranial brain outflow [18], the clinical application of the present model seems highly desirable such as building the advanced adult and paediatric model to study a group of vascular malfunction diseases.

The most adaptable parameters in the model is each veins conductance which we focused our attention on changes in conductances in the venous pathways who is responsible to impose the disorder to the system. Indeed, IJVs as the main study target are collapsible vessels which reflect the changes in their cross sectional depending on the pressure difference between inside and outside of the vessel wall called transmural presser.

In this study symmetric and asymmetric collapsing or expansion in IJVs in our different study conditions were considered to be evaluated according to the tube law [67, 86]. In this regard, each conductance under examination was varied from the baseline value, that is representative of physiological condition, to zero value that simulates total absence of drainage from a section of the network; simulations of posture variation were performed in both situations. Analysis of the correlation between vessels conductance and posture variation and the subsequent pressures and flows changes might give information about the parameters that have greater impact on intracranial hemodynamics (and then on related disorders). From our particular point of view, analysis of the results before and after the variation of a conductance is meaningful, since it provides information on how the closure of a particular drainage tract affects important physiological parameters, such as venous sinuses pressure  $P_{vs}$  (and so intracranial pressure  $P_{ic}$  and cerebral circulation).

## 2.2 Anatomy and physiology of the cerebral drainage system

Due to the large cross-sectional area, internal jugular veins are the main blood outflow pathway from the brain in the supine position [59]. The internal jugular veins connect the superior vena cava to the venous sinus in the skull. Each of the two IJVs is conventionally subdivided into three segments (J3, J2 and J1, from the head to the heart) and its cross-sectional area increases along the same direction [56,58] (See Figure 2.1).

- left and right lower segments (J1) correspond to the point close to the junction of the IJVs with the subclavian vein, at the confluence with the brachiocephalic vein trunk;
- the middle segments (J2) correspond to the point where IJVs are in an anatomical relationship with the more lateral contour of the thyroid gland;
- the upper segments (J3) correspond to the point before the passage through the jugular foramen into the skull.

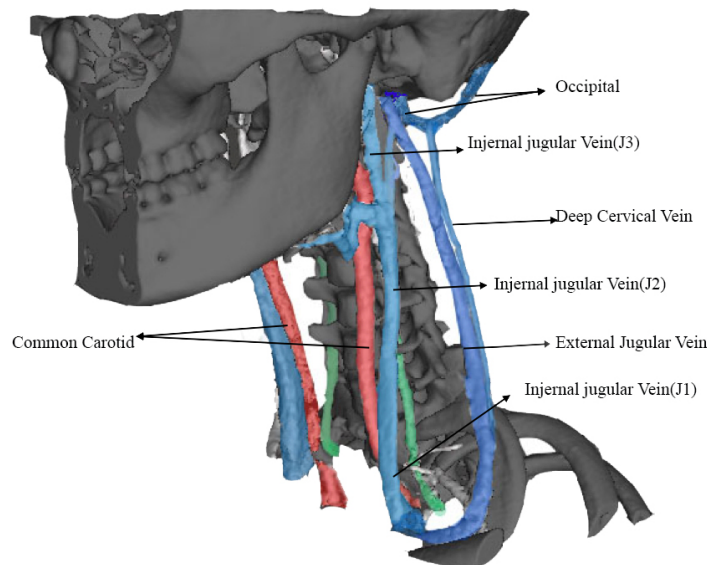


Figure 2.1: Schematic representation of the main vessels of the neck drainage system.

Vertebral veins, internal venous plexus, and deep cervical veins are alternative pathways [16,62] that can carry the brain venous outflow in the case of IJV collapsing. In the absence of other routes for extracranial outflow, this flow limitation would have dramatic and dangerous effects on the cerebral circulation, such as increase in intracranial pressure.

The external carotid arteries enter the facial and extracranial compartment to join external jugular vein. Cerebral venous outflow is the flow that originates from the straight sinus which

is divided into right and left transverse sinuses and supplies the IJVs and vertebral veins. Moreover, there are important communicating pathways between external jugular veins (which collect blood from temporal branches [56, 58]) and deep cervical veins and IJVs. There is a quota of the head inflow that is conveyed into the IJV more caudally with respect to the J3 position, through intra- and extra-cranial anastomosis [59]. These network all together are playing an important role in improving the accuracy of the model output.

## 2.3 Mathematical Modelling Description

The model consists of an anatomically informed 1D arterial network and two 0D networks of the brain and venous drainage, respectively. The arterial network is designed by a compartmental method in which the vessels are treated as monomode 1D waveguides. The parameters such as vessels length, mean blood velocity, topology of the arterial segments and the characteristic impedance of each segment are used to simulate the arterial hemodynamic characteristics [53]. In the 0D networks, vasculature is considered as an electric circuit, and the veins are electric elements with given values of capacitance and conductance. The model equations satisfy the momentum and mass conservation laws and describe the pressure-area relationship in accordance with literature and experimental data [21, 54]. The model is managed by the software package MATLAB-Simulink 2019b (version 9.0.0.341360, developed by The MathWorks Inc., Natick, MA, 2016).

### 2.3.1 Description of the 0D Brain and venous submodel

In the 0D algorithm, the intracranial autoregulation mechanisms and cerebral outflow were modelled according to the model by Ursino et al [15, 54]. Each vessel was considered as an electric element with a given value of resistance, capacitance and conductance (i.e., pressure  $P_x$ , conductance  $G_x$ , and capacity  $C_x$  in a specific point  $x$ ) [20, 21, 53, 54]. Equations satisfy the momentum and mass conservation laws and describe the pressure-area relationship. Table 2.1 provides a glossary of terms.

The value of  $C_{pa}$  at the denominator accounts for the ability of the duct to store blood without variations of transmural pressure: the higher the value of  $C_{pa}$  the lower the change in pressure over time.

Table 2.1: Glossary of terms related to the 0D part of the model.

<i>Symbol</i>	<i>Quantity</i>
$A$	Parameter related to the elasticity of the jugular wall segments and collapsibility
$AZY$	Lumbo-azygos system
$azy1$	Distal azygos
$azy2$	Proximal azygos
$c3$	Upper segment of the collateral network
$cj2$	Lower anastomoses
$cj3$	Upper anastomoses
$C_{azy}$	Capacity of the azygos system
$C_{c2}$	Capacity of the middle segment of the collateral network
$C_{c3}$	Capacity of the upper segment of the collateral network
$C_{ic}$	Intracranial capacity
$C_{jl2}$	Capacity of the middle segment of the left internal jugular vein
$C_{jl3}$	Capacity of the upper segment of the left internal jugular vein
$C_{jr2}$	Capacity of the middle segment of the right internal jugular vein
$C_{jr3}$	Capacity of the upper segment of the right internal jugular vein
$C_{pa}$	Capacity of the pial arterioles
$C_{pan}$	Basal capacity of the pial arterioles
$C_{svc}$	Capacity of the superior vena cava
$C_{vi}$	Capacity of the intracranial veins
$C_{vs}$	Capacity of the terminal intracranial veins
$C_{vv}$	Capacity of the vertebral veins
$C_x$	Capacity of the generic segment $x$ of the circulatory system
$\Delta C_{pa}$	Amplitude of the curve of the pial arterioles capacity
$\Delta C_{pa1}$	Value of the capacity of the pial arterioles during vasodilation simulation
$\Delta C_{pa2}$	Value of the capacity of the pial arterioles during vasoconstriction simulation
$G_0$	Conductance of the cerebrospinal fluid outflow tract
$G_{aut}$	Gain of the autoregulation mechanism related to CBF variations
$G_{azy1}$	Conductance of the distal azygos
$G_{azy2}$	Conductance of the proximal azygos
$G_{c1}$	Conductance of the lower segment of the collateral network
$G_{c2}$	Conductance of the middle segment of the collateral network
$G_{c3}$	Conductance of the upper segment of the collateral network
$G_{cjl2}$	Conductance of the lower anastomotic connection (left side)
$G_{cjl3}$	Conductance of the upper anastomotic connection (left side)
$G_{cjr2}$	Conductance of the lower anastomotic connection (right side)
$G_{cjr3}$	Conductance of the upper anastomotic connection (right side)
$G_{ex}$	Conductance of the external carotid arteries
$G_{jl1}$	Conductance of the lower segment of the left internal jugular vein
$G_{jl2}$	Conductance of the middle segment of the left internal jugular vein
$G_{jl3}$	Conductance of the upper segment of the left internal jugular vein
$G_{jr1}$	Conductance of the lower segment of the right internal jugular vein
$G_{jr2}$	Conductance of the middle segment of the right internal jugular vein
$G_{jr3}$	Conductance of the upper segment of the right internal jugular vein
$G_{lv}$	Conductance of the lumbar vein
$G_{svc1}$	Conductance of the upper segment of the superior vena cava (jugular confluence)
$G_{svc2}$	Conductance of the lower segment of the superior vena cava
$G_{vs}$	Conductance of the terminal intracranial veins
$G_{vv2}$	Conductance of the lower part of the vertebral vein
$G_{vvl}$	Conductance of the left vertebral vein
$G_{vvr}$	Conductance of the right vertebral vein
$G_x$	Conductance of the generic segment $x$ of the circulatory system
$hb_f$	Mock cerebrospinal fluid possibly injected into or subtracted from the cranial cavity
$IJV$	Internal jugular vein
$kC_{pa}$	Parameter for the capacity of the pial arterioles
$k_E$	Intracranial elastance coefficient
$k_{jl1}$	Parameter for the basal conductance of the lower segment of the left internal jugular vein
$k_{jl2}$	Parameter for the basal conductance of the middle segment of the left internal jugular vein
$k_{jl3}$	Parameter for the basal conductance of the upper segment of the left internal jugular vein
$k_{jr1}$	Parameter for the basal conductance of the lower segment of the right internal jugular vein
$k_{jr2}$	Parameter for the basal conductance of the middle segment of the right internal jugular vein

All other mass conservation equations have a similar meaning. Mass conservation at the node of cerebral veins  $vi$  implies the following equation:

$$\frac{d(P_v - P_{ic})}{dt} = \frac{1}{C_{vi}} \left[ \frac{P_c - P_v}{R_{pv}} - \frac{P_v - P_{vs}}{R_{vs}} \right] \quad (2.1)$$

The relationship between  $C_{vi}$  and pressure is given by the following equation:

$$C_{vi} = \frac{1}{k_{ven} (P_v - P_{ic} - P_{v1})} \quad (2.2)$$

Control mechanisms work at the level of the arteriolar cerebrovascular bed by modifying  $R_{pa}$  and  $C_{pa}$ . Autoregulation activated by relative changes in  $Q$  is given by the following equation:

$$\frac{dx_{aut}}{dt} = \left( \frac{1}{\tau_{aut}} \right) \left[ -x_{aut} + G_{aut} \left( \frac{Q - Q_n}{Q_n} \right) \right] \quad (2.3)$$

where the minus sign of  $x_{aut}$  simulates the fact that a fall in blood flow causes a rapid dilatation of resistance vessels, whereas a rise in blood pressure causes vasoconstriction. The existence of maximal limits for the vascular response (total vasodilation and maximal vasoconstriction) is simulated by a sigmoidal relationship with upper and lower saturation levels acting on pial arteries capacity  $C_{pa}$ , so that:

$$C_{pa} = \frac{\left( C_{pan} - \frac{\Delta C_{pa}}{2} \right) + \left( C_{pan} + \frac{\Delta C_{pa}}{2} \right) \exp \left[ \frac{-x_{aut}}{kC_{pa}} \right]}{1 + \exp \left[ \frac{-x_{aut}}{kC_{pa}} \right]} \quad (2.4)$$

The sigmoidal curve cannot be symmetrical because the increase in blood volume induced by vasodilation is higher than the blood volume decrease induced by vasoconstriction. Hence, two different values must be chosen for the parameter  $\Delta C_{pa}$ , depending on whether vasodilation or vasoconstriction is considered.

$$\text{if } x_{aut} < 0 \text{ then } \Delta C_{pa} = \Delta C_{pa1} \text{ and } kC_{pa} = \Delta C_{pa1}/4 \quad (2.5)$$

for the vasodilation simulation, and

$$\text{if } x_{out} > 0 \text{ then } \Delta C_{pa} = \Delta C_{pa2} \text{ and } kC_{pa} = \Delta C_{pa2}/4 \quad (2.6)$$

for the vasoconstriction simulation.

The value of pial arteriolar resistance is given by the formula:

$$R_{pa} = \frac{k_R C_{pan}^2}{[(P_{pa} - P_{ic}) C_{pa}]^2} \quad (2.7)$$

The following equations account for cerebrospinal fluid formation rate  $Q_f$  and outflow rate  $Q_0$

$$Q_f = \frac{P_c - P_{ic}}{R_f} \text{ if } P_c > P_{ic}, \text{ else } Q_f = 0 \quad (2.8)$$

$$Q_0 = \frac{P_{ic} - P_{vs}}{R_0} \text{ if } P_{ic} > P_{vs}, \text{ else } Q_0 = 0 \quad (2.9)$$

An expression for the resistance of the terminal intracranial veins  $R_{vs}$  is computed as follows:

$$R_{vs} = \frac{P_v - P_{vs}}{P_v - P_{ic}} R_{vs1} \text{ if } P_v > P_{vs}, \text{ else } R_{vs} = R_{vs1} \quad (2.10)$$

Application of mass conservation at the intracranial volume leads to the following equations:

$$\frac{dP_{ic}}{dt} = \frac{1}{C_{ic}} \left[ \frac{d(P_{pa} - P_{ic})}{dt} C_{pa} + \frac{d(P_v - P_{ic})}{dt} C_{vi} + \frac{dC_{pa}}{dt} (P_{pa} - P_{ic}) + Q_f - Q_0 + hbf \right] \quad (2.11)$$

and

$$C_{ic} = \frac{1}{k_E P_{ic}} \quad (2.12)$$

This formula states that the variation in time of the intracranial pressure is the result of several factors. The first and the second term in brackets at the right side of Equation 2.11 refer to changes in transmural pressure at the level of arterioles and cerebral veins, the third term refers to change on pial artery capacity, while the other terms refer to CSF inflow or

outflow. Intracranial capacity  $C_{ic}$  at the denominator accounts for the ability of the skull to store volume of fluid.

The structure of the cerebral venous outflow model has been developed starting from the work of Zamboni et al in 2013 [59]. It is build by using two types of equations. Equations from 2.13 to 2.22 are the state equations of the model and implement the mass conservation at all the circuit nodes. In fact, the pressure change over time ( $dP/dt$ ) is calculated according to the Kirchhoff law for each vessel of the whole network. We can see how the pressure at a given point (e.g.  $j_r3$  in Equation 2.14) is related to capacity, conductances, and drops of pressure.

$$\begin{aligned} \frac{dP_{vs}}{dt} = \frac{1}{C_{vs}} & [(P_v - P_{vs}) G_{vs} - (P_{vs} - P_{ic}) G_0 - (P_{vs} - P_{jr3}) G_{jr3} - (P_{vs} - P_{jl3}) G_{jl3} \\ & - (P_{vs} - P_{c3}) G_{c3} - (P_{vs} - P_{vv}) G_{vvl} - (P_{vs} - P_{vv}) G_{vvr}] \end{aligned} \quad (2.13)$$

$$\frac{dP_{jr3}}{dt} = \frac{1}{C_{jr3}} [(P_{vs} - P_{jr3}) G_{jr3} - (P_{jr3} - P_{c3}) G_{cjr3} - (P_{jr3} - P_{jr2}) G_{jr2}] \quad (2.14)$$

$$\frac{dP_{jr2}}{dt} = \frac{1}{C_{jr2}} [(P_{jr3} - P_{jr2}) G_{jr2} - (P_{jr2} - P_{c2}) G_{cjr2} - (P_{jr2} - P_{suc1}) G_{jr1}] \quad (2.15)$$

$$\frac{dP_{jl3}}{dt} = \frac{1}{C_{jl3}} [(P_{vs} - P_{jl3}) G_{jl3} - (P_{jl3} - P_{c3}) G_{cjl3} - (P_{jl3} - P_{jl2}) G_{jl2}] \quad (2.16)$$

$$\frac{dP_{jl2}}{dt} = \frac{1}{C_{jl2}} [(P_{jl3} - P_{jl2}) G_{jl2} - (P_{jl2} - P_{c2}) G_{cjl2} - (P_{jl2} - P_{suc1}) G_{jl1}] \quad (2.17)$$

$$\begin{aligned} \frac{dP_{c3}}{dt} = \frac{1}{C_{c3}} & [(P_{vs} - P_{c3}) G_{c3} + (P_{jr3} - P_{c3}) G_{cjr3} + (P_{jl3} - P_{c3}) G_{cjl3} + (P_a - P_{c3}) G_{ex} \\ & - (P_{c3} - P_{c2}) G_{c2}] \end{aligned} \quad (2.18)$$

$$\frac{dP_{c2}}{dt} = \frac{1}{C_{c2}} [(P_{c3} - P_{c2}) G_{c2} + (P_{jr2} - P_{c2}) G_{cjr2} + (P_{jl2} - P_{c2}) G_{cjl2} - (P_{c2} - P_{cv}) G_{c1}] \quad (2.19)$$

$$\frac{dP_{svc}}{dt} = \frac{1}{C_{svc}} [(P_{svc1} - P_{svc}) G_{svc1} + (P_{azy} - P_{svc}) G_{azy2} - (P_{svc} - P_{cv}) G_{svc2}] \quad (2.20)$$

$$\frac{dP_{vv}}{dt} = \frac{1}{C_{vv}} [(P_{vs} - P_{vv}) G_{vvl} + (P_{vs} - P_{vv}) G_{vvr} - (P_{vv} - P_{azy}) G_{azy1} - (P_{vv} - P_{lv}) G_{vv2}] \quad (2.21)$$

$$\frac{dP_{azy}}{dt} = \frac{1}{C_{azy}} [(P_{vv} - P_{azy}) G_{azy1} + (P_{lv} - P_{azy}) G_{lv} - (P_{azy} - P_{svc}) G_{azy2}] \quad (2.22)$$

Starting from the work on the intracranial circuit [15], we moved around several experimental data to choose the right inputs for the jugular-extra jugular network, adopting reasonable criteria to determine parameters not available from literature.

### 2.3.2 Description of the 1D arterial submodel

The arterial network of our model previously was published by Majka et al in 2017 in which the model has a set of 55 main arteries as named in table 2.2 and depicted in Figure 2.2 [20,53]. Table 2.2 shows the number of the vessel in the reduced model (the same numbers were used in the figures 2.2 and 2.3, name, length, mean value of the velocity, characteristic impedance, time delay and reflection coefficient of the peripherals.

An anatomically detailed model consisting of a network of electric transmission lines is used here to simulate propagation of the pulse waves in humans. It is a new numerical simulation method that allows one to predict the time dependence (waveform) of pressure at any location of the arterial system in humans [53]. This kind of models are particularly effective in the description of large scale properties of the entire arterial system and of its response to some

Table 2.2: Parameters of the arterial model.  $No.$  is the vessel number in the model,  $L$  is the length of the vessel,  $c$  is the mean velocity,  $Z_0$  is the characteristic impedance,  $t_d$  is the time delay, and  $R_f$  is the reflection coefficient of the peripherals [53].

$No.$	$Vessel$	$L$ [m]	$c$ [ $ms^{-1}$ ]	$Z_0$ [ $\Omega$ ]	$t_d$ [s]	$R_f$
1	Ascending aorta	0.0400	5.3400	8.4935e+06	0.0075	-
2	Aortic arch A	0.0200	5.4708	1.4576e+07	0.0037	-
3	Brachiocephalic artery	0.0340	5.9351	5.1604e+07	0.0057	-
4	Subclavian (R)	0.0680	6.4731	1.3522e+08	0.0105	-
5	Common carotid (R)	0.1880	6.5757	1.6054e+08	0.0286	-
6	Vertebral (R)	0.1480	10.9677	1.0154e+09	0.0135	0.3583
7	Brachial artery (R)	0.2350	7.1998	3.6688e+08	0.0326	-
8	Radial artery (R)	0.2340	11.6832	1.5253e+09	0.0200	0.4740
9	Ulnar artery (R)	0.1520	23.0143	2.0393e+09	0.0066	-
10	Interossea artery (R)	0.0790	17.7770	7.3352e+09	0.0044	0.7068
11	Ulnar artery (R)	0.0850	11.0889	1.0266e+09	0.0077	0.3535
12	Internal carotid (R)	0.1180	11.8060	1.8018e+09	0.0100	0.9487
13	External carotid (R)	0.1180	11.9252	1.7714e+09	0.0099	0.5150
14	Aortic arch B	0.0390	5.4901	1.6027e+07	0.0071	-
15	Common carotid (L)	0.2090	6.5757	1.6054e+08	0.0318	-
16	Internal carotid (L)	0.1180	11.8060	1.8018e+09	0.0100	0.9487
17	External carotid (L)	0.1180	11.9252	1.7714e+09	0.0099	0.5150
18	Thoracic aorta A	0.0520	5.5203	1.8450e+07	0.0094	-
19	Subclavian (L)	0.0680	6.4731	1.3522e+08	0.0105	-
20	Vertebral (L)	0.1480	10.9677	1.0154e+09	0.0135	0.3583
21	Brachial artery (L)	0.2350	7.1998	3.6688e+08	0.0326	-
22	Radial artery (L)	0.2340	11.6832	1.5253e+09	0.0200	0.4740
23	Ulnar artery (L)	0.1520	23.0143	2.0393e+09	0.0066	-
24	Interossea artery (L)	0.0790	17.7770	7.3352e+09	0.0044	0.7068
25	Ulnar artery (L)	0.0850	11.0889	1.0266e+09	0.0077	0.3535
26	Intercostals	0.0920	5.1642	1.6054e+08	0.0178	0.5353
27	Thoracic aorta B	0.0520	5.5685	2.0622e+07	0.0093	-
28	Abdominal aorta A	0.0530	5.9701	6.1414e+07	0.0089	-
29	Coeliac artery A	0.0100	6.4555	1.4185e+08	0.0015	-
30	Coeliac artery B	0.0100	6.4555	1.4185e+08	0.0015	-
31	Hepatic artery	0.0660	7.5207	5.1934e+08	0.0088	0.3944
32	Gastric artery	0.0710	7.9679	8.2193e+08	0.0089	0.5290
33	Splenic artery	0.0630	6.9332	2.9557e+08	0.0091	0.2132
34	Superior mesenteric	0.0590	6.3835	1.1539e+08	0.0092	0.1696
35	Abdominal aorta B	0.0530	5.9701	6.1414e+07	0.0089	-
36	Renal artery (L)	0.0320	7.1949	3.5573e+08	0.0044	0.2656
37	Abdominal aorta C	0.0530	5.9701	6.1414e+07	0.0089	-
38	Renal artery (R)	0.0320	7.1949	3.5573e+08	0.0044	0.2656
39	Abdominal aorta D	0.0530	5.9701	6.1414e+07	0.0089	-
40	Inferior mesenteric	0.0500	8.2613	1.0786e+09	0.0061	0.5970
41	Abdominal aorta E	0.0530	5.9701	6.1414e+07	0.0089	-
42	Common iliac (L)	0.0580	6.0922	7.5303e+07	0.0095	-
43	Common iliac (R)	0.0580	6.0922	7.5303e+07	0.0095	-
44	External iliac (L)	0.0830	6.9399	2.7580e+08	0.0120	-
45	Internal iliac (L)	0.0500	14.2533	1.1910e+09	0.0035	0.1903
46	Femoral artery (L)	0.1270	10.2865	5.9687e+08	0.0123	-
47	Deep Femoral artery (L)	0.1270	10.2865	5.9687e+08	0.0123	0.1717
48	Posterior tibial artery (L)	0.3220	15.9357	1.6439e+09	0.0202	0.2376
49	Anterior tibial artery (L)	0.3250	15.3211	4.3267e+09	0.0212	0.7324
50	External iliac (R)	0.0830	6.9399	2.7580e+08	0.0120	-
51	Internal iliac (R)	0.0500	14.2533	1.1910e+09	0.0035	0.1903
52	Femoral artery (R)	0.1270	10.2865	5.9687e+08	0.0123	-
53	Deep Femoral artery (R)	0.1270	10.2865	5.9687e+08	0.0123	0.1717
54	Posterior tibial artery (R)	0.3220	15.9357	1.6439e+09	0.0202	0.2376
55	Anterior tibial artery (R)	0.3250	15.3211	4.3267e+09	0.0212	0.7324

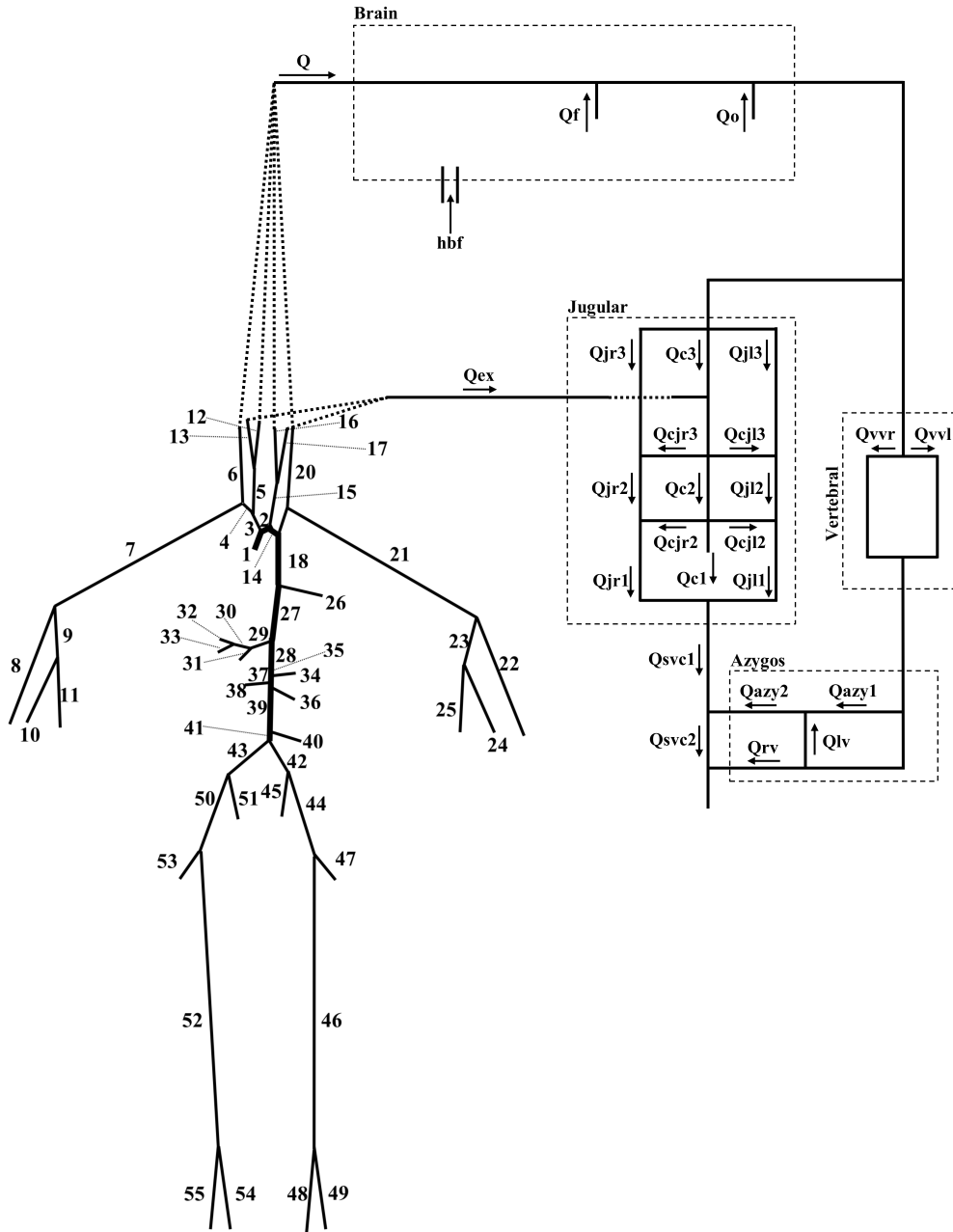


Figure 2.2: Previously published model for the study of the cerebral and extracerebral circulation. Box on the top part is the scheme of the intracranial 0D submodel. Right part is the representation of the 0D submodel for the cerebral drainage system, while in the left part the 1D submodel for the human arterial tree is depicted. [20]

lesions and/or external hazards. Starting from experimental data collected at rest [68], the 1D model can simulate blood pressure during rest and exercise condition, changes in the heart rate, basal properties of left ventricle valve and its disfunctions.

The input data include the geometry and the elastic properties of the arteries as well as the rheological parameters of blood [69]. Thus, the method can account for individual anatomic details of the subject examined. In its simplest realization the model involves lengths and

topology of the arterial segments as well as the propagation parameters: the phase velocity and the characteristic impedance of each segment. This allows the reflection and transmission coefficients to be calculated at each bifurcation [68, 70]. The elasticity of vessel walls is at the origin of the wave-like character of blood flow in arteries. In principle the number of propagation modes is infinite [71], but the most significant effect belongs to the Young mode easily palpable at wrist. Restricting the attention to this mode allows one to treat the vessels as monomode 1D waveguides.

The method of obtaining 1D equation of motion in a distensible vessel of varying cross section has been developed in [68]. The governing equations involve conservation of mass and the momentum balance in a control volume of the 1D vessel [79]. The volumetric flow  $Q(x, t) = AU$ , as a function of space  $x$  and time  $t$ , relates the cross section area  $A$  and the average axial velocity  $U$  tethered in longitudinal direction. The pressure  $P$  is assumed constant across the section, whereas the radial and azimuthal components of velocity are neglected. For what concerns the arterial part of the model, gravitational effects on pressure are ignored.

## 2.4 Mathematical Modelling Advancement

### 2.4.1 Extending the vessels anatomy map of the model

Recent literature has mentioned the considerable role of peripheral vessels in the head and neck drainage [6, 10, 59]. In cases of obstructions of the main pathways, alternative routes compensate the blood outflow [16, 58, 59]. We adjusted the anatomic map of the model to improve its ability to evaluate both physiological and pathological cases. The full list of vessels added in this work is reported in Table 2.3.

We worked in order to keep the proper relative magnitude among flow rates in the three segments of the IJV [59, 65]. A summary of our work strategy is reported in the flowchart in Figure 2.4, which shows all the contributions used to build the paediatric model. We started from mathematical models previously validated and published by our group to have a solid basis from the mathematical point of view. Beside, we used both literature and data acquisition to collect all the parameters we need to switch from an adult to a paediatric model, by a proper tuning of the parameters of the mathematical equations.



Table 2.3: Parameters of the arterial model.  $No.$  is the vessel number in the model,  $L$  is the length of the vessel,  $c$  is the mean velocity,  $Z_0$  is the characteristic impedance,  $t_d$  is the time delay, and  $R_f$  is the reflection coefficient of the peripherals.

$No.$	$Vessel$	$L$ [m]	$c$ [ $ms^{-1}$ ]	$Z_0$ [ $\Omega$ ]	$t_d$ [s]	$R_f$
56	Basilar	0.0290	15.8377	2.0170e+09	0.0018	-
57	Posterior cerebral segment A (R)	0.0050	16.0107	4.6739e+09	0.0003	-
58	Posterior cerebral segment A (L)	0.0050	16.0107	4.6739e+09	0.0003	-
59	Posterior comm (R)	0.0150	19.1237	2.5566e+10	0.0008	-
60	Posterior comm (L)	0.0150	19.1237	2.5566e+10	0.0008	-
61	Anterior comm	0.003	19.6477	2.6267e+10	0.0002	-
62	Anterior cerebral segment A (R)	0.0120	15.8681	3.8743e+09	0.0008	-
63	Anterior cerebral segment A (L)	0.0120	15.8681	3.8743e+09	0.0008	-
64	External carotid (R)	0.118	11.9252	1.7714e+09	0.0099	-
65	External carotid (L)	0.118	11.9252	1.7714e+09	0.0099	-
66	Posterior cerebral segment B (R)	0.0860	15.8603	4.8081e+09	0.0054	0.6548
67	Posterior cerebral segment B (L)	0.0860	15.8603	4.8081e+09	0.0054	0.6548
68	Ophthalmic artery (R)	0.03	17.0360	1.1620e+10	0.0018	0.8188
69	Ophthalmic artery (L)	0.03	17.0360	1.1620e+10	0.0018	0.8188
70	Middle cerebral artery (R)	0.03	18.4010	1.7084e+10	0.0016	0.8535
71	Middle cerebral artery (L)	0.03	18.4010	1.7084e+10	0.0016	0.8535
72	Cerebral artery (R)	0.0580	18.1695	9.4886e+09	0.0032	0.7563
73	Cerebral artery (L)	0.0580	18.1695	9.4886e+09	0.0032	0.7563
74	Internal carotid (R)	0.0590	11.2683	1.1624e+09	0.0052	-
75	Internal carotid (L)	0.1480	11.2683	1.1624e+09	0.0052	-
76	Facial A	0.04	17.4567	5.8345e+09	0.0023	0.6552

that, the following equations have been included in the model:

$$\frac{dP_{jr1}}{dt} = \frac{1}{C_{j1}} [(P_{jr2} - P_{jr1}) G_{jr1} - (P_{jr1} - P_{svcl}) G_{svcl}] \quad (2.23)$$

$$\frac{dP_{jl1}}{dt} = \frac{1}{C_{j1}} [(P_{jl2} - P_{jl1}) G_{jl1} - (P_{jl1} - P_{svcl}) G_{svcl}] \quad (2.24)$$

$$\frac{dP_{IVP}}{dt} = \frac{1}{C_{vp}} [(P_{vs} - P_{vp}) G_{vp} - (P_{vp} - P_{azy}) G_{azy1} - (P_{ej1} - P_{jcl}) G_{jc}] \quad (2.25)$$

$$\frac{dP_{ejr}}{dt} = \frac{1}{C_{ej}} [(P_{ex} - P_{ejr}) G_{ej} - (P_{ejr} - P_{jcl}) G_{jc} - (P_{ejr} - P_{svcl}) G_{svcl}] \quad (2.26)$$

$$\frac{dP_{ejl}}{dt} = \frac{1}{C_{ej}} [(P_{ex} - P_{ejl}) G_{ej} - (P_{ejl} - P_{jcl}) G_{jc} - (P_{ejl} - P_{svcl}) G_{svcl}] \quad (2.27)$$

$$\frac{dP_{dvr}}{dt} = \frac{1}{C_{dv}} [(P_{ex} - P_{dvr}) G_{dv} - (P_{dvr} - P_{ejr}) G_{ej}] \quad (2.28)$$

$$\frac{dP_{dvl}}{dt} = \frac{1}{C_{dv}} [(P_{ex} - P_{dvl}) G_{dv} - (P_{dvl} - P_{ejl}) G_{ej}] \quad (2.29)$$

$$\frac{dP_{jcr}}{dt} = \frac{1}{C_{jc}} [(P_{ejr} - P_{jcr}) G_{jc} - (P_{jcr} - P_{jr2}) G_{jr2}] \quad (2.30)$$

$$\frac{dP_{jcl}}{dt} = \frac{1}{C_{jc}} [(P_{ejl} - P_{jcl}) G_{jc} - (P_{jcl} - P_{jl2}) G_{jl2}] \quad (2.31)$$

Conductance parameter (G-function) has a switch-like function to simulate the collapsibility behaviour of the IJV [67]. The G-function for the all segments of IJV were segment-specifically modified as written in Equations below:

$$G_{jr3} = k_{jr3} \left[ 1 + \left( \frac{2}{\pi} \right) \arctan \left( \frac{P_{vs} - P_{j3ext}}{A_{j3}} \right) \right]^2 \quad (2.32)$$

$$G_{jl3} = k_{jl3} \left[ 1 + \left( \frac{2}{\pi} \right) \arctan \left( \frac{P_{vs} - P_{j3ext}}{A_{j3}} \right) \right]^2 \quad (2.33)$$

$$G_{jr2} = k_{jr2} \left[ 1 + \left( \frac{2}{\pi} \right) \arctan \left( \frac{P_{jr3} - P_{thor}/2 - P_{j2ext}}{A_{j2}} \right) \right]^2 \quad (2.34)$$

$$G_{jl2} = k_{jl2} \left[ 1 + \left( \frac{2}{\pi} \right) \arctan \left( \frac{P_{jl3} - P_{thor}/2 - P_{j2ext}}{A_{j2}} \right) \right]^2 \quad (2.35)$$

$$G_{jr1} = k_{jr1} \left[ 1 + \left( \frac{2}{\pi} \right) \arctan \left( \frac{P_{jr2} - P_{thor} - P_{j1ext}}{A_{j1}} \right) \right]^2 \quad (2.36)$$

$$G_{jl1} = k_{jl1} \left[ 1 + \left( \frac{2}{\pi} \right) \arctan \left( \frac{P_{jl2} - P_{thor} - P_{j1ext}}{A_{j1}} \right) \right]^2 \quad (2.37)$$

### 2.4.2 Modelling Physiology Advancements

#### Arterial physiology Adjustment: Modelling Age-Related Parameters in paediatric study

The procedure of how we improved the age-related physiological parameters is shown in Figure 2.4. Physiology of paediatric cardiovascular system is different from the adult and wrongly based on studies involving adults [30]. Thus, the adult model needs appropriate modifications. Heart rate (HR), systolic blood pressure (SBP) and diastolic blood pressure (DBP) in paediatric subjects are different than in adults [31]. The mean age of the volunteers enrolled in our dataset was  $12 \pm 5$  years, while the measured average HR was  $83 \pm 16$  beats per min (mean  $\pm$  standard deviation [SD]). Therefore, we set the duration of one cardiac cycle to 0.7 s (against a duration of 0.8 s in the adult model). The mean value of SBP (in mmHg) was calculated by using the Equation  $SBP=90+2(Age)$ , where age is measured in years [72]. Therefore, the SBP for our dataset was equal to  $114 \pm 9$  mmHg (mean  $\pm$  SD).

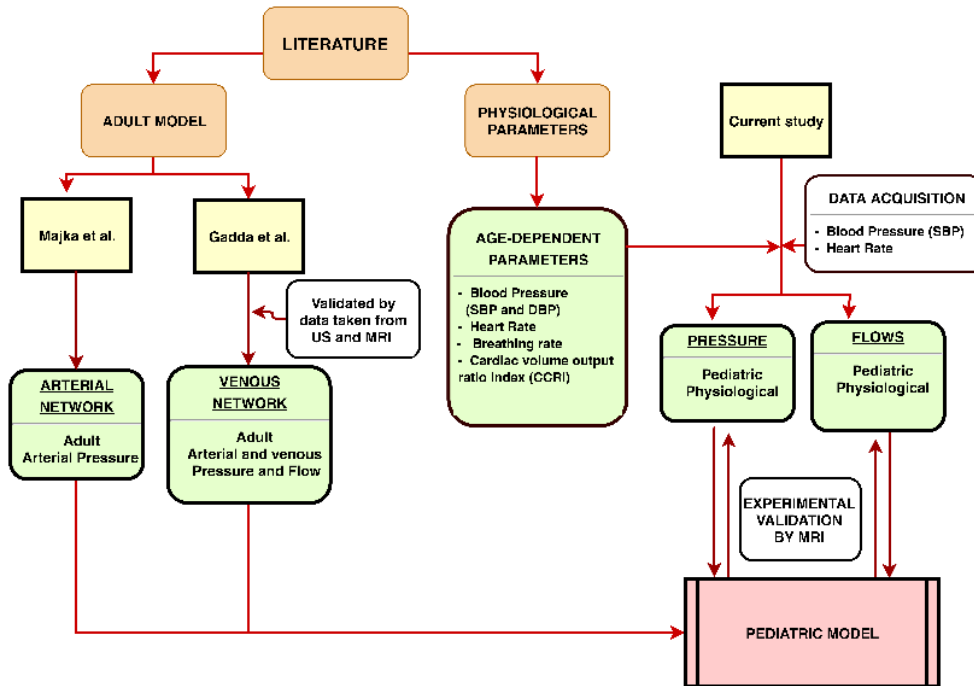


Figure 2.4: Flowchart of all the contributions used to build the paediatric model.

For what concern the mean value of DBP, we referred to literature [72, 74, 75]. From the literature we know that the respiratory rate in adults and old-children are about 15 and 20 breaths/min, respectively [75]. We tuned the respiratory rate in the model accordingly. By setting the model with these new parameters, the new simulated cardiac pulse waves at the level of aorta and ventricle were representative of a paediatric cohort. In Figure 2.5 such pulse

waves are presented and compared with the results of the adult setting. The generated pulse wave is compared with the physiologic reference pattern for adults [1] represented in the inset of Figure 2.5. The parameters were also regulated to generate the pressure waveform at the level of ascending aorta to satisfy the SBP and DBP according to the mean values from our database and the paediatric cardiopulmonary care guide [76]. More modifications were not necessary because there is no significant correlation between the mean value of systolic to diastolic ratio and age or body surface [77].

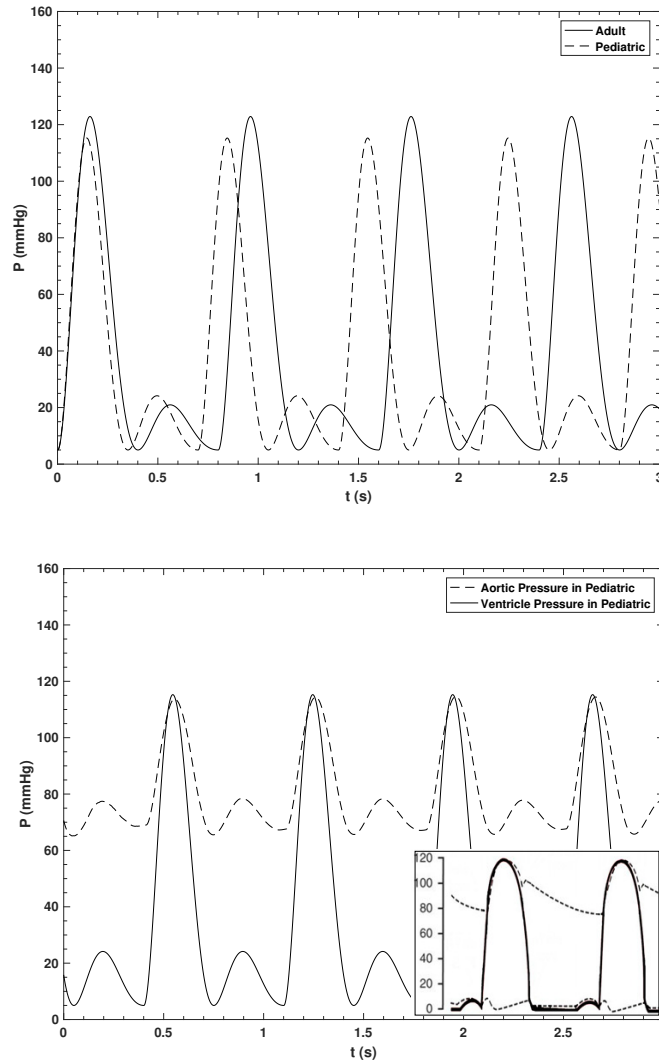


Figure 2.5: The simulated cardiac pressure waveform. a Comparison of the aortic and ventricle pressure wave in paediatric. b Comparison of the ventricle pressure wave in paediatric and adult. The inset shows the physiological pattern

Other relevant age-related parameters to regulate the pressure and flow rate in the 1D part of the model are total blood volume (TBV), cerebral blood volume (CBV), and cardiac volume output ratio index (CBV/CO) [5]. The CO is calculated by multiplying HR by the difference between end-diastolic volume and end-systolic volume [59]. Since the ascending

aorta was not in the selected region of our study, we were not able to calculate the cardiac volume output ratio index. This value was taken from literature. Its mean value in infants, paediatric subjects with the same mean age of our dataset, and adults is 34.0%, 22.9%, and 14.3%, respectively [5, 78]. The simulated flow ratio percentage of CBF to the ascending aorta flow was tuned to be about 22.9%. According to literature, the paediatric TBV and CBF have the mean value of  $3.4 \pm 1.2$  L (mean  $\pm$  SD) and  $1,101 \pm 258$  mL/min (mean  $\pm$  SD) (80 mL blood/100 mL brain), respectively [30, 77]. The weight of the brain is reported as  $1,100.7 \pm 209.6$  g (mean  $\pm$  SD) and  $1,189 \pm 99$  g (mean  $\pm$  SD) in paediatric subjects and adults, respectively [5, 78]. For adults, the reported mean TBV and CBF are  $5.6 \pm 0.3$  L and 750 (490–770) mL/min (mean and min to max range) (70 mL blood/100mL of brain), respectively [5, 16, 78].

#### Arterial physiology Adjustment: Modelling orthostatic stress

Arterial 1D compartments consist of 55 blocks that simulate the arterial tree and 11 blocks that simulate the Willis circle, respectively. By that, in total 76 main arteries were modelled in the current advanced model. Each block calculates the pressure pulse behaviour of a given artery by solving 1D equations and considering the pressure as a transient wave pulse. In order to solve the equations, parameters such as segment length, mean velocity of blood in the vessel, characteristic impedance, time delay and reflection coefficient are imported into the mode as explained in the publication by Majka et al [53]. Since enough information to adjust the 1D compartments has not been reported in literature, we decided to adjust the arterial pressure  $P_a$  (Equation 2.38) and external carotid arteries pressure  $P_{ex}$  (Equation 2.39) by using  $P_{hydrox}$  and  $P_{TW}$ .

$$P_a = P_{a0} + P_{hydrox} \quad (2.38)$$

$$P_{ex} = P_{ex0} + P_{hydrox} + P_{TW} \quad (2.39)$$

To do this, we followed the format of equation for ICP reported in the work of Magnæs [43]

(Equation 2.40):

$$P_{ic} = P_{ic0} + \rho g L \sin(\Theta) \quad (2.40)$$

Where  $P_{ic0}$ ,  $P_{a0}$ , and  $P_{ex0}$  are the intracranial, arterial, and external carotid pressure in supine position on Earth.

### Venous Compartment Upgrade

To take into account the IJV collapsibility and the dynamics of pressure change due to posture variation, conductance function should vary according to each segment and vessels CSA and collapsibility. In this regards, the parameters in G-function needs to be analyzed in this section in order to discover how we can take the benefit from it. In fact, the G-function (conductance function) is a nonlinear switch like (arc-tangent) function to simulate the vessels capability in collapsing or dilatation [64, 67]. The G-function for the given segment of  $x$  in IJV is written in Equation 2.41. In this equation, if the negative or low transmural pressure  $P_{xint} - P_{xext}$  at a given point  $x$ , the related vessel conductance  $G_x$  is low, while for high transmural pressure, vessel conductance approaches a maximum value [16].

$$G_x = k_x \left[ 1 + \left( \frac{2}{\pi} \right) \arctan \left( \frac{P_{xint} - P_{xext}}{A} \right) \right]^2 \quad (2.41)$$

$$k_x = \frac{V_0^2}{8\pi\mu L^3} \quad (2.42)$$

where  $L$  is the segment length,  $V_0$  is related to the volume of blood,  $\mu$  is the blood viscosity, and  $A$  is the slope of the pressure-volume relationship or elastance [20, 64, 67]. The sensitivity of Equation 2.41 to pressure variation due to posture changes (e.g. from supine to upright position) on a gravity field is implemented in the difference between internal ( $P_{xint}$ ) and external ( $P_{xext}$ ) pressure. This difference is defined as transmural pressure ( $P_T = P_{xint} - P_{xext}$ ) [64, 67]. Therefore, following the G-function (Equation 2.41), if transmural pressure has positive values IJV is fully open, while if P-T reaches null or negative values IJV is partially or fully collapsed.

To properly define  $P_{xext}$ , we introduced the following equations:

$$P_{xext} = P_{xhydro} + P_{TW} \quad (2.43)$$

$$P_{hydrox} = \rho \times \left( \frac{g}{g_{Earth}} \right) \times L \times \sin(\Theta) \quad (2.44)$$

$$P_{TW} = \left[ 1 - \frac{g}{g_{Earth}} \right] \times R \quad (2.45)$$

where  $\rho$  is the blood density,  $\Theta$  is the body orientation with respect to the gravity acceleration vector of modulus  $g$ ,  $g_{Earth}$  is the modulus of gravity acceleration vector on Earth,  $P_{xhydro}$  and  $P_{TW}$  are the hydraulic and surrounding tissue weight pressure on vessel  $x$  [28].  $P_{TW}$  is related to body size and it emphasizes inter-individual differences [35]. Buckey and colleagues introduced the variable  $R$  as the radius of the body section in which external pressure is measured [28]. We borrowed that concept to tune such parameter in accordance to the characteristic of our model. To include in the orthostatic stress effects on the intra- and extracranial hemodynamic in gravity field or in the absence of it (microgravity) in all three segments of IJV, conductances are upgraded to the following versions. The G-function for supine Equation 2.46, upright and HDT Equation 2.47 and microgravity Equation 2.48 are defined:

$$G_{jl3} = k_{jl3} \left[ 1 + \left( \frac{2}{\pi} \right) \arctan \left( \frac{P_{vs}}{A_{j3}} \right) \right]^2 \quad (2.46)$$

$$G_{jl3} = k_{jl3} \left[ 1 + \left( \frac{2}{\pi} \right) \arctan \left( \frac{P_{vs} - P_{hydro-j3}}{A_{j3}} \right) \right]^2 \quad (2.47)$$

$$G_{jl3} = k_{jl3} \left[ 1 + \left( \frac{2}{\pi} \right) \arctan \left( \frac{P_{vs} - P_{hydro-j3} - P_{TW}}{A_{j3}} \right) \right]^2 \quad (2.48)$$

In this work we assumed the same  $P_{TW}$  for all the IJV segments (J1, J2, and J3), while values of  $P_{hydro}$  were calculated from Equation 2.44 taking into account the average distance of each segment from the hydrostatic indifference point (HIPCSF, Figure 2.6), and assuming that CSF pressure is constant [36]. ICP gradient can be predicted according to the hydrostatic pressure gradients from the HIPCSF [36].

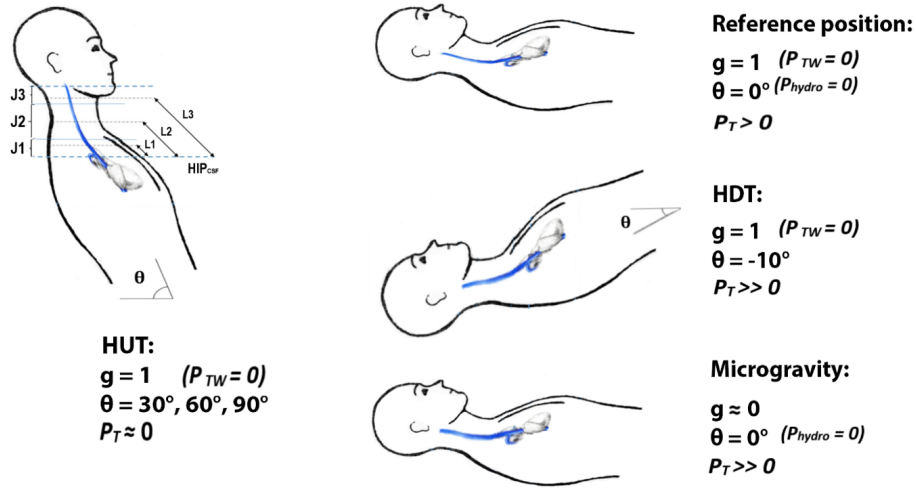


Figure 2.6: Illustration of the three modelled segments of IJV heights from the  $H_{IPCSF}$ .

### Brain Compartment physiology Upgrade

According to the Ursino et al [54] well accepted intracranial dynamics model, at the intracranial level storage capacitance ( $C_{ic}$ ) is inversely proportional to ICP (see equation 2.12 which  $k_E$  is introduced as the intracranial elastance parameter. In the same manner, intracranial venous capacitance ( $C_{vi}$ ) in equation 2.2 and hydraulic pial artery resistance ( $R_{pa}$ ) in equation 2.7 introduced the  $k_{ven}$  and  $k_R$  constants, respectively. By that, the intracranial resistance depends to the capacitance and these  $k$  values ( $k-x$ ) [9]. Taking into account the literature [9,36,42,44], the effect of gravity on cerebral blood circulation is considered by multiplying the supine value  $k-x_0$  in the aforementioned  $k-x$  parameters to a factor as written below:

$$k_x = k_{x0} \times (1 - \alpha \times \sin(\theta) + \beta \times P_{TW}) \quad (2.49)$$

where  $\alpha$  and  $\beta$  are parameters properly settled to adjust the output.

### 2.4.3 Flow Analysis

In order to analyze the flow in the head and neck network of the model, the following definitions of flow rate proposed by Zamboni et al [59] were used and adjusted with respect to the latest anatomical updates of the model published by Mohammadyari et al [22]. The hydraulic map of the model is illustrated in Figure 2.7. The head blood inflow (QHBin) indicates the amount

of blood entering the head through the vertebral artery (VA) and the two branches of common carotid (CC), that is the internal common carotid (IC) and external common carotid (EC).

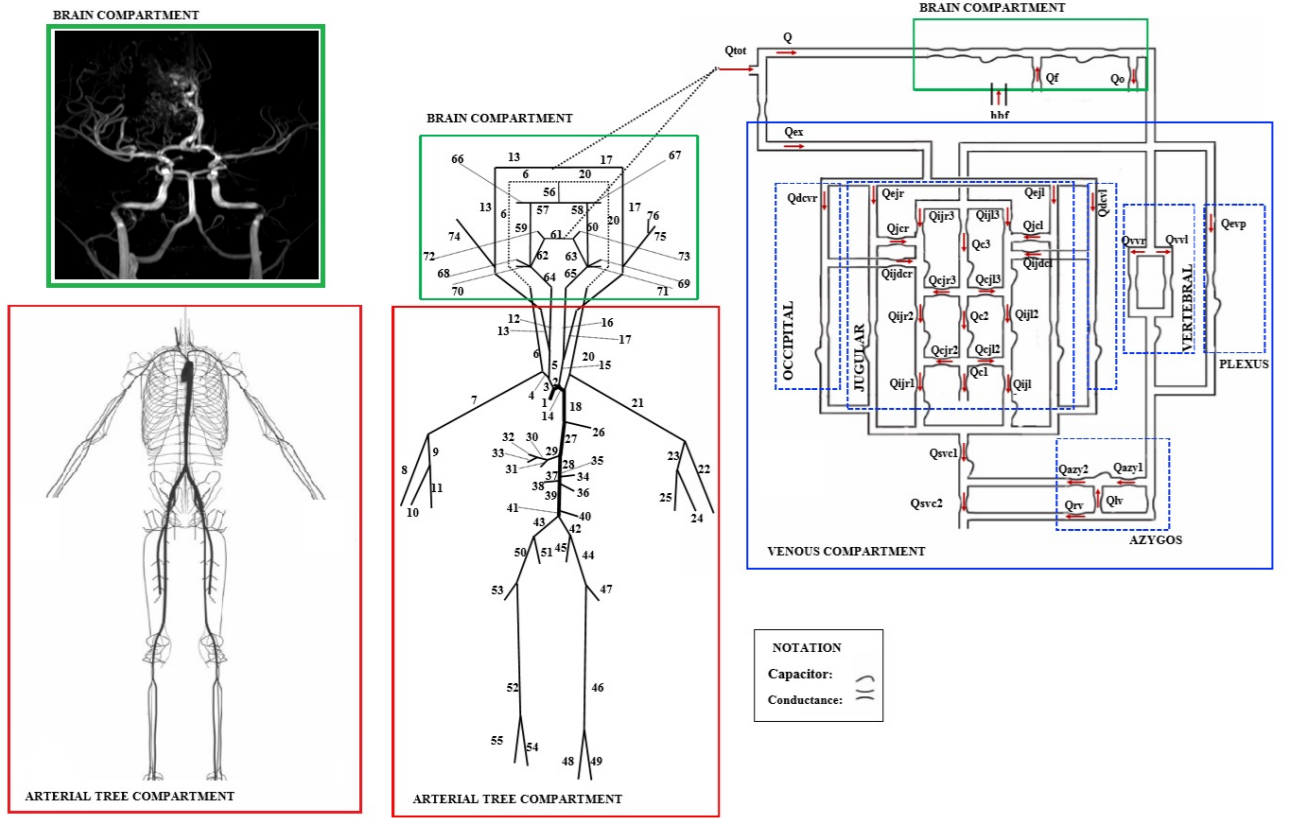


Figure 2.7: Simulated hydraulic map to model human circulation. Red boxes are the anatomy (left) and scheme (right) of the arterial tree. Green boxes are the anatomy (left) and scheme (middle) of the Willis circle tree, and the scheme of the intracranial 0D submodel (right). Blue box is the scheme (left) and anatomy (right) of the venous compartment

$$Q_{HBin} = \frac{Q_{CC} + (Q_{IC} + Q_{EC})}{2} + Q_{VA} \quad (2.50)$$

Cerebral blood flow ( $Q_{CBF}$ ) indicates the incoming flow into the Willis circle of brain compartment which supplies by IC and VA.

$$Q_{CBF} = Q_{IC} + Q_{VA} \quad (2.51)$$

The ECAs enter the facial and extracranial compartment and then are mainly drained by the temporal and facial veins to join external jugular vein (EJV) and the rest of neck venous network. The previous version of the venous network model [12,40] assumed that the ECA flow rate supplies the anastomosis network of the neck. Our latest published update allows us to change the previous assumption, by stating that all the extracranial inflow ( $Q_{Ex}$ ) is

supplying the deep cervical vein (DCV) and EJV (see the venous compartment scheme in the left blue box of Figure 2.7).

In addition to the drainage through the jugular system, collateral veins play an important role in blood redistribution. There are many other small and numerous channels arising from the skull base, such as occipital deep cervical and venous plexus veins and other anastomoses, that communicate with the lower jugular system and with the vertebral venous system [10,60]. In order to take into account the role of peripheral veins in our simulation, the collateral vein flow ( $Q_{cv}$ ) is defined as the summation of the blood flow in external jugular vein, internal venous plexus and occipital deep cervical veins [16,41].

Cerebral venous outflow ( $Q_{CVO}$ ) is the flow that originates from the intracranial compartment and is defined by the sum of IJVs-J3, vertebral veins (VVs) and the epidural veins (EDVs), including DCV and internal venous plexus vein (IVP)):

$$Q_{CVO} = Q_{J3} + Q_{VV} + Q_{EDV} \quad (2.52)$$

It is important to add the IVP because of the well-known role of this vein and VV as a main outstream pathway of blood from brain to superior vena cava (SVC) in the upright position, when the IJV is collapsed [22,59,61]. The head blood outflow ( $Q_{HBout}$ ) is equivalent to the sum of the flow of the IJV-J1, EJV, VV and EDV:

$$Q_{HBout} = Q_{J1} + Q_{VV} + Q_{EJV} + Q_{EDV} \quad (2.53)$$

In order to analyze the role of collateral vessels in head and neck drainage, the collateral-distal ( $Q_{C-D}$ ) and collateral-proximal flows ( $Q_{C-P}$ ) were defined as the outflows which directly goes into the brain and neck collaterals, respectively:

$$Q_{C-D} = Q_{CBF} - Q_{CVO} \quad (2.54)$$

$$Q_{C-P} = Q_{HBin} - Q_{HBout} \quad (2.55)$$

Collateral flow index (CFI) and delta cerebral venous outflow (DCVO) are the two factors that Zamboni et al [59] defined to examine the percentage of blood entering the head and the

normalized outflow difference:

$$CFI = \frac{Q_{C-P}}{Q_{HBin}} \times 100 \quad (2.56)$$

$$DCVO_{Upright} = [(Q_{HBout}/Q_{HBin})|_{Supine} - (Q_{HBout}/Q_{HBin})|_{Uprigh}] \times 100 \quad (2.57)$$

We also defined the  $DCVO|_{HDT}$  and  $DCVO|_{\mu G}$  to investigate the outflow differences during HDT and uG with respect to supine position, and the peripheral veins outflow index (PVI), which is equal to the percentage difference of blood that passes from the peripheral veins (except the IJV):

$$DCVO_{HDT} = [(Q_{HBout}/Q_{HBin})|_{Supine} - (Q_{HBout}/Q_{HBin})|_{HDT}] \times 100 \quad (2.58)$$

$$DCVO_{\mu G} = [(Q_{HBout}/Q_{HBin})|_{Supine} - (Q_{HBout}/Q_{HBin})|_{\mu G}] \times 100 \quad (2.59)$$

$$PVI = \left( \frac{Q_{HBout} - Q_{J3}}{Q_{HBout}} \right) \times 100 \quad (2.60)$$

With these equations we can study the posture change effects on the haemodynamic model from  $-10^\circ$  HDT to  $90^\circ$  HUT (upright). The model parameters have been taken from previous published article by Gadda et al [20,54].



## Chapter 3

### Experimental validation by Real Medical data

As we said in Chapter 2, the model requires to be validated according to experimental data and literature results, concerning aging, jugular stenosis, the effect of a posture change from head down tilt to supine and head up tilt, and microgravity effect. In particular, the extracranial venous circulation in humans is specifically adapted to the maintenance of any interrupt in head and neck blood circulation and prevents from brain damage. To study these particular subjects, we deal with some blood biomechanical and physiological parameter measurements on volunteers, using MRI and literature, to assess blood flow changes in the different age ranges and different head portions of the circulatory system and to provide a complete quantitative set for model validation.

To validate the model outcomes, we used supine average arterial and venous extracerebral blood flow obtained by using PC-MRI data. Ultrasound-based techniques and 2-dimensional (2D) phase-contrast (PC) MRI have been used previously to measure cerebral and cardiac vascular flow and velocities [5, 17, 21]. Ultrasound measurements, however, are operator dependent and limited by an inadequate acoustic window when measuring blood flow in cerebral vessels distal to the circle of Willis. Moreover, 2D PCMRI requires multiple scans with manual 2D plane placement perpendicular to the intracranial vessels of interest. Recently, the promising imaging modality to measure blood flow is 4-dimensional phase contrast magnetic resonance imaging (4D PC-MRI) [89, 90]. This technique provides the time-resolved full volumetric images instead of conventional 2D planes multiple scans. By that, 4D flow images offers the advantage of three-dimensional coverage of the vessels inside the selected field of view (FOV) over the time of one cardiac cycle in addition with ability in retrospective flow quantification at any vessel position within the imaging volume. Moreover, 4D flow MRI has been reported to

provide reliable flow assessment consistent with 2D PC-MRI for the measurement of pulsatile flow in cerebral arteries [5,90]. Hence, we decided to take advantage from 2D and 4D PC-MRI techniques to have the most reliable dataset concerning the model validation necessities.

Details including the patients selection procedures, MRI used techniques and data processing are reported in this Chapter. Two different data sets were acquired, one to analyse the age-related parameters and providing the paediatric hemodynamic model and the another one to evaluate asymmetric IJV stenosis by head rotation. Taking advantage of the MRI data helped us to improve the model anatomy map and physiology of the model.

## 3.1 Patients Selection Procedures

### 3.1.1 Study group I

Patient selection and MRI acquisition took place at the Sant Joan de Déu Hospital (Barcelona, Spain). Twenty-nine healthy volunteers participated in the study (Table3.1). Subjects were chosen among all the patients for whom a brain MRI had been requested. We considered only subjects with recognized normal neck and brain blood circulation that signed the informed consent to participate as a volunteer. The study was approved by the ethical committee of the hospital. The list of clinical characteristics of the volunteers can be seen in the Table3.1. Non of these pathologies interrupted the head and neck hemodynamic system. Therefore, those cases recognized healthy and eligible for our study by a radiologists.

### 3.1.2 Study group II

MRI acquisition was performed at the Radiology Department of the Sant Joan de Déu Hospital (Barcelona, Spain). Eight healthy volunteers (mean age  $19 \pm 6$  years) participated in the study. Table 3.2 reports the characteristics of the study group. Subjects were chosen among all the collaborative paediatric patients for whom a brain MRI had been requested and other young volunteers (between 18 and 23 years old). The imaging time was about 9 minutes per sequence (depending on the heart rate). Each subject underwent four MRI sequences: imaging of neck and brain with head in neutral orientation ,and imaging neck and brain with head in rotated position. The quite long duration of scanning time reduced the number of lower age volunteers. For this reason, we decided to enrol other subjects with age up to 23

Table 3.1: Characteristic of the enrolled subjects

Demographic characteristics	
Total number of subjects	29
Sex (females:males)	14:15
Age (years)	12 $\pm$ 5
Age range (years)	2–18
Weight (kg)	43 $\pm$ 15
Systolic blood pressure (mmHg)	114 $\pm$ 9
Heart rate (betas per min)	83 $\pm$ 16
Clinical characteristics	
Headache	10
Epilepsy	4
Cyst	2
Hearing loss	2
Down syndrome	1
Acondroplasia	1
Diplopia	1
Tremor	1
Vertigo	1
Encephalopathy (NBIA-PKAN mutation)	1
Unknown encephalopathy-genetic origin	2
Cavernoma	1
Psychosis	1
Control trauma	1

Data are given as absolute frequencies or mean  $\pm$  standard deviation.

years old, i.e. volunteers that could stay collaborative till the end of examination. The study was approved by the ethical committee of the hospital, and the informed consent were signed by participates or their parents in the case of children.

Table 3.2: Volunteers demographic characteristic

Demographic characteristics	
Total number of subjects (4D-flow :2D-flow )	8 (6:2)
Sex (females:males)	3:5
Average Age (years)	19 $\pm$ 6
Age range (years)	9–23
Weight (kg)	54 $\pm$ 11
Average Hight (cm)	156 $\pm$ 11
Average BMI (kg/m2)	22 $\pm$ 3
Heart rate before rotation (beats per min)	77 $\pm$ 10
Heart rate after rotation (beats per min)	73 $\pm$ 9

Data are given as absolute frequencies or mean  $\pm$  standard deviation.

## 3.2 MRI protocols

Cardiovascular magnetic resonance imaging (MRI) is an essential tool in the diagnosis, monitoring, and treatment of cardiac diseases, and has the potential of evaluating both anatomy and function of the cardiovascular system [87, 88]. Traditionally, MRI imaging of flow is accomplished using methods that resolve two spatial dimensions (two-dimensional) in individual slices. Standard two-dimensional (2D) phase-contrast (PC) MRI was introduced in the late 1980s to enable through-plane assessment of blood flow fields and velocities, particularly in the cardiovascular system. The 4D flow MRI was introduced in the 1990s [87]. Since then, the development of in-plane phase-contrast sequences has allowed acquisition of a time-resolved cine sequence amenable to three-dimensional (3D) velocity encoding, a technique known as four dimensional (4D) (3D plus time) flow MRI. Although . In addition to providing the basic phase-contrast findings such as peak velocity, flow volume, and flow direction, 4D flow MRI delivers unprecedented capabilities for comprehensive blood flow assessment, offering various modalities of blood flow pathway visualization and thereby helping one understand blood flow changes and retrospectively perform accurate flow measurements [88]. 4D flow MRI technique permits the volumetric assessment of blood flow in the entire vasculature of interest and enables the volumetric quantification and retrospective analysis of blood flow in any arbitrary angle, which is not possible with conventional 2D PC-MRI. 2D PC-MR images are acquired with single-direction (through-plane) velocity encoding during a breath hold. When flow must be measured at several sites, the acquisition must be repeated at each site, taking care to position the acquisition plane perpendicular to the long axis of the vessel of interest, a technically challenging and time-consuming process that may also be difficult for patients, particularly those with complex drainage [91]. Whereas the standard 2D PC sequence provides an image with a single velocity and magnitude, 4D flow PC-MRI provides sets of 3D volumes over time. Each 4D volume contains one magnitude volume and three velocity volumes encoded in the three dimensions of space. The visualization of 4D PC-MRI data using vector field, streamline, pathline, isosurface, and volume rendering has been effective in identifying the abnormal alteration of blood flow in various vessels, such as the aorta, carotid arteries, and cerebral vessels. Volumetric acquisition of the blood flow also enables better visualization and quantification of the complex nature of intracardiac blood flow [88]. 4D PC-MRI provides not only the conventional flow quantifications, but also various fluid dynamic biomarkers with potential clinical utility, such as wall shear stress (WSS), pressure gradient (21-23) and pulse wave velocity [90, 92].

### 3.2.1 2D-Flow PC-MRI technique

The volunteers were imaged using a 3-T scanner (Ingenia, Philips, Amsterdam, Netherlands) with a 32-channel head coil. Phase-contrast sequences were used to collect 2D quantitative flow images of the neck at the vertebral level C2/C3 (J3), C5/C6 (J2), and at the brain level including the Willis circle and Sylvian aqueduct, with the subject in the supine position. The common technical parameters of the sequences were presented in Table 3.3. Acquisitions were synchronized with the electrocardiogram of the scanned volunteer. We used phase images to extract data such as flow rate and pressure, and magnitude images to check the anatomy and improve the anatomic map of the model. Two ranges of velocity encoding were tested in three subjects to improve the image quality and avoid aliasing effects. After this test, we chose the velocity encoding of 60 and 120 cm/s for veins and arteries, respectively. The MRI were performed at the level of C2/C3 and C5/C6 of neck vertebrae. Seven sequences were performed for each subject (Table ??). As it can be seen in figure 3.2 Resulting images were named by vein or artery at a specified anatomic location. Also, MR images of the neck vessels obtained from a subjects of Group II at the two neck orientations are shown in Figure 3.1.

Table 3.3: 2D-MR imaging parameters.

parameters	Value
Flip angle	15°
TR (ms)	9.1
TE (ms)	5.4
Slice thickness (mm)	4
Frame rate (fps)	15
Reconstruction Voxel size AP (mm <sup>2</sup> )	0.6×0.6
Field of view (mm <sup>3</sup> )	150×150
In-plane spatial resolution (mm <sup>2</sup> )	1

### 3.2.2 4D-Flow PC-MRI technique

The same MR scanner were used to acquired the images. Phase-contrast sequences were used to collect 4D quantitative flow images. The imaging anatomical volume includes neck at the vertebral volume level C2/C5 (J3 and J2) and brain including the Willis circle and occipital veins (sagittal sinus, straight sinus and transvers sinus). The imaging parameters were reported in Table 3.4. All subjects were first asked to stand in the supine with neutral head orientation and then to rotate the head left up to the maximum capability (about 80°).

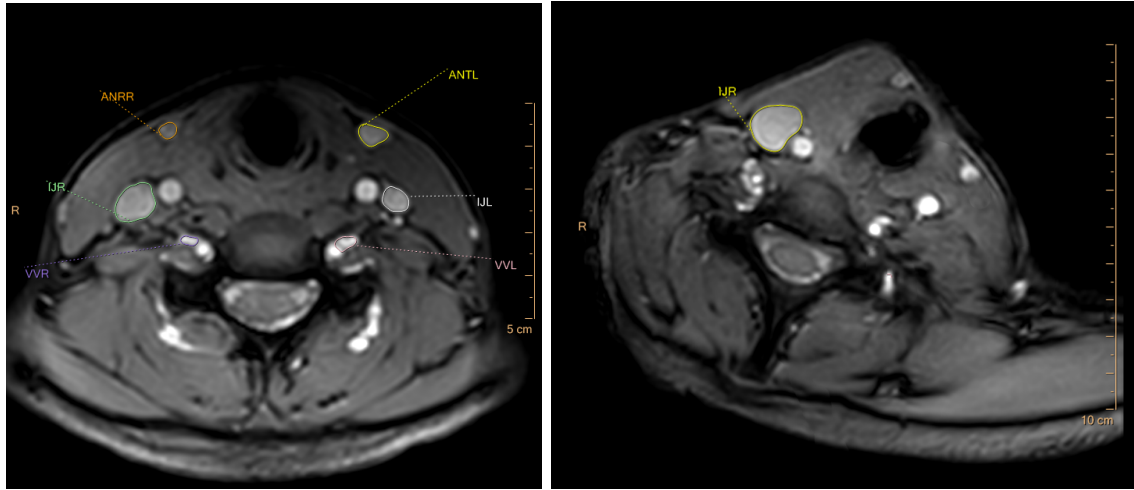


Figure 3.1: 2D-flow PC-MRI of the neck vessels at the vertebral level C5/C6 (J2) in neutral (left) and rotated (right) position.

Acquisitions were synchronized with the real time electrocardiogram of the subject.

Table 3.4: 4D-MR imaging parameters.

parameters	Value
Velocity Encoding (cm/s)	50
Flip angle	7°
TR (ms)	5.0
TE (ms)	3.2
Frame rate (fps)	28
Reconstruction Voxel size (mm <sup>3</sup> )	0.9×0.9×1.3
Field of view (mm <sup>3</sup> )	170× 170 × 50
Average Scan time (min)	9

The vessels considered in this study are the common carotid artery (CCA) and internal carotid artery (ICA), vertebral artery (VA), IJV and vertebral veins (VV). These vessels are known as the main neck drainers. The velocity encoding must be chosen carefully to avoid the velocity aliasing defects. For this reason, two velocity encoding of 70 and 50 cm/s were tested in two subjects to improve the image quality. After this test, and since only one velocity is required to set the MRI sequence, velocity encoding of 50 cm/s was chosen.

In the 75% of the selected volunteers, the MR scan prescribed for clinical reasons was short enough to allow for an extra time acquisition to perform 4D flow examination. Since the 4D flow MRI has been reported to provide compatible flow assessment with 2D-flow PC-MRI [5], the former sequence were performed in the 25% of volunteers not allowed to 4D flow. Such 2D sequence was already tested and validated for this purposes in a recent published study [22].

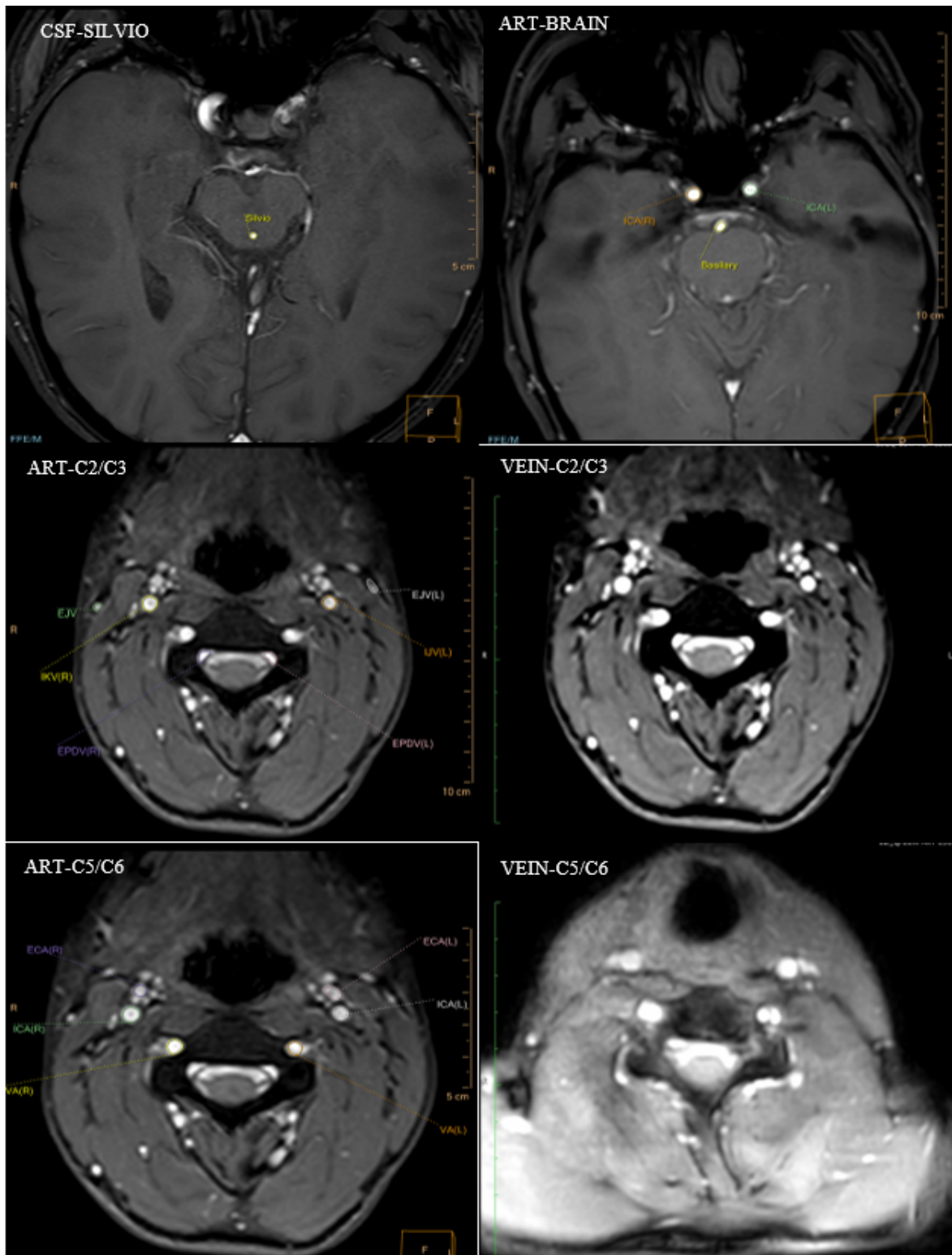


Figure 3.2: The 2D PC-MR Images acquired from one of the volunteers.

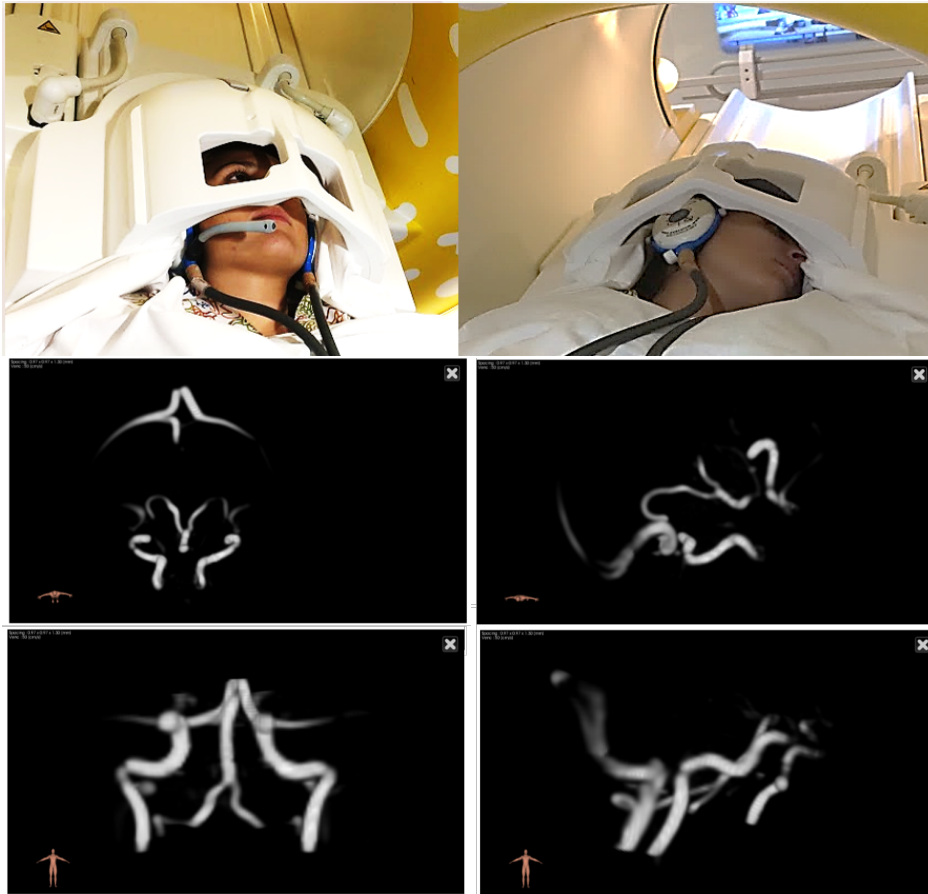


Figure 3.3: The 4D PC-MR Images acquired from one of the volunteers.

The duration of the 2D-flow sequence was about half of the 4D sequence.

### 3.3 MRI data processing

#### 3.3.1 2D-flow PC-MRI data

We measured the flow rate at different vessels (vessels with flow rate less than 0.05 mL/s were eliminated from the study because of the low signal-to-noise ratio). Regions of interest (ROIs) were drawn manually on all the vessels on each sequence and then cross-sectional area of the vessels, blood flow, velocity, delay time, and pressure gradients were extracted by the Philips software (Philips IntelliSpace Portal, version 10). Blood flow was calculated by multiplying the mean velocity by the cross-sectional area of the region of interest, while pressure gradient was calculated by using the modified Bernoulli equation ( $\Delta P = 4V_p^2$ ), where  $V_p$  is the peak velocity of blood [63]. After drawing the regions of interest on all the 15 frames acquired at each anatomical plane, the software calculated all the parameters. If the signal intensity was low (mostly in the temporal veins), the software did not calculate the pressure gradient.

In other words, we eliminated from the study all the vessels with flow rate less than 0.05 mL/s because of the low signal-to-noise ratio. Otherwise, resolution was enough to include the acquired data in the dataset.

### 3.3.2 4D-flow PC-MRI data

The 4D image series were analysed by using the Pie Medical imaging software (CAAS MR Solutions, Pie Medical Imaging B.V., version 5.1). Besides the anatomical information, physiological parameters were obtained such as vessels blood volume, flow rate and CSA at the considered vessels. After importing the image series, ROIs were manually drawn on all the vessels during systole with the maximum flow rate [90,91]. Then, the 3D image reconstruction command were applied and the software extrapolated the segmentation to the all 37 frames. Cross-sectional area of the vessels, blood flow rate and velocity were automatically calculated by the software.

4D PC-MRI and the Pie medical imaging software provide the data and functionality to visualize WSS in a 3D segmented model of the vessel of interest [90,92]. WSS by definition is the frictional shearing force on the vessel walls. To perform the 3D segmentation, the vessels centreline selection and plane by plane vessel lumen segmentation need to be performed manually along the vessel length. Then, WSS is calculated by multiplying the viscosity of the fluid (4 mPa.s for blood) by the local velocity gradient at the wall [89,92]. The quantitative values of WSS is shown along the vessel in the colour coded spectrum. The colour bar is adjusted to the maximum value of the WSS [90,92].

The last information that we could extract indirectly by the software was measuring the flow rate change over the length of IJVs before and after head rotation. In this regards, the flow rate was measured along the length of IJV at maximum ten points with the same distance from each other. The distances were measured and recorded for each subject. The measurement were repeated for all IJVs in neutral and rotated head position.



# Chapter 4

## Results and discussion

In this chapter, the results are explained in three different sections in which clinical or research applications for the model are discussed. In this work, three main projects were performed as explained in chapter 1 and 2. The first section refers to the built paediatric model results. The model was updated to simulate the aging effects on the hemodynamic physiology to calculate the paediatric blood circulation at the level of head and neck. Paediatric results were compared with results of the adult version of the model [22]. In the second section, the head rotation effects on head and neck hemodynamic in imposing the asymmetric non-invasive IJV stenosis were explained. The results of the MRI study were compared with simulation. In the third section, the results of imposing human body to different gravity fields and the effects on the blood circulation system were discussed. At last, the limitations that we were faced with during performing my projects are explained.

All variables were expressed in terms of mean  $\pm$  standard deviation (mean  $\pm$  SD) or the percentile. RStudio software (version 1.3.959, Boston, USA) was used for statistical analysis. Significance between two different settings was determined using the t-test. The effect of head rotation on flow parameters gradient with P-value  $< 0.05$  was considered as statistically significant difference.

### 4.1 Paediatric Hemodynamic Model: Aging study

Based on a well-developed mathematical model for the simulation of blood circulation in adult humans [20], the present model has been tuned with respect to paediatric physiological parameters (average age 12 years, supine position). Paediatric hemodynamic circulation was

modelled for the first time by using a parameter model consisting of a 0-D and 1-D algorithm. The previous well-described model was adjusted in accordance to the differences between paediatric and adult subjects. The model is able to compute blood pressures and flow rates in accordance to the collected phase-contrast MRI data and literature. Moreover, it has the potential to simulate pathological conditions due to aging.

#### 4.1.1 Arterial adjustments results

The pressure pulse wave of Figure 2.5, together with the contribution of the respiratory pulse are the input to the model. As shown in Figure 4.1, the simulated pressure in the ascending aorta was 114/65 mmHg, in accordance with the paediatric cardiopulmonary care guide [76]. Figure 4.1 also reports the pressure pulse in the intracranial artery, extracranial artery, vertebral artery, and facial arteries calculated by the model.

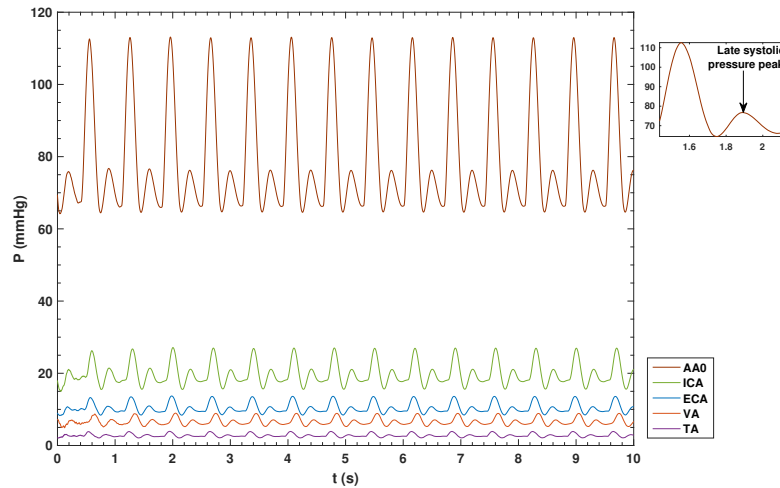


Figure 4.1: Cardiac and arterial pressure waveforms. The inset shows the zoom of one cardiac cycle. AAO Ascending aorta, ECA Extracranial artery, ICA Intracranial artery, FA Facial artery, VA Vertebral artery

The backward wave from ascending aorta to heart generate the late systolic or early diastolic pressure peak [1, 62]. This late pulse can be seen in Figure 4.1. Moreover, the blood flows from the heart to the vessels and is divided among many branches. This must correspond to a change in the venous pressure. We can see from Figure 4.1 that the model properly simulates both decrease in pressure amplitudes and mean values in the following order: ascending aorta > intracranial artery > extracranial artery > facial arteries [1, 16].

In 2017, Cattermole et al. [81] reported a measured values of ascending aorta pressure of 80.7 mmHg (range 65.3 to 103.7 mmHg) in the same age range as this study (see Figure 4.1).

my simulated pressure in the intracranial artery ( $22 \pm 4$  mmHg, mean  $\pm$  SD, age range 2 to 18 year-old) follows the trend of the data reported in literature (age range 20 to 60 year-old and older), where blood pressure in intracranial artery increases with age. Indeed, on 2006 Hirata et al. [82] investigated blood velocity and pressure in intracranial artery and reported a mean value of  $29.3 \pm 6.4$  mmHg (mean  $\pm$  SD) for the age range from 20 to 40 years,  $35.9 \pm 8.0$  mmHg (mean  $\pm$  SD) from 40 to 60 years and higher values for higher ages.

Figure 4.2 compares the simulated intracranial artery pressure and venous sinus pressure in paediatric subjects and adults. It can be seen that the mean pressure values were less in lower age. Indeed, the mean values of intracranial artery pressure are  $5.6 \pm 0.2$  (mean  $\pm$  SD) and  $8.3 \pm 0.8$  mmHg (mean  $\pm$  SD), while the mean values of venous sinus pressure are  $4.9 \pm 0.6$  and  $5.9 \pm 1.0$  mmHg in paediatric subjects and adults, respectively. Moreover, We see that intracranial artery pressure was lower than venous sinus pressure. Hence, the simulated intracranial artery pressure and venous sinus pressure values were in agreement with the literature. The normal range of intracranial artery pressure was variable between 3 to 7 mmHg for paediatric subjects and less than 10 to 15 mmHg for adults [65, 66].

#### 4.1.2 Venous adjustments results

The venous part of the model was adjusted to simulate the main blood pathways from the brain. In the majority of individuals, IJVs are the main pathway and the flow at each segment (J1, J2, and J3) is more than that of vertebral veins or internal venous plexus flow [21, 66]. In this work, we refer to the flow rate in VV and DCV as summation of the left and right veins due to the low value of them.

Due to regulation between arterial and venous compartment, the CBF is calculated on the base of arterial out put. The intracranial flow rate is calculated by the summation of ICA left and right and basilar arteries [5]. Moreover, total blood flow is the flow rate at the level of neck arteries that supplies the intracranial and extracranial subsystems [20, 21]. Figure 4.3 shows the amount of the simulated flow rates at rest, and makes a comparison between paediatric and adult flow rates. There was good agreement between model response and paediatric MRI flow data. Moreover, flow rates were higher in paediatric rather than adult subjects, as expected.

The CBV increases rapidly from early childhood to preschool age up to 6 years, and then

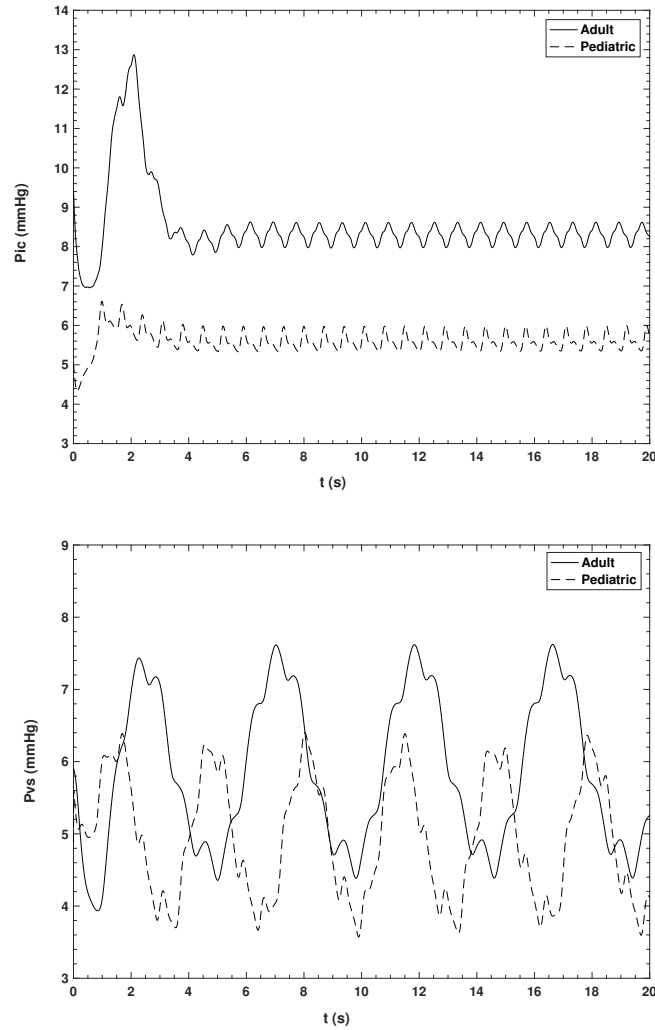


Figure 4.2: Comparison between intracranial (Pic) and venous sinus (Pvs) pulse in paediatric (dashed line) and adult (solid line)

continuously decreases till adulthood [5, 84]. Moses et al. reported a normalized different value of  $10.6 \pm 5.2$  mL/100mL/min between the mean age of 12 years and adults (mean age of 22 years) [84]. Wu et al. reported a blood flow reduction rate of about 48% from the age of 12 to 40 years [5]. According to Figure 4.3, the average inflow toward head and brain are 18.7 mL/s and 13.4 mL/s that is a 34% and 24% augmentation in paediatric rather than adult subjects. These values are within the range of previous reports [5, 30, 84]. Additionally, we can see from Figure 4.3 the asymmetric behaviour of the cerebral venous drainage. Indeed, the right side flow rate is about 10% more than the left, as reported by the literature [21, 65, 66, 83].

Figures from 4.4a to 4.4f show how the model simulates the pressure and flow rate both in paediatric (dashed line) and adult (solid line) setting in IJV and vertebral veins. Figures from 4.4g to 4.4i compares the simulated flow waveforms in IJV and VV against PC-MRI data. In this figure, the simulation of respiratory rate and so the effects on modelled flow

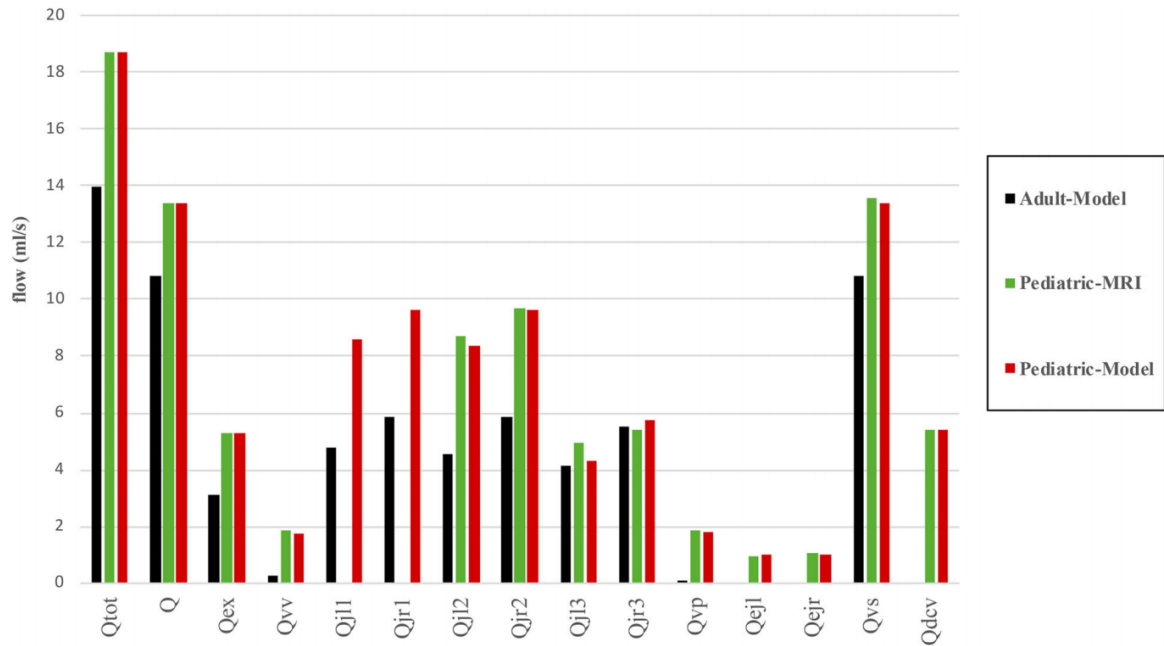


Figure 4.3: Comparison of simulated paediatric and adult flow rates, and paediatric experimental data. Q Cerebral blood flow, dcv Deep cervical vein, ejl Left external jugular vein, ejr Right external jugular vein, Qex Extracerebral blood flow, jl1 Lower segment of the left jugular vein, jl2 Middle segment of the left jugular vein, jl3 Upper segment of the left jugular vein, jr1 Lower segment of the right jugular vein, jr2 Middle segment of the right jugular vein, jr3 Upper segment of the right jugular vein, Qtot Blood flow to the head, vp Venous plexus, vs Venous sinus, vv Vertebral vein

rate was eliminated in order to make a comparison with phase-contrast data of one cardiac cycle. In order to quantify the agreement shown by Figures from 4.4g to 4.4i, the time-averaged difference between simulated (dashed line) and measured (dotted line) flow rates were calculated, during the reported cardiac cycle, for left J3, left J2 and vertebral vein. Such time-averaged difference was  $1.1 \pm 0.3$  mL/s (mean  $\pm$  SD),  $3.7 \pm 0.1$  mL/s (mean  $\pm$  SD), and  $0.3 \pm 0.2$  mL/s (mean  $\pm$  SD), respectively.

The mean value of central venous pressure and EJV pressure in adults were studied by Leonard et al. [83]. They stated that mean EJV pressure is slightly higher than IJV pressure. They measured  $8.3 \pm 2.6$  mmHg (mean  $\pm$  SD) for IJV and  $8.6 \pm 2.8$  mmHg (mean  $\pm$  SD) for EJV in adults with a mean age of 66 years. As depicted in Figure 4.4, mean IJV pressure in all three sections and vertebral vein pressure were  $4.7 \pm 0.8$  mmHg (mean  $\pm$  SD) and  $4.8 \pm 0.7$  mmHg (mean  $\pm$  SD) in paediatric subjects, and  $5.6 \pm 1.1$  mmHg (mean  $\pm$  SD) and  $5.8 \pm 0.7$  mmHg (mean  $\pm$  SD) in adults, respectively, showing that the model results are quite satisfactory. However, there is the need of more paediatric measurement at the IJV level and peripheral veins in order to produce a model with more details.

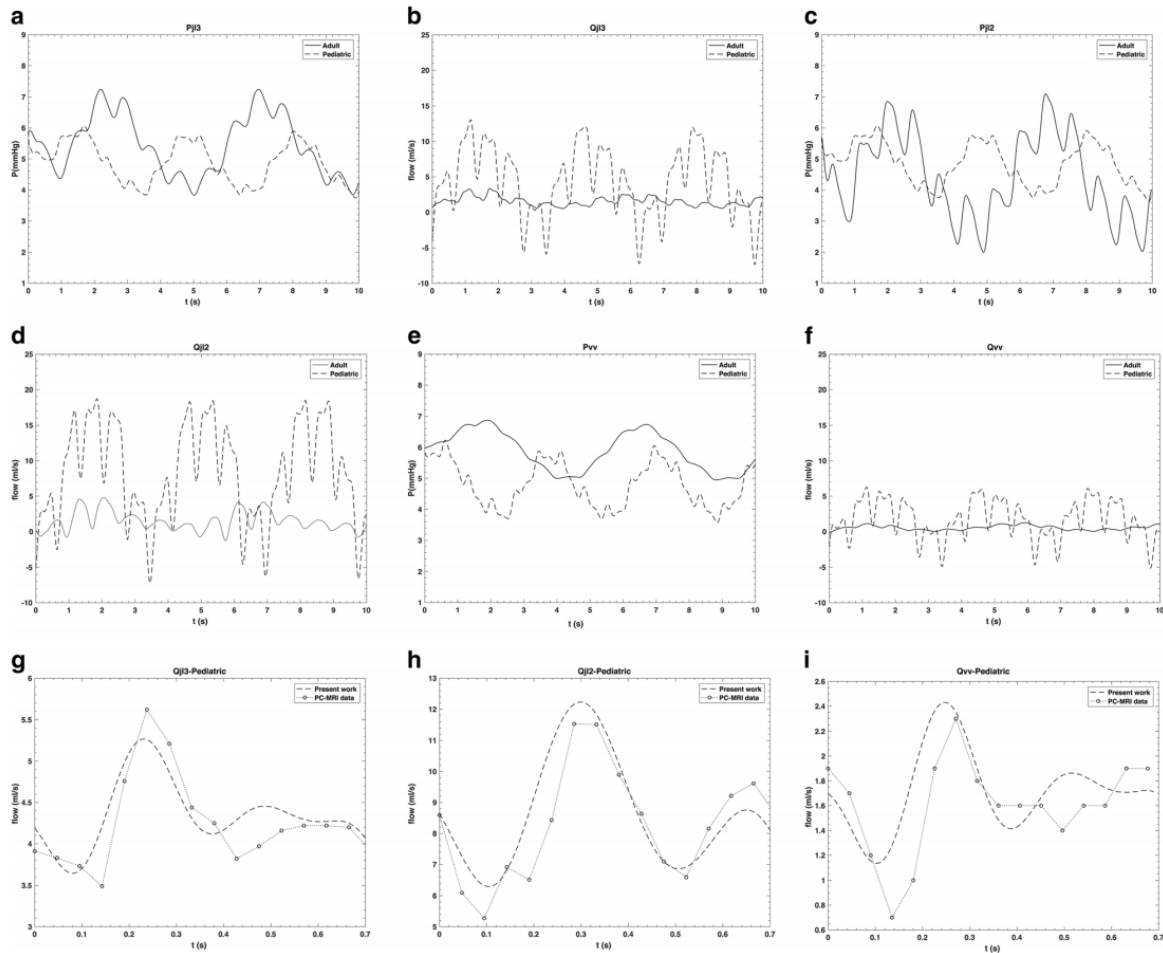


Figure 4.4: Comparison between intracranial (Pic) and venous sinus (Pvs) pulse in paediatric (dashed line) and adult (solid line)

Results reported in Figure 4.4 from 4.4a to 4.4f were satisfactory because the simulated pressure values were higher in adult than paediatric subjects, while flow rates were lower [5,84]. Figure 4.4g, 4.4h, and 4.4i represent a comparison between the simulated and measured flow rates in J3, J2 and vertebral vein as an example of the accuracy of my paediatric model. The correlation value between the simulated and PC-MRI data was 88%. The positive value of all the calculated time-averaged differences between simulated and measured flow rates means that, in the investigated anatomical regions, the mathematical model slightly overestimates the flow rate. The low SDs are index of good agreement between simulated and measured flow rates. As previously reported in literature [80], there is interest in properly simulate flow rate and pressure waveforms to discriminate between physiologic and pathologic subjects. The present model is able to simulate such waveforms for a paediatric setting.

## 4.2 Asymmetric IJV stenosis study: Head Rotation

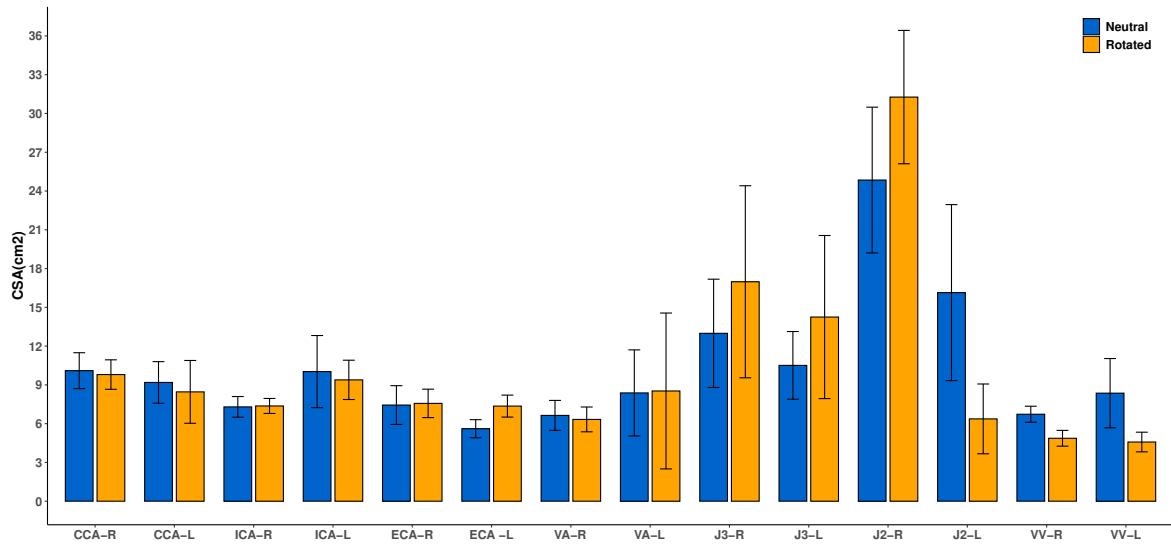
In this study, we were able to visualise the CCAs, VAs, IJVs and VVs with MRI at the neck of all subjects in neutral position. However, after head rotation and depending on inter-individual characteristics, some veins like left IJV and VV appear absent, probably due to low blood flow and small vessel size.

All the study cases had jugular dominant drainage and no cases with complex venous drainage network. Of the 8 patients we examined four subjects (50%) were right jugular dominant, two (25%) were left jugular dominant, and two (25%) were codominant. The distribution of mean CSA values for both head position were reported in Figure 4.5a. Significant differences between the IJV-CSAs before and after head rotation were observed. CSA at left j2 decreased of 9.8 cm<sup>2</sup> (61%) while right j2, right and left j3 were expanded of 6.4 cm<sup>2</sup> (26%), 4.0 cm<sup>2</sup> (31%) and 3.7 cm<sup>2</sup> (36%), respectively. The mean flow rate for both head positions were reported in Figure 4.5b. Partially and fully left IJV collapsing were seen equally, each in 38% of my volunteers. Moreover, the average flow rate gradient due to the rotation shows significant decreases in  $\Delta Q_{CBF} = 2.1$  ml/s (26%),  $\Delta Q_{vs} = 4.0$  ml/s (63%) and  $\Delta Q_{jl2} = 2.1$  ml/s (53%). Flow rate change showed significant increased in  $\Delta Q_{jr2} = 1.9$  ml/s (47%) and  $\Delta Q_{jr3} = 1.2$  ml/s (36%) with  $P < 0.05$ . There were no other statistically significant changes in flow rate for any other vessels at any position.

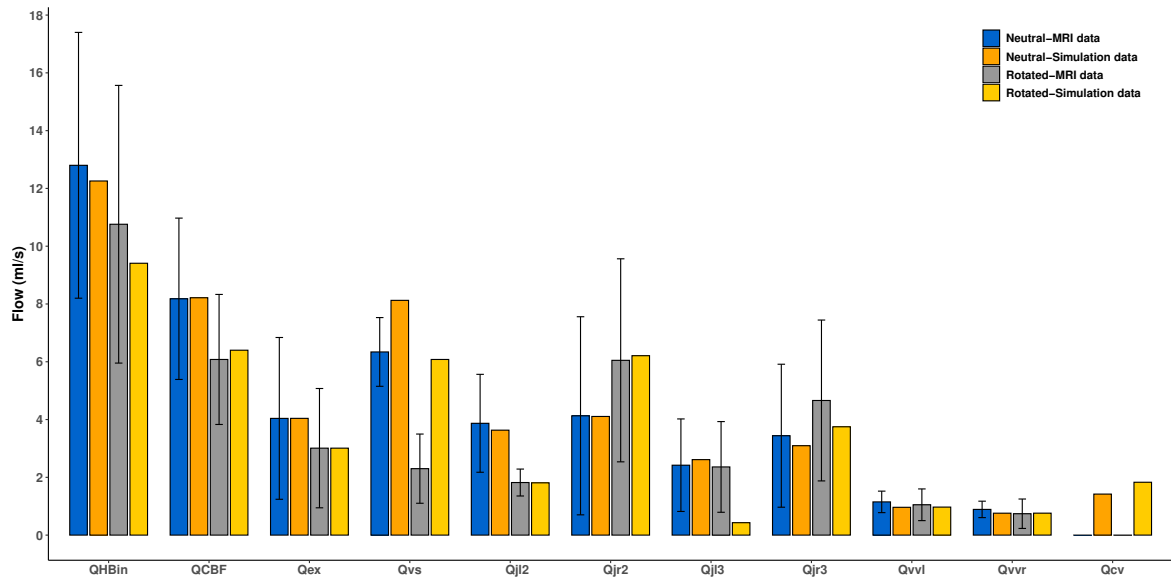
The standard deviation in error bars for measured and simulated data are presented in Figure 4.5.b. Neutral MRI data and neutral simulation data showed a correlation of 0.98 ( $P < 0.0005$ ) and rotated MRI data and rotated simulation data showed 0.87 ( $P < 0.0005$ ) that indicates a strong relationship between simulated and experimental data.

Our study confirmed that turning head to left side causes obstruction in the ipsilateral IJV by decreasing the effective CSA at the middle segment of left IJV (j2). As reported in Figure 4.5, due to the torsion-compression force the mean CSA and flow rate in left j2 reduced significantly about 61% and 53% in left j2, respectively with respect to neutral head orientation values.

Figure 4.6 shows the flow rate change over the IJV vessel length before and after the rotation for three different neck-drainage type. Case #1 has a codominant jugular drainage, while the case #2 and #3 have a right and left dominant jugular drainage, respectively. In case #1 and #2, flow rate in the right jugular increased as a compensatory response to the head rotation. In



(a)



(b)

Figure 4.5: a) CSA Comparison for both neutral and rotated head position including the standard deviation in error bars on the MRI extracted data. b) Comparison of measured and simulated cycle-averaged flow rates for both neutral and rotated orientation.

case #3, right jugular was not as functional as left jugular. However, this case showed a slight increase in the left jugular flow rate at the upper segment (j13), a decrease at the j12 level and decrease in overall flow rate. Left jugular flow rate in case #2 dropped down to zero value because the IJV was fully collapsed and absent in the MRI measurement platform, while in case #1 it remained almost unchanged. Cases with the same neck-drainage type showed the same results.

Regarding the compensatory act of human body, three main differences induced by head

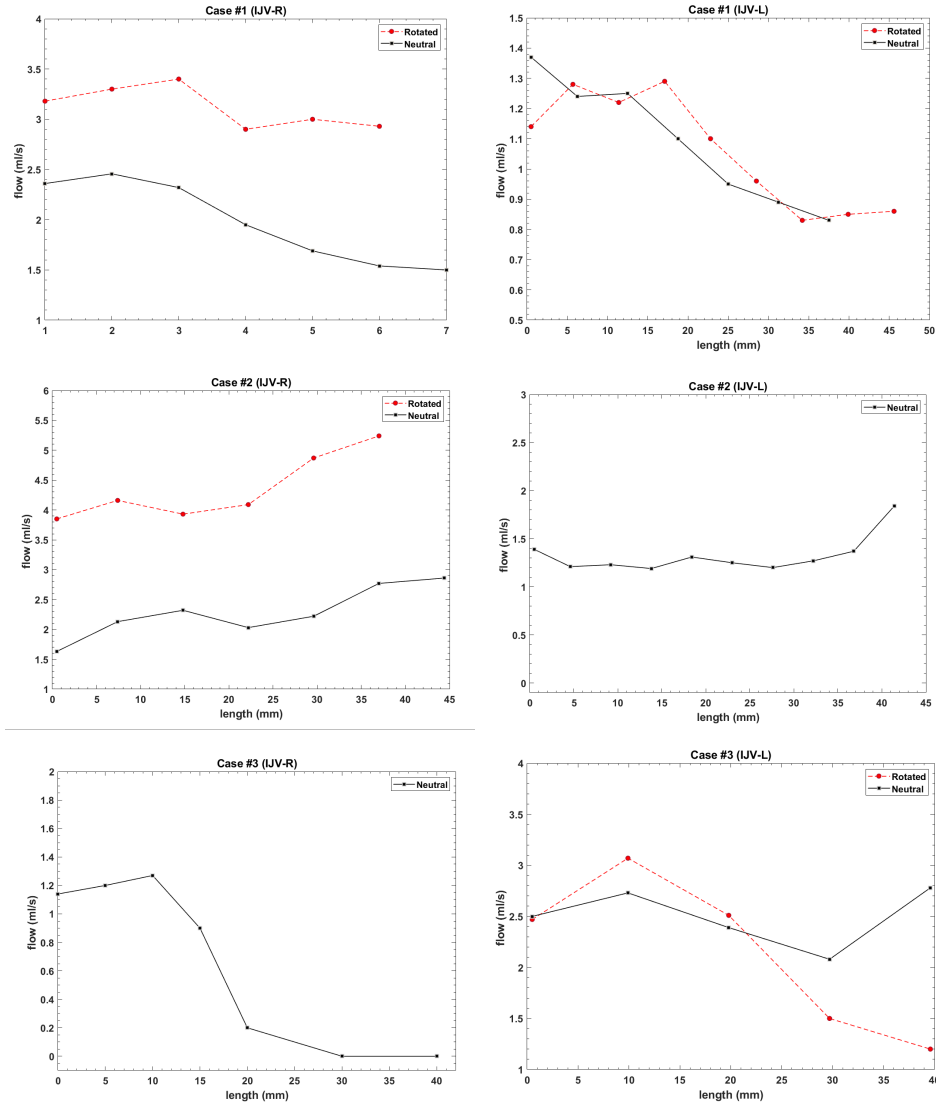


Figure 4.6: Measured flow rate change over the length of left and right IJV for both neutral (black line) and rotated (red dashed line) head position for all of the 4D PC-MRI cases. Flow in Case#2 IJV-L and Case#3 IJV-R subplots are not reported because the IJV is fully collapsed and absent in the MRI measurement platform.

rotation were recorded: first a slight mean heart rate value reduction about  $4 \pm 14$  bpm (5%) (see Table 3.2). Second a significant intracranial inflow (QCBF) and outflow (Q<sub>vs</sub>) reduction about 26% and 63%, respectively while the total blood volume remained almost unchanged (see Figure 4.5.b). Third, an asymmetric flow rate change between the right and left side transverse sinus and IJV according to the interindividual characteristic (see Figure 4.6 and 4.7). Overall right IJV flow rate increased significantly about 47% and 36% ( $P < 0.05$ ). These findings corresponded to what has been reported previously as explained in the following.

Hojlund et al in 2012 measured the effects of posture change from supine to prone on heart rate, mean arterial blood pressure and bilateral IJV diameter [93]. They reported a reduction in heart rate and increase in blood pressure and IJV diameter. Hence, the slight reduction in

measured heart rate in my study is in agreement with Hojlund et al findings. Watson et al in 1974 and Farina et al in 2013 stated that the head rotation to one side causes occlusion of the ipsilateral IJV and affect the intracranial venous flow rate in children [10,94]. Gwak et al in 2009 measured the IJV-CSA in infants and children. They reported that as the head was rotated, the right IJV-CSA was significantly larger (about 44% at 80° head rotation) with respect to the neutral position [85]. These findings shows good agreement with what we reported in result section, right IJV reduction ( $j_2 = 26\%$ ,  $j_3 = 31\%$ ).

Glor et al in 2004 measured the influence of the head leftward rotation on carotid hemodynamic in young adults [95]. They reported no remarkable change in CA-CSA and flow rate due to head rotation. Similarly, Lorchirachoonku in 2012 reported that left and right CAs were similar in size and were not affected by head rotation [96]. Aristokleous et al in 2015 measured the hemodynamic alteration in VAs and reported no statistically significant difference in VA-CSA [97]. Thomas et al in 2014 reported that the total cerebral inflow was not significantly affected by rotation in either direction. The same results were achieved by my simulation model in which the main and collateral veins are both included [98]. According to my measurements, the total cerebral blood inflow and outflow gradients with respect to the neutral position were considered significant ( $P < 0.05$ ). However, the total neck inflow and outflow change ( $P = 0.1$ ) is not meaningful. By that, my results approve the literature findings that the total neck blood flow remains unchanged after leftward head rotation, while the cerebral blood flow decreased.

Moreover, the collateral veins blood flow ( $Q_{cv}$ ) calculated by my model shows 36% increase in flow rate with respect to the neutral head orientation in order to compensate the cerebral outflow reduction. Therefore, collaterals impact explains the reason that compression of one jugular vein has no significant impact on the overall head and neck blood flow [62,93].

Glor et al stated that WSS changed significantly with head rotation, but the variations were very subject dependent. In accordance, results of this study highlighted the impact of the dependency of WSS distribution on the morphological and vascular anatomical characteristic [95].

Figure4.7 shows the WSS dependency to head orientation and vasculature functionality. Comparison of the WSS distributions show that the wall stress of left IJV decreases despite a significant increase in the right IJV wall stress. As it can be seen in Figure4.7 case #1, leftward head rotation caused decrease in the left jugular WSS while increased the right jugular WSS.

In the case #2, WSS did not show significant changes in the right jugular while the left jugular WSS increased slightly. In the case #3, the left jugular were the dominant veins which after rotation the flow in right IJV and left j2 decreased dramatically (collapsed fully) while the shear stress on the left j3 wall increased. Figure4.7 represents the WSS distribution in sigmoid sinus and upper part of j3 for the first and third cases. The jugular codominant cases showed almost the same WSS distribution as the right jugular dominant drainers. Due to the impact of head rotation in case #1 and #2, blood flow passing the left transverse and sigmoid sinus decreased dramatically which contributes to an increase in flow and WSS of right j3. In case #3, the result is opposite, right transverse sinus was absent partially before and fully after rotation. Comparing the WSS distribution before and after rotation shows the wall stress increased in left transverse sinus.

The main topic in Figure4.6 and 4.7 beside evaluating the flow rate and WSS change over the vein length is to categorize such changes into three subgroups according to the interindividual drainage characteristics. In the intracranial compartment investigation, after turning the head, blood flow was decreased significantly at one or both transverse sinuses. In the cases of fully collapsed left IJV, left transverse sinus disappeared (see Figure4.7.b case #1; case #2 showed similar results). According to my findings, jugular vein obstruction on the side of the dominant venous drainage could result in severely limited neck venous drainage (case #3). Figure4.7.b shows how the right IJV and consequently right transverse sinus are affected, while the blood flow and WSS in left transverse sinus increased. Therefore, my findings confirmed what reported in previous literature about the strong relationship of extracranial hemodynamic alteration on intracranial physiological parameters [59].

After the analysis of all the data extracted from MRI, we properly tuned the model in order to simulate the flow rate mean values and their variations due to leftward head rotation. Since the brain compartments pressure are critical parameters to monitor in brain trauma cases, the simulated pressure values were computed and represented in Figure4.10. Indeed, these values are the indirect indicators of hemodynamic alteration physiology. Results show that the head rotation increased the intracranial pressure by 2 mmHg (20%), and decreased the venous sinus and IJV pressure almost the same by 1.4 mmHg (32%). Note worthy, the model was tuned based on the average data consider generally the jugular dominant condition in which the right IJV has more flow rate at all three segments [20, 22].

Finally, as reported in Figure 4.10, my mathematical model calculates a 20% in ICP, that

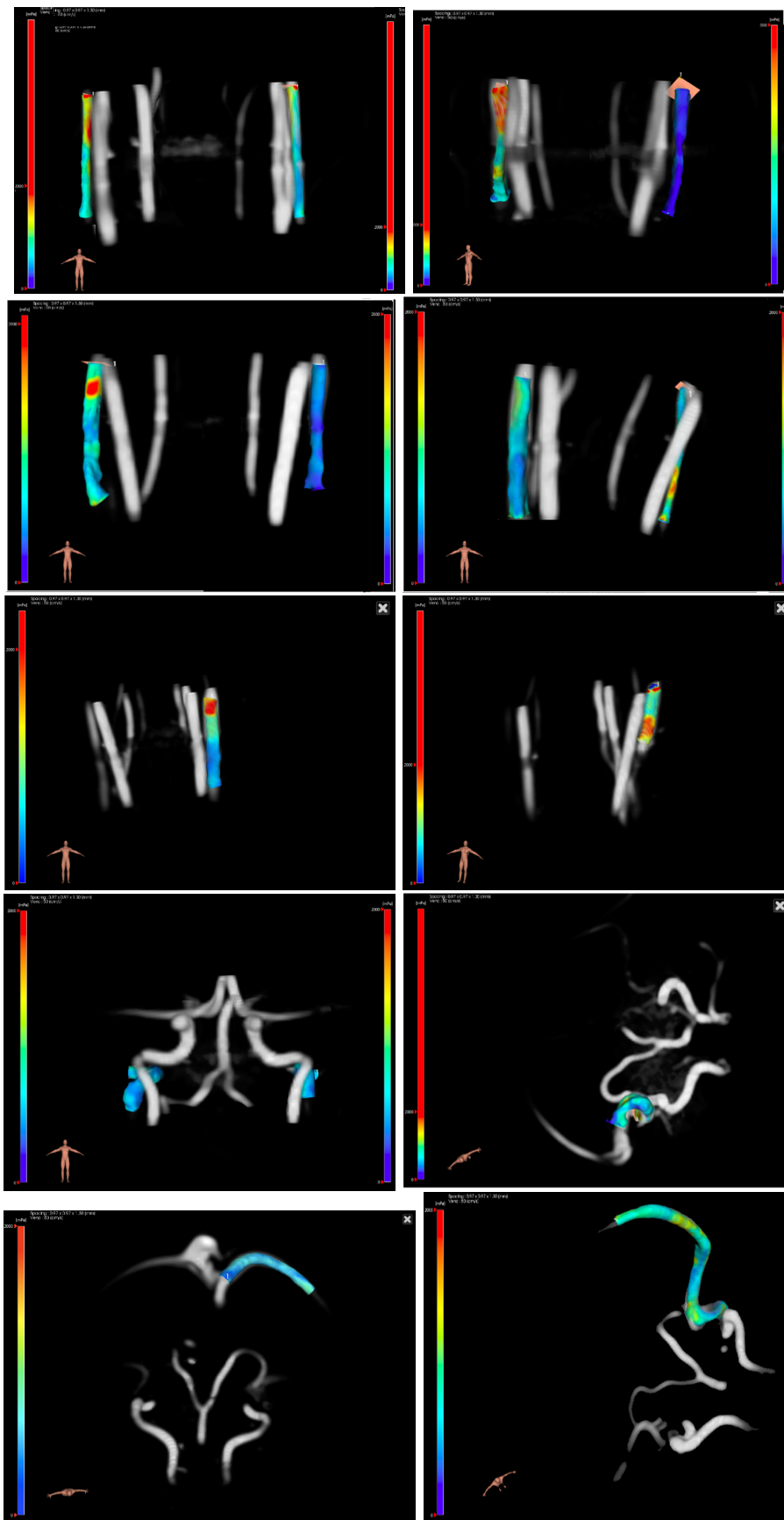
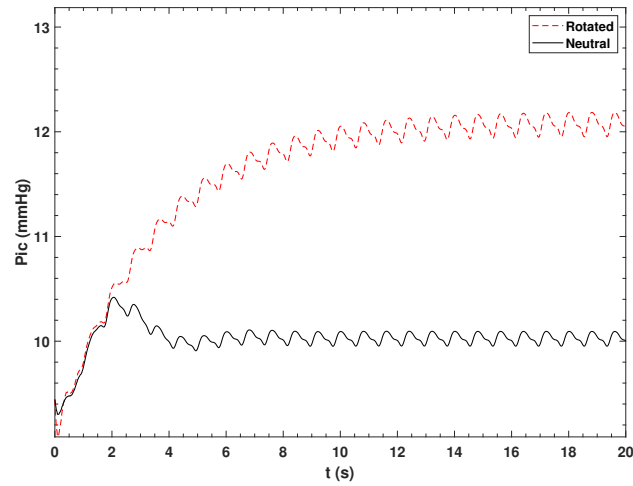
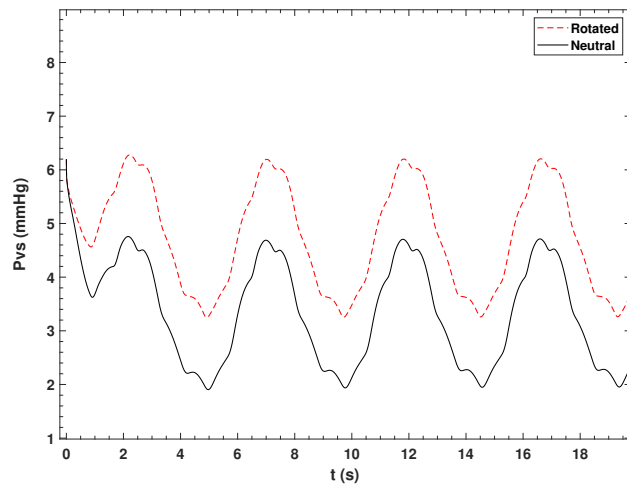


Figure 4.7: Contour plots of WSS for neutral and rotated head position at the level of neck for three different drainage cases and brain images of the case #1 and #2, the two most visualized intracranial blood redistribution.



(a)



(b)

Figure 4.8: Comparison of the simulated pressure of (a) intracranial ( $P_{ic}$ ), (b) venous sinus ( $P_{vs}$ ).

is in a strong agreement with Grover et al 2003 left rotation of the head (22.2% in healthy adult [99]) and Hung et al 2000 (about 50% in patients with tumour [100]).

### 4.3 Modelling microgravity and orthostatic stress effects

In this work, the mathematical haemodynamic model to simulate the hydrostatic pressure changes and weightlessness condition were adjusted. The model is calibrated in accordance to the data taken from literature. Noteworthy, the lack of knowledge, discordant literature and measured data about hemodynamic adaptation over time during a spaceflight mission limit the computational approach. To deal with these restrictions, the current model is tuned

Table 4.1: Comparing the computed pressure values (mmHg) (value  $\pm$  standard deviation) of my model with measurement and modelling in literature.

	Supine	30°	60°	Upright-Seated	HDT	$\mu$ G (0g)
Present study - modelling result						
Pa	100.8	85.8	74.8	70.8	106.0	100.8
Pic	9.5	6.7	3.7	2.1	10.5	8.3
CVP	4.2	3.3	2.7	2.5	4.4	3.9
Lindén et al (2018) – measurement						
Pic	10.5 $\pm$ 1.5	-	-	-0.8 $\pm$ 3.8	-9°: 15.8 $\pm$ 1.2	-
Lawley et al (2017) – measurement						
Pa	100	-	-	$\Delta$ -13 $\pm$ 7.1	-	$\Delta$ -1.85 $\pm$ 5.1
Pic	15 $\pm$ 2	-	-	4 $\pm$ 1	-6°:15 $\pm$ 4( $\Delta$ 1.8 $\pm$ 0.5)	13 $\pm$ 2
CVP	7 $\pm$ 3	-	-	2 $\pm$ 3	-6°: $\Delta$ -0.49 $\pm$ 0.5	4 $\pm$ 2
Eklund et al (2016)– measurement						
Pic	10.5 $\pm$ 1.5	-	-	-0.8 $\pm$ 3.8	-9°:15.8 $\pm$ 1.3	-
Petersen et al (2016)– measurement						
	Supine	10°	20°	Upright-Standing	-10°:	
Pa	103 $\pm$ 19	88 $\pm$ 9	87 $\pm$ 7	87 $\pm$ 8	86 $\pm$ 11	
Pic	9.4 $\pm$ 3.8	4.8 $\pm$ 3.6	1.3 $\pm$ 3.6	-2.4 $\pm$ 4.2	14.3 $\pm$ 4.7	
Qvarlander et al (2013) – measurement						
	Supine	27°	57°	71°-Seated		
Pic	11 $\pm$ 2.1	2.3 $\pm$ 2.5	-1.0 $\pm$ 3.0	-1.8 $\pm$ 3.2		
Mekišl and Kamenik (2010) – measurement						
Pa	72.9 $\pm$ 11.6	20°:65.1 $\pm$ 13.1	-	-	-20°:85.4 $\pm$ 14.0	-
CVP	8.1 $\pm$ 4.9	20°:4.5 $\pm$ 3.8	-	-	-20°:12.7 $\pm$ 4.7	-
Buckey et al (2017) - modelling results						
Pic	6.1	-	-	-	-	2.4
CVP	3.5	-	-	-	-	-6

with literature reporting data of hemodynamic physiology alteration in a short-time space mission or during a parabolic flight, whose experimental conditions and measurement data are compatible.

The study focus was on the head and neck part of the haemodynamic system. Table 4.1 presents the considered literature pressure values (mean  $\pm$  standard deviation) and the simulated mean values of pressure at the level of aorta ( $P_a$ ), braincase (ICP), and SVC (CVP).

As it can be seen from Table 4.1 and Figure ??, subject posture affects the measured pressure values. In particular, transition from supine to upright causes a pressure decrease, while transition from supine to HDT causes a pressure increase.

In the following simulations of pressure from my model, gradients are explained and compared with literature.

Arterial BP is hypothesised to be about 100 mmHg in supine, to decrease by increasing

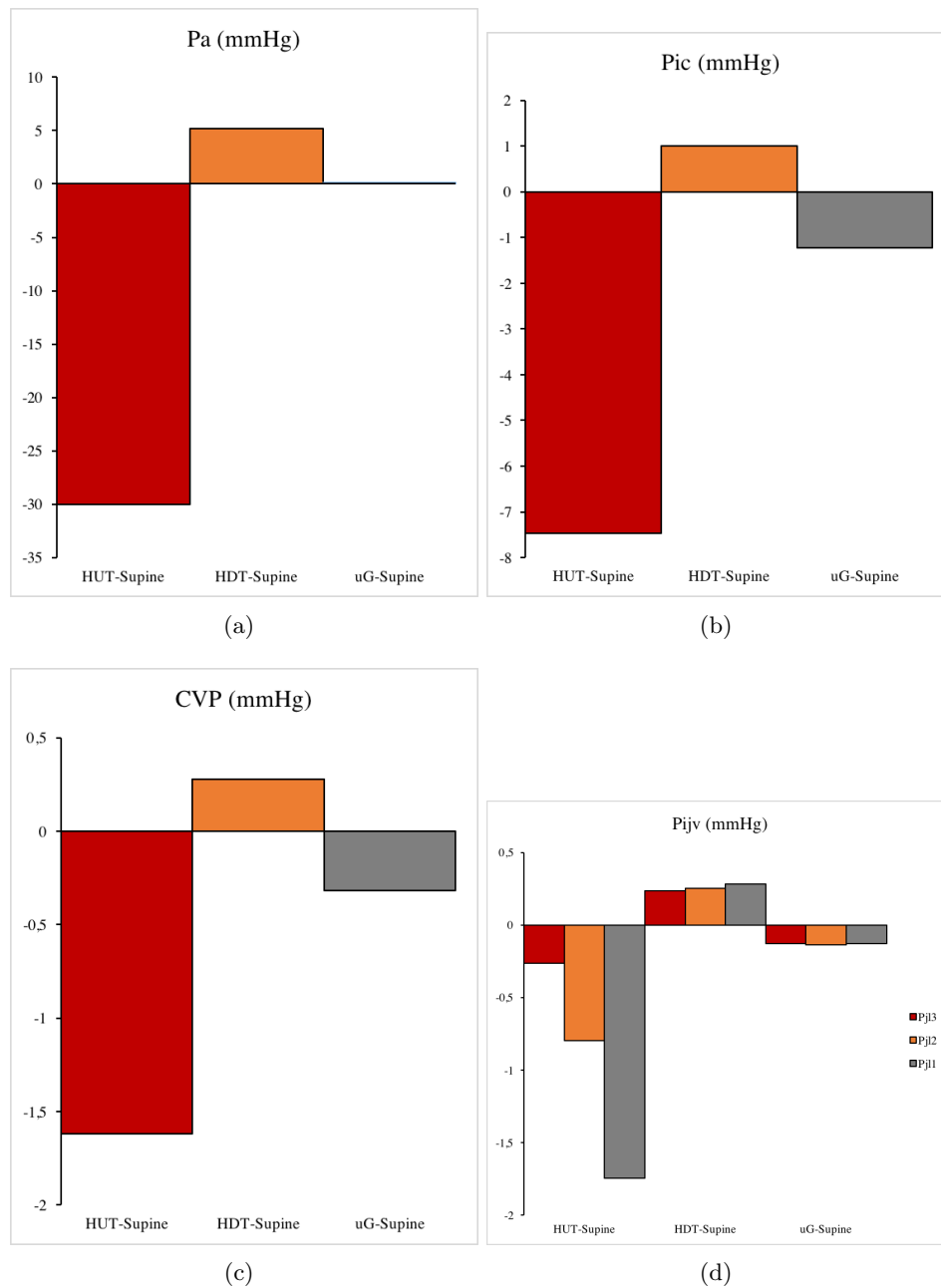


Figure 4.9: Simulated pressure difference caused by hydraulic pressure change and weightlessness at the level of a) aorta, b) braincase, c) SVC, d) upper, middle, and lower left IJV segments (Jl3, Jl2, Jl1)

the HUT angle till the value of 70 mmHg in upright, and to increase to 105 mmHg at a HDT angle of  $6^\circ$  [102]. Also, it is reported that in microgravity it remains unaffected with respect to measurement performed in the supine position before the flight [35] around the mean value of 100 mmHg [103]. Petersen et al reported a 17 mmHg drop in arterial BP when passing from supine to  $-10^\circ$  HDT (Table 4.1) [36]. The current model shows good agreement with aforementioned literature when simulations of arterial BP in HUT,  $-10^\circ$  HDT, and weightlessness condition are performed. As reported in Figure ??-A, the mean simulated arterial BP decreases of 30 mmHg in upright with respect to the supine position, while it

increases of 5 mmHg in HDT, and it remains constant in microgravity condition.

ICP are frequently reported in literature, and a significant reduction during HUT posture change from supine is always measured [34, 36, 104, 110]. Moreover, the normal range of ICP for a supine adult is about 7 to 15 mmHg, and in general less than 20 mmHg [106]. Figure ??-B shows that in model simulations ICP decreases of 7.4 mmHg in upright with respect to the supine position, while it increases of 1 mmHg in HDT. Referring to Table 4.1, Lawley et al [34] reported a slight increase ( $\Delta 1.8 \pm 0.5$  mmHg) in  $-6^\circ$  HDT which is comparable with my finding. However, Lindén et al [] and Eklund et al [104] measured the same increase in the mean value of ICP about (5.3 mmHg) after  $-9^\circ$  HDT. As we can understand, such high value of differences can not be calculated by known hydrostatic pressure equation (equation 2.39). This difference reported in literature might be due to the measurement dependency to experimental conditions [28, 103, 107].

According to Lawley et al (Table 4.1) the ICP in microgravity environment has a slight reduction ( $\Delta -1.9 \pm 5.1$ ) with respect to supine position on Earth [34]. During simulation of microgravity condition, my model calculates a ICP of 8.3 mmHg, and a ICP reduction of 1.2 mmHg with respect to supine position on Earth, in agreement with literature.

Measurements of CVP reported by Lawley et al [34] indicated that such value does not change when passing from supine to  $-6^\circ$  HDT. Mekiš and Kamenik [] measured a 4.6 mmHg augmentation for  $-20^\circ$  HDT. Results from my model (Figure ??-C) shows a 1.6 mmHg reduction of CVP in upright with respect to the supine position on Earth, while it is almost unchanged in HDT.

Noteworthy, the equation used in the model to calculate CVP [(Gadda et al. 2015; Gadda et al. 2016; Mohammadyari2020)] is not directly related to gravity changes, and it is affected by IJV changes as explained in the chapter 2 section 2.3.1. Therefore, the simulated CVP in microgravity condition shows a slight decrease (7.6%) with respect to the simulation in supine position on Earth. Therefore, the trend of my model results in different conditions shows good agreement with the literature of Table 4.1.

Figure ??-D compares the pressure variation in the three segments of left IJV for HUT, HDT and uG with respect to the supine condition. Due to the relatively larger CSA of segment J1, in this section there is the lowest pressure supine value, and consequently the higher pressure variation in upright and HDT ( $\Delta P_{j1} > \Delta P_{j2} > \Delta P_{j3}$ ).

In Figure ?? the simulated flow rates are reported and compared for different vessels and posture and gravity condition.

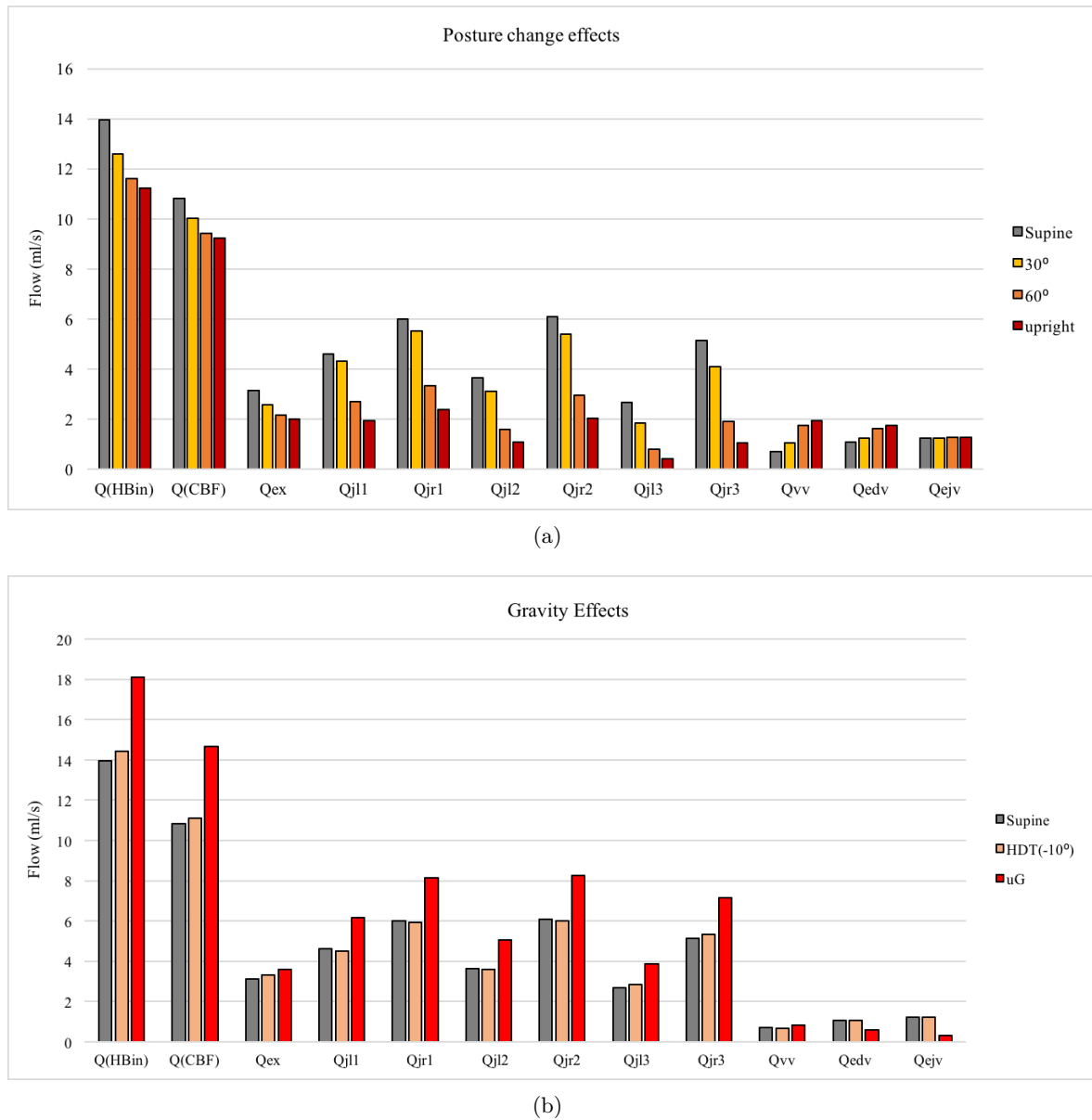


Figure 4.10: Comparison of simulated flow rates for a) different posture condition on Earth (1g) and a) supine and HDT on Earth (1g), and weightlessness (uG).

In this work we refer to the flow rate at VVs, EDV and EJVs as the summation of the right and left veins due to the low value of them.

On 2013 Zamboni et al stated that the blood flow at each segment of IJV is more than that of VVs or EDV [59]. Moreover, in the publication of Gadda et al it is reported that blood flow in J3 is lower than in the other segments ( $QJ1 > QJ2 > QJ3$ ) with the subject in standing position [20,21]. Therefore, it means that the higher segment (with respect to the HIPCSF zero level) is more collapsed. The simulated flow rates reported in Figure ?? (summation of left and right, J1: 10.6, J2: 9.7 and J3: 7.8 ml/s) are in agreement with the cited literature.

It is proven that increasing the tilt angle contributes to the IJVs collapse and expansion of peripheral veins as a compensatory mechanism [16, 47, 59, 110]. In this regard, the G-function for all the simulated neck veins has been integrated in the model (Equation 2.41). Therefore, the model is able to simulate the different degree of collapse at IJV segments, other than the slight dilatation in VV, IVP, and DCV. In other words, the model takes into account the increase of IJV resistance and the TPR decrease during upright simulations. As a consequence, flow is driven to the peripherals. Hence, results showed in Figure ??-A are in agreement with literature reports. The model simulates a reduction in  $Q_{HBin}$ ,  $Q_{CBF}$ ,  $Q_{Ex}$ , and  $Q_{IJV}$  flow rates, and augmentation of VVs and EDV flow rates. The extracranial veins such as EJVs do not show significant changes. The total  $Q_{HBin}$  and  $Q_{CBF}$  reductions after  $90^\circ$  posture change from supine to upright are about 20% and 15% (from 14.0 and 10.8 ml/s in supine to 11.2 and 9.2 ml/s in upright), respectively. The modelled  $Q_{CBF}$  reduction is comparable with the 12% reduction reported by Alperin et al [41]. Similarly, Zhang and Levine reported 10 to 20% reduction in CBF velocity in the middle cerebral artery [37]. Moreover, Sato et al [49] and Serrador and Freeman [50] showed that the inflow augmentation is due to the functionality of central arteries, and not to the peripheral ones during upright tilt. Therefore, the change in flow rate can be directly related to change in flow velocity. By that, the 20% reduction in  $Q_{HBin}$  is also in agreement with literature.

In Figure ??-B the environmental variables are HDT angle and weightlessness. Considering the fluid shift in the head-down position and microgravity, the augmented  $Q_{HBin}$  leads to an outflow increase. Such increased outflow is mainly supported by the IJVs, with a consequent increase of IJV-CSA, since the flow rate can be calculated by multiplying CSA and mean velocity [64, 67]. Moreover, the 30% reduction in blood flow velocity during parabolic flight reported by Bondar et al can be interpreted as 30% reduction in total blood inflow which is the same as my model response reduction (4 ml/s) [51]. For what concern effects of microgravity, literature highlighted the role of tissue weight on pressure changes and flow rates [28, 40, 102]. HDT is only able to model the headward fluid shift in inherently ground-based simulation condition. Beside, astronauts after a long-term space mission shows a puffy face suggesting that the fluid volume in head and neck is augmented also by the microgravity environment rather than exclusively by HDT. The model simulates higher  $Q_{HBin}$ ,  $Q_{CBF}$  and IJV flow rate in microgravity with respect to supine position on Earth (microgravity,  $Q_{HBin}$  : 18.1,  $Q_{CBF}$  : 14.7,  $Q_{IJV}$ : 6.4 ml/s vs supine,  $Q_{HBin}$  : 14.0,  $Q_{CBF}$ : 10.8,  $Q_{IJV}$ : 4.7 ml/s). Therefore, model results are satisfying and in agreement with what highlighted by literature reports and

Table 4.2: Comparing the computed flow rates (ml/s) of my model with measurement in literature.

	Primary pathway (IJV)	Secondary pathway	
Present study - modelling result			
Supine	9.4	VV: 0.7	EDV:1.1
30°	8.1	VV: 1.0	EDV:1.2
60°	4.4	VV: 1.7	EDV:1.6
Upright	3.0	VV: 2.0	EDV:1.7
HDT (-10°)	9.4	VV: 0.7	EDV: 1.1
Microgravity	12.9	VV: 0.8	EDV: 0.6
Ciuti et al (2013) - measurement			
Supine	5.6±3.9	VV: 0.6±2.8	
Upright	2.0±2.1	VV: 0.4±0.4	
Zamboni t al (2013) - measurement			
Supine	6.2±4.5	VV: 0.6±0.5	
Upright	5.0±5.3	VV: 1.1±0.9	
Alperin et al (2005) - measurement			
Supine	10.2±2.4	-	
Upright	5.1±4.4	-	
Cirovic et al (2003)- measurement			
Supine	15.5±8.0	-	
Upright	6.2±3.2	-	
Valdueza et al (2000) - measurement			
Supine	11.7±4.5	VV: 0.67±0.3	
15°	2.5±2.2	VV: 1.50±1.0	
30°	2.3±3.3	VV: 1.83±1.2	
45°	1.8±2.5	VV: 2.17±1.2	
Upright	1.2±1.7	VV: 3.50±2.0	

The values for internal jugular vein is the average value of the three segments (J1, J2, and J3). IJV: internal jugular vein, VV: vertebral vein, EDV: epidural vein (equals the summation of VV and DCV).

predictions [(Grigoriev et al. 2011; Norsk et al. 2006, 15,30)].

Niggemann et al [47], Valdueza et al [61] and Ciuti et al [109] emphasized the important role of peripheral veins such as EDV in venous drainage in the upright position. However, due to the difficulty to properly assess flow rate in small and inaccessible veins, it has not been quantitatively reported. Therefore, the calculated QEDV can be assumed as a predicted mean value [47].

Table 4.2 shows the mean flow rates computed by my model and measurement (mean ± standard deviation) in literature.

As shown in Table 4.2, Valdueza et al [61] reported a 90% reduction of IJV flow and a 425% increase of VV flow in upright posture compared with supine. Ciuti et al [109], Cirovic et al [42] and Alperin et al [41] measured 64%, 60% and 50% reduction in the IJV flow rate

Table 4.3: Simulated mean pressure and literature pressure values (mean  $\pm$  standard deviation) considered in this study. All values are reported in mmHg.

parameter		Supine	Upright	HDT	uG
CFI	Present work	3.4%	13.1%	8.3%	10.7%
	Zamboni et al 2013	1 $\pm$ 3 %	9 $\pm$ 19 %	-	-
DCVO	Present work	-	9.7%	4.9%	7.3%
	Zamboni et al 2013	-	5 $\pm$ 10 %	-	-
PVI	Present work	42.1%	78.0%	57.0%	53.2%

Total head blood inflow  $Q_{HBin}$ , cerebral blood inflow  $Q_{CBF}$ , total head blood inflow  $Q_{CVO}$ , cerebral blood outflow  $Q_{HBout}$ , Collateral flow index (CFI), Delta Cerebral Venous Outflow (DCVO) and peripheral veins outflow index (PVI).

during the transition from supine to sitting posture, respectively. Zamboni et al measured flow in the three segments of IJV [59]. They reported a flow reduction of 20%, 37%, and 34% in J1, J2, and J3 respectively, with an overall reduction of 30%. They also measured a 26% increase of VV flow after the posture change from supine to upright.

The presented model simulates a IJV flow reduction of 68% (from 9.4 ml/s supine to 3.0 ml/s in upright). Conversely, the modelled secondary pathway (sum of VVs and DCVs flows) shows an increase of 108% (from 1.8 ml/s supine to 3.7 ml/s in upright) as compensatory system response of the model.

Alperin et al reported the percentage of the venous drainage that passes through IJV in supine and upright position as 75%  $\pm$  14% and 42%  $\pm$  34%, respectively [41]. The same values calculated by my model are 67% and 26%. The results are comparable, if we consider the large uncertainty in the experimental values. Up today, there is no literature report about direct measurements of venous flow rates for what concern HDT and microgravity. Model results did not show significant differences in the mean flow rate values in supine and after HDT, however it shows a dramatic increase of IJV flow rate in microgravity condition. On the other side, the modelled secondary pathway flows did not change neither by HDT nor microgravity conditions.

The simulated mean values of CFI, DCVO and PVI indexes are reported in Table 4.3, and compared with results from Zamboni et al [59] who proposed the two first indexes.

The new index of PVI indicates that, in simulation of supine position, 42% of the brain and head outflow is passing through peripheral veins. This index is highly sensitive to posture change so that in upright, HDT (-10°), and microgravity it increases up to 78%, 57%, and 53%, respectively. The model simulations shows that, in supine position, 3% of the blood

entering into the head and neck circulation goes to the collateral (CFI). This percentage increases up to 13% in upright position, 8% in HDT, and 11 % in microgravity condition. The DCVO index emphasises the importance of posture change and weightlessness condition on the blood circulation by normalizing values to the supine reference condition. Zamboni et al only reported this index just for the upright posture [59]. Table 4.3 shows that my simulated values are in agreement with the experimental findings of Zamboni et al [59].

## 4.4 Study Limitations

Our study has limitations. The patient selection protocol was affected by limitations that decrease the number of cases. Subjects were chosen among patients with brain MRI prescription. We considered two conditions to select a patient for the study: normal neck and brain blood circulation, and no sedation during MRI due to the influence of the anaesthesia medication on the brain flows [73].

According to Doepp et al. [56] there are two main categories of human blood drainage: jugular drainage (75% of the population) and non-jugular drainage (25% of the population). My dataset is in perfect agreement, showing a subset of jugular drainers equal to 74% (26% non-jugular). Nevertheless, we decided to not separate the two subgroups in this study, focusing on the problem to tune an “adult based” model to paediatrics. Moreover, paediatric subjects are categorized in three subgroups: infants, preschool and old-children while there is no such a categorization for adults. This implies a poor accuracy when we want to compare paediatric and adult subjects because the value of biofactors changes with age constantly. Insufficiency in the number of experimental studies and age categorization may have affected the quality of numerical studies and modelling.

Moreover, to retrieve flow measurements from phase contrast imaging is sometimes not easy in small vessels, and even more difficult in veins due to the lower yields of the parameters in paediatric subjects. Furthermore, the small size of the vessels cross-sections area, the sensitivity of selecting a proper velocity encoding for arteries and veins in order to have comprehensive information and time consuming process of MRI data acquisition and manual vessels segmentation are other limitation in MRI data acquisition and processing in such study.

The literature measurement discordant is another restriction in such study. This difference

reported in literature might be due to the measurement dependency to experimental conditions and lack of a standard measurement protocol. In case of microgravity study, this limitation is more highlighted. Since the space environment is not easily accessible, there is not a united protocol to measure the physiological parameters in astronauts and then tune the simulation model accordingly. The other limitation mentioned by literature is that measurement results are highly dependent on the study conditions, such as the duration of the spaceflight and inter-individual differences (e.g. body size and weight) [28]. Moreover, this current version of the model is not able to follow the haemodynamic changes and body adaptation concerning the long-term and short-term space mission. This model offers the possibility of investigation about counteracting procedures to reduce the orthostatic stress in returning astronauts in future updates.

# Chapter 5

## Conclusions

The cardiovascular modelling is known as a challenging subject of study due to the complexity in human anatomy, the high number of enrolled physiological parameters which they are highly related to each other and inter-individual decency in normal and healthy cardiovascular system. Moreover, many biophysical factors affect cerebral circulation such as aging, posture change and vessel stenosis that they are known as the biological and mechanical factors in both physiological and pathological conditions.

In this filed of research, the measurement results highly depend on the study conditions and accuracy of the measurements. For instance, results from Earth-based simulations might not be used to infer conclusions about the microgravity environment. Moreover, the results of some clinical studies are discordant due to the lack of standard data collection protocol on older experiments. These restrictions lead to a poor understanding of the cardiovascular responses. For all these reasons, the necessity to have a reliable computed simulation tool is highlighted in the hemodynamic research framework. An important advantage of computational modelling is that it provides a virtual laboratory and allows the exploration of a wide range of pathological and physiological situations such as orthostatic stresses and their complex physiological chain of events on the intra- and extracranial compartments at a low medical and computational cost. Many valuable models of the cerebral circulation (like the works of Gisolf et al. [16] and Buckey et al. [28]) focused on intracranial segments and related control mechanisms, by providing a simplified description of the main arterial inflow and extracranial venous return. Whole body models such as the one developed by Zhang et al. and Gallo et al do not include brain compartments, and only the main outflow routes (IJV and VV) are included in the vascular network. Peripheral vessels play an important role in the brain and head drainage,

so that the choice to not account for them in order to simplify the model is not reasonable. Hence, we realized the need of a comprehensive model that considers both extracranial and intracranial compartments with their interactions to adapt the whole hemodynamic system to physiological changes. In this work we improved the mathematical haemodynamic model to satisfy the aforementioned needs.

This dissertation introduces our mathematical model as a powerful tool that investigate the causes and effects of hemodynamic alteration in specific cases including altered hydrostatic pressures by posture change from head-down tilt position to supine and upright (head-up tilt), microgravity environment, aging (paediatric study) and venous stenosis (head rotation study) in addition to their reciprocal effects on both intracranial and extracranial compartments. The additional capability of such advancement was provided through modifying and introducing a set of proper equations and parameters to reproduce the physiological changes as reported by literature. In this study the focus was on head and neck hemodynamic modelling. The purpose of this work was to validate the simulation results by using data extracted from MR images and volunteers medical records that were recognised with normal neck and brain blood circulation. The model presented here is tuned by using two different MRI datasets, one in paediatric cases (mean age of  $12\pm 5$ ) and second in young adult (mean age of  $19\pm 6$ ). We benefited from the use of two and four dimensional quantitative-flow phase contrast MRI techniques to have a detailed map of the vessels and of the blood circulating in them. Taking advantage from the most recent MRI techniques provided further refine and validate of the model. However, four-dimensional flow protocols were highly time consuming to study blood flows at the neck level because of the volume involved.

The current version of our model is an open-loop system with a more sophisticated description of the collateral pathways, including not only the internal jugular and vertebral veins but also the external jugular veins, the vertebral plexus (including internal epidural venous plexus and deep cervical veins) and other anastomoses that carry blood to the downstream sections. Therefore, the current model allows simulation of blood flows and pressures in the main vessels and collateral routes taking into account the collapsibility of the veins. Additionally, a model of arterial system upgraded to simulate 76 main arteries (including 55 arterial tree blocks [53], circle of Willis and temporal arteries) which this format of the arterial compartment provides new applications to study a wide range of arteries stenosis as well as venous stenosis and thrombosis. The other approach of this research was to introduce a hemodynamic computational model for paediatrics with keeping all the previously published

abilities for adults [19, 21, 53]. In this project, physiological age-related parameters such as respiratory rate, heart rate and blood pressure together with MR images were acquired. Data taken from both the experiments and literature were used to adjust cardiac output and cerebral blood flow for paediatrics. Every simulated data fell inside the standard error from the corresponding average experimental value, as well as the simulated extracerebral arterial flow. The model outcomes indicated about 88% correlation with MRI data.

The other approach of this work is the successfully simulating the head rotation effects on the rotated-side IJV stenosis. This study took the benefits of 4D PC-MRI techniques to assess the wall shear stress variation as a new parameter to measure. MR image acquisition and numerical simulation were performed in two situations: the neutral and 80° left head rotation. The model is capable of full range head rotation effects, while the results are just validated for two measured situations. Flow rate and wall shear stress analysis within IJVs demonstrated a strong interindividual dependency. we examined four subjects (50%) were right jugular dominant, two (25%) were left jugular dominant, and two (25%) were co-dominant. Noteworthy, the model was tuned based on the average data consider generally the jugular dominant condition in which the right IJV has more flow rate at all three segments. Experimental data and simulation results showed strong agreement in both neutral and rotated position with 98% and 87% correlation coefficient, respectively. Moreover, our study shows the impact of extracranial hemodynamic alteration on intracranial physiological parameters, besides the role of neck collateral veins in hemodynamic adaptation to head rotation. Since MRI techniques faced some aforementioned difficulties in measuring the flow parameters, the mathematical model is introduced as a strong tool which is capable of reproducing the known hemodynamic effects of head rotation by literature and direct measurements. Since little has been published about the biomechanical effects of head rotation on head and neck hemodynamic, we strongly state further researches are warranted. In addition, assessment of the effects of head rotation in the presence of neck hemodynamic pathology cases to evaluate deeply the effect of extracranial hemodynamic change on the intracranial physiological parameters are required. As well as studying the effect of inter-individual anatomical differences on the hemodynamic variation influenced by head rotation.

The microgravity physiology is a complex subject with restricted number of concordant measurement data. Cardiovascular mathematical modelling is a well-known useful method to study the human physiology change during a space mission. Our model is the first full-body map that provides comprehensive insights into the effect of microgravity on human body

physiology, including the effects of hydraulic pressure change and weightlessness. Noteworthy, this is a multiscale model tuned by literature data and it is not able to assess any change in distal part of human haemodynamic system. The main capability and purpose of such modelling is the calculation of physiological changes if the pertinent equations and parameters are correctly introduced. Another advantage of the presented model is the possibility to modify the equations of the 0-D compartment in order to simulate additional orthostatic stress causes. Limitations aside, this model offers the possibility to investigate counteracting procedures to reduce the orthostatic stress in returning astronauts, and it will be the subject of future work.

The methods presented here can be used to predict the response of the hemodynamic system in many other physiological and pathological conditions in both paediatric and adult.

# Bibliography



# Bibliography

- [1] Guyton AC (1991) The veins and their functions. In: Textbook of medical physiology, 8th edn. Saunders, Philadelphia
- [2] Beggs CB (2013), “Venous hemodynamics in neurological disorders: an analytical review with hydrodynamic analysis,” *BMC Med*, Vol. 11, pp. 142.
- [3] Folkow B, Neil E (1973), “Circulation,” *New York: Oxford University Press*.
- [4] Aaslid R, Lindegaard KF, Sorteberg W, Nornes H (1989), “Cerebral autoregulation dynamics in humans,” *Stroke*, Vol. 20(1), pp. 45-52.
- [5] Wu C, Honarmand AR, Schnell S et al (2016)“Age-related changes of normal cerebral and cardiac blood flow in children and adults aged 7 months to 61 years.” *J Am Heart Assoc* vol. 5(1), pp. 1-13.
- [6] Bhalla TDewhirst ESawardekar ADairo OTobias J (2012) “Perioperative management of the pediatric patient with traumatic brain injury ”  
textitPaediatric Anaesthesia Vol. 22(7), pp. 627–640.
- [7] Toro EF (2016) “Brain venous haemodynamics, neurological diseases and mathematical modelling. A review.” *Appl Math Comput* 272:542–579.
- [8] Casas B, Lantz J, Dyverfeldt P, Ebbers T. (2016)“4D Flow MRI-based pressure loss estimation in stenotic flows: Evaluation using numerical simulations.”  
textitMagn Reson Med. 2016 Apr;75(4):1808-21. doi: 10.1002/mrm.25772. Epub 2015 May 28. PMID: 26016805.
- [9] Slesnick TC (2017) “Role of computational modelling in planning and executing interventional procedures for congenital heart disease. ” *Can J Cardiol* 33:1159–1170.

- [10] Farina M, Novelli E, Pagani R. (2013) “Cross-sectional area variations of internal jugular veins during supine head rotation in multiple sclerosis patients with chronic cerebrospinal venous insufficiency: a prospective diagnostic controlled study with duplex ultrasound investigation.” *BMC Neurol* 5;13:162. doi: 10.1186/1471-2377-13-162. PMID: 24188184; PMCID: PMC4229316.
- [11] Chambers B, Chambers J, Churilov L, Cameron H, Macdonell R (2014), “Internal jugular and vertebral vein volume flow in patients with clinically isolated syndrome or mild multiple sclerosis and healthy controls: results from a prospective sonographer-blinded study,” *Phlebology*, Vol. 29(8), pp. 528–535.
- [12] Feng W, Utriainen D, Trifan G, Haacke EM (2012), “Quantitative Flow Measurements in the Internal Jugular Veins of Multiple Sclerosis Patients Using Magnetic Resonance Imaging,” *Rev Recent Clin Trials*, Vol. 7(2), pp. 117–126.
- [13] Moghadam ME, Vignon-Clementel IE, Figliola R, Marsden AL (2013) , “A modular numerical method for implicit 0D/3D coupling in cardiovascular finite element simulations.” *J Comput Phys* 244:63–79.
- [14] Qureshi MU, Vaughan GD, Sainsbury C et al (2014) “Numerical simulation of blood flow and pressure drop in the pulmonary arterial and venous circulation.” *Biomech Model Mechanobiol* 13:1137–1154.
- [15] Ursino M, Lodi CA (1997) “A simple mathematical model of the interaction between intracranial pressure and cerebral hemodynamics.” *J Appl Physiol* 82:1256–1269.
- [16] Gisolf J, van Lieshout JJ, van Heusden K, Pott F, Stok WJ, Karemaker JM (2004) “Human cerebral venous outflow pathway depends on posture and central venous pressure.” *J Physiol* 560:317–327.
- [17] Carlsson M, Andersson R, Bloch KM, et al (2012) “Cardiac output and cardiac index measured with cardiovascular magnetic resonance in healthy subjects, elite athletes and patients with congestive heart failure.” *J Cardiovasc Magn Reson* 14:51.
- [18] Zivadinov R, Galeotti R, Hojnacki D, Menegatti E, Dwyer MG, Schirda C, Malagoni AM, Marr K, Kennedy C, Bartolomei I, Magnano C, Salvi F, Weinstock-Guttman B, Zamboni P (2011), Value of MR Venography for Detection of Internal Jugular Vein Anomalies in Multiple Sclerosis: A Pilot Longitudinal Study“, *AJNR Am J Neuroradiol*, Vol. 32 pp.

- 938–946.
- [19] Gadda G, Majka M, Zieliński P, Gambaccini M, Taibi A (2018) “A multiscale model for the simulation of cerebral and extracerebral blood flows and pressures in humans.” *Eur J Appl Physiol* 118:2443–2454.
- [20] Gadda G, Taibi A, Sisini F, Gambaccini M, Zamboni P, Ursino M (2015), “A new hemodynamic model for the study of cerebral venous outflow,” *Am J Physiol Heart Circ Physiol*, Vol. 308(3), pp. H217–H231.
- [21] Gadda G, Taibi A, Sisini F, Gambaccini M, Sethi SK, Utriainen DT, Haacke EM, Zamboni P, Ursino M (2016), “Validation of a hemodynamic model for the study of the cerebral venous outflow system using MR imaging and echo-color Doppler data,” *AJNR Am J Neuroradiol*.
- [22] Mohammadyari P, Gadda G, Taibi A, Munuera Del Cerro J (2020) “Paediatric haemodynamic modelling: development and experimental validation using quantitative flow MRI.” *Eur Radiol Exp* 4:16.
- [23] Mohammadyari P, Gadda G, Taibi A, Munuera Del Cerro J (2021) “Head rotation Effects on youth Head and Neck hemodynamic using PC MR Imaging and Mathematical Modelling.” Submitted to *Eur Radiol Exp*.
- [24] Mohammadyari P, Gadda G, Taibi A (2021) “Modelling physiology of haemodynamic adaptation in short-term Microgravity exposure and orthostatic stress on Earth.” *Scientific Reports* 11:4672.
- [25] Mader, G., Olufsen, M., Mahdi, A. (2015) “Modeling cerebral blood flow velocity during orthostatic stress.” *Ann. Biomed. Eng.* 43, 1748–1758.
- [26] Diaz-Artilles, A., Heldt, T., Young, L. R. (2016) “Effects of artificial gravity on the cardiovascular system: Computational approach.” *Acta Astronaut.* 126, 395–410.
- [27] Zhang, X., Noda, S., Himeno, R., Liu, H. (2017) “Gravitational effects on global hemodynamics in different postures: A closed-loop multiscale mathematical analysis.” *Acta Mech. Sinica* 33, 595–618.
- [28] Buckey JC, Anderson A, Chepko AB, Archambault-Leger V, Masterova K, Fellows AM,

- Cowan DR (2017) “The importance of tissue weight and tissue compressive forces in human spaceflight.” Paper presented at the international astronautical congress, Adelaide, Australia, 25-29 September 2017.
- [29] Gallo, C., Ridolf, L., Scarsoglio, S.(2020)“Cardiovascular deconditioning during long-term spaceflight through multiscale modeling. ”  
textitNPJ Microgravity 6, 27.
- [30] Figaji AA (2017) “Anatomical and physiological differences between children and adults relevant to traumatic brain injury and the implications for clinical assessment and care.”  
*Front Neurol* 8:685.
- [31] Macfarlane F (2005) “Paediatric anatomy and physiology and the basic of paediatric anaesthesia. ” *World Anaesthesia Tutorial of the week.AnaesthesiaUK*. Available via <https://www.AnaesthesiaUK.com/WorldAnaesthesia>. Accessed 12 Oct 2015.
- [32] Law-ye B, Saliou G, Toulgoat F et al (2016) “Early-onset stroke with moyamoyalike syndrome and extraneurological signs: a first reported paediatric series.” *Eur Radiol* 26:2853–2862.
- [33] Manto M, Huisman T (eds) (2018) “The cerebellum: disorders and treatment.”  
textitElsevier.
- [34] Lawley JS, Petersen LG, Howden EJ, Sarma S, Cornwell WK, Zhang R, Whitworth LA, Williams MA, Levine BD (2017) “Effect of gravity and microgravity on intracranial pressure. ” *J Physiol* 595:2115-2127.
- [35] Norsk P, Damgaard M, Petersen L, Gybel M, Pump B, Gabrielsen A, Christensen NJ (2006) “Vasorelaxation in space.” *Hypertension* 47:69–73.
- [36] ]Petersen LG, Petersen JC, Andresen M, Secher NH, Juhler M (2016)“Postural influence on intracranial and cerebral perfusion pressure in ambulatory neurosurgical patients.” *Am J Physiol Regul Integr Comp Physiol* 310:R100-R104.
- [37] Zhang R, Levine BD (2007) “Autonomic ganglionic blockade does not prevent reduction in cerebral blood flow velocity during orthostasis in humans. ” *Stroke* 38, 1238–1244.
- [38] Mader TH, Gibson CR, Pass AF, Kramer LA, Lee AG, Fogarty J, Tarver WJ, Dervay JP, Hamilton DR, Sargsyan A, Phillips JL, Tran D, Lipsky W, Choi J, Stern C, Kuyumjian

- R, Polk JD (2011) “Optic disc edema, globe flattening, choroidal folds, and hyperopic shifts observed in astronauts after long-duration space flight.” *Ophthalmology* 118:2058-2069.
- [39] Keil LC, McKeever KH, Skidmore MG, Hines J, Severs WB (1992) “The effect of head-down tilt and water immersion on intracranial pressure in nonhuman primates.” *Aviat Space Environ Med* 63:181–185.
- [40] Marshall-Goebel K, Damani R, Bershad EM (2019) “Brain physiological response and adaptation during spaceflight.” *Neurosurgery* 85:E815-E821.
- [41] Alperin N, Lee SH, Sivaramakrishnan A, Hushek SG (2005), “Quantifying the effect of posture on intracranial physiology in humans by MRI flow studies,” *J Magn Reson Imaging*, Vol. 22, pp. 591-596.
- [42] Cirovic S, Walsh C, Fraser WD, Gulino A (2003) “The effect of posture and positive pressure breathing on the hemodynamics of the internal jugular vein.” *Aviat Space Environ Med* 74:125–131.
- [43] Magnaes B (1976) “Body position and cerebrospinal fluid pressure. Part 2: clinical studies on orthostatic pressure and the hydrostatic indifferent point.” *J Neurosurg* 44:698–705.
- [44] Convertino VA, Cooke WH (2007) “Vascular functions in humans following cardiovascular adaptations to spaceflight.” *Acta Astronaut* 60:259–266.
- [45] Nayman A, Ozkan Onal I, Apiliogullari S, et al. (2015) “Ultrasound validation of Trendelenburg positioning to increase internal jugular vein cross-sectional area in chronic dialysis patients.” *Renal Failure*, 37:8, 1280-1284.
- [46] Hargens AR, Vico L (2016) “Long-duration bed rest as an analog to microgravity.” *J Appl Physiol* 120:891-903.
- [47] Niggemann P, Kuchta J, Grosskurth D, Beyer HK, Krings T, Reinges M (2011) “Position dependent changes of the cerebral venous drainage – implications for the imaging of the cervical spine. ” *Cent Eur Neurosurg* 72:32-37.
- [48] Nicogossian AE, Williams RS, Huntoon CL, Doarn CR, Polk JD, Schneider JS (eds) (1993) *Space physiology and medicine*. Springer, New York.
- [49] Sato K, Fisher JP, Seifert T, Overgaard M, Secher NH, Ogoh S (2012) “Blood flow in inter-

- nal carotid and 17 vertebral arteries during orthostatic stress.” *Exp Physiol* 97:1272–1280.
- [50] Serrador JM, Freeman R (2017) “Enhanced cholinergic activity improves cerebral blood flow during orthostatic stress.” *Front Neurol* 8:103.
- [51] Bondar RL, Stein F, Kassam MS, Dunphy PT, Bennett BS, Johnston KW (1991) “Cerebral blood flow velocities by transcranial Doppler during parabolic flight.” *J Clin Pharmacol* 31:915–919.
- [52] Zhang LF (2001) “Vascular adaptation to microgravity: what have we learned? ” *J Appl Physiol* 91:2415–2430.
- [53] Majka M, Gadda G, Taibi A, Gałazka M, Zieliński P (2017) Protective properties of the arterial system against peripherally generated waves. *Math Biosci* 286:16–21.
- [54] Ursino M, Magosso E (2000), “Acute cardiovascular response to isocapnic hypoxia. I. A mathematical model,” *Am J Physiol Heart Circ Physiol*, Vol. 279(1), pp. H149–H165.
- [55] Takahashi T, Shirane R, Sato S, Yoshimoto T (1999) Developmental changes of cerebral blood flow and oxygen metabolism in children. *AJNR Am J Neuroradiol* 20:917–922
- [56] Doepp F, Schreiber SJ, von Münster T, Rademacher J, Klingebiel R, Valdueza JM (2004) “How does the blood leave the brain? A systematic ultrasound analysis of cerebral venous drainage patterns.” *Neuroradiology* 46:565–570.
- [57] Zamboni P, Menegatti E, Weinstock-Guttman B, Schirda C, Cox JL, Malagoni AM, Hojnacki D, Kennedy C, Carl E, Dwyer MG, Bergsland N, Galeotti R, Hussein S, Bartolomei I, Salvi F, Ramanathan M, Zivadinov R (2010), “CSF dynamics and brain volume in multiple sclerosis are associated with extracranial venous flow anomalies: a pilot study,” *Int Angiol*, Vol. 29(2), pp. 140–148.
- [58] Zamboni P, Morovic S, Menegatti E, Viselner G, Nicolaidis AN (2011) “Screening for chronic cerebrospinal venous insufficiency (CCSVI) using ultrasound-recommendations for a protocol. ” *Int Angiol* 30:571–597.
- [59] Zamboni P, Menegatti E, Occhionorelli S, Salvi F (2013) “The controversy on chronic cerebrospinal venous insufficiency.” *Veins and Lymphatics* 2:14.
- [60] Gooding CA, Stimac GK. (1984) “Jugular vein obstruction caused by turning of the

- head. ” *AJR Am J Roentgenol* 142(2):403-6. doi: 10.2214/ajr.142.2.403. PMID: 6421115.
- [61] Valdueza JM, von Münster T, Hoffman O, Schreiber S, Einhüpl KM (2000) “Postural dependency of the cerebral venous outflow.” *Lancet* 355:200–201.
- [62] Tobinick E, Vega CP (2006) “The cerebrospinal venous system: anatomy, physiology, and clinical implications.” *MedGenMed* 8:53.
- [63] Caruthers SD, Lin SJ, Brown P et al (2003) “Practical value of cardiac magnetic resonance imaging for clinical quantification of aortic valve stenosis: comparison with echocardiography.” *Circulation* 108:2236–2243.
- [64] Braakman R, Sipkema P, Westerhof N (1989) “A dynamic nonlinear lumped parameter model for skeletal muscle circulation.”  
textitAnn Biomed Eng 17:593-616. <https://doi.org/10.1007/bf02367465>.
- [65] Stover JF, Stocker R (2011) “Intensive care treatment options of elevated intracranial pressure following severe traumatic brain injury. In: Oestern HJ, Trentz O, Uraunes S (eds) Head, thoracic, abdominal, and vascular injuries, ”cap. 2. Springer-Verlag Berlin Heidelberg.
- [66] Wilson MH (2016) “Monro-Kellie 2.0: The dynamic vascular and venous pathophysiological components of intracranial pressure.” *J Cereb Blood Flow Metab* 36:1338–1350.
- [67] Fung YC (1997), “Biomechanics Circulation,” *New York: Springer Science & Business Media*.
- [68] Alastruey J, Parker KH, Sherwin SJ (2012), “Arterial pulse wave haemodynamics,” *11th International Conference on Pressure Surges* pp. 401–442.
- [69] Nichols W, O’Rourke M, Vlachopoulos C (2011), “McDonald’s blood flow in arteries, sixth edition: theoretical, experimental and clinical principles,” *Boca Raton: CRC Press*.
- [70] Reymond P, Merenda F, Perren F, Rüfenacht D, Stergiopoulos N (2009), “Validation of a one-dimensional model of the systemic arterial tree,” *Am J Physiol Heart Circ Physiol*, Vol. 297(1), pp. H208–H222.
- [71] Jagielska K, Trzuppek D, Lepers M, Pelc A, Zieliński P (2007), “Effect of surrounding tissue on propagation of axisymmetric waves in arteries,” *Phys Rev E Stat Nonlin Soft Matter Phys*, Vol. 76(6 Pt 2).

- [72] Moses S (2019) “Pediatric vital signs, vital signs in children.” *In: Cardiovascular medicine book*. <https://fpnotebook.com/cv/exam/pdtrcvtlsgns.htm>. Accessed 13 May 2019.
- [73] Gribkov AV, Boiarinov GA, Bolonichev AM, Grigor’eva VV (2001) “Changes in cerebral blood flow, intracranial and cerebral perfusion pressure in neurosurgical patients during anesthesia induced with diprivan. ” *Anesteziol Reanimatol* 2:43–45.
- [74] Boville B, Caulette Young L (2015) “ECCE Quick guide to pediatric cardiopulmonary care.” *Edwards*, California.
- [75] Butterworth JF, Mackey DC, Wasnick JD (2013) “Clinical Anesthesiology.” McGraw-Hill Education, New York.
- [76] Larrabide I, Blanco PJ, Urquiza SA et al (2012) “HeMoLab – Hemodynamics Modelling Laboratory: an application for modelling the human cardiovascular system.” *Comput Biol Med* 42(10):993–1004.
- [77] Sarnari R, Kamal RY, Friedberg MK, Silverman NH (2009) “Doppler assessment of the ratio of the systolic to diastolic duration in normal children: relation to heart rate, age and body surface area.” *J Am Soc Echocardiogr* 22(8):928–932.
- [78] Xing CY, Tarumi T, Liu J et al (2017) “Distribution of cardiac output to the brain across the adult lifespan.” *J Cereb Blood Flow Metab* 37(8):2848–2856.
- [79] Peiro J, Veneziani A (2009), “Reduced models of the cardiovascular system,” *Cardiovascular Mathematics*, Vol. 1, pp. 347–394.
- [80] Muller LO, Toro EF (2014) “Enhanced global mathematical model for studying cerebral venous blood flow.” *J Biomech* 47(13):3361–3372.
- [81] Cattermole GN, Mia Leung PY, Ho GYL et al (2017) “The normal ranges of cardiovascular parameters measured using the ultrasonic cardiac output monitor.” *Physiol Rep* 5(6):e13195.
- [82] Hirata K, Yaginuma T, ORourke MF, Kawakami M (2006) “Age-related changes in carotid artery flow and pressure pulses: possible implications for cerebral microvascular disease.” *Stroke* 37(10):2552–2556.
- [83] Leonard AD, Allsager CM, Parker JL, Swami A, Thompson JP (2008) “Comparison of central venous and external jugular venous pressures during repair of proximal femoral

- fracture.” *Br J Anaesth* 101(2):166–170.
- [84] Moses P, Hernandez LM, Orient E (2014) “Age-related differences in cerebral blood flow underlie the BOLD fMRI signal in childhood.” *Front Psychol* 5:300.
- [85] Gwak M. et al. (2009) “Effects of head rotation on the right internal jugular vein in infants and young children.” *Anaesthesia* 65, 272–276. DOI: 10.1111/j.1365-2044.2009.06209.x
- [86] Bassez S, Flaud P, Chauveau M (2005), “Modeling of the deformation of flexible tubes using a single law: application to veins of the lower limb in man,” *J Biomech Eng*, Vol. 123(1), pp. 58–65.
- [87] Pelc NJ, Herfkens RJ, Shimakawa A, Enzmann DR.(1991) “Phase contrast cine magnetic resonance imaging.” *Magn Reson Q*, 7(4):229–254.
- [88] Markl M, Chan FP, Alley MT, et al. (2003) “Time-resolved three-dimensional phase-contrast MRI.” *J Magn Reson Imaging*, 17(4):499–506.
- [89] Ha H, Kim GB, Kweon J, Lee SJ, Kim YH, Lee DH, Yang DH, Kim N.(2016) “Hemodynamic Measurement Using Four-Dimensional Phase-Contrast MRI: Quantification of Hemodynamic Parameters and Clinical Applications.” *Korean J Radiol* Jul-Aug;17(4):445-62. doi: 10.3348/kjr.2016.17.4.445.
- [90] Azarine A, Garçon P, Stansal A, Canepa N, Angelopoulos G, Silvera S, Sidi D, Marteau V, Zins M. (2019) “Four-dimensional Flow MRI: Principles and Cardiovascular Applications.” *Radiographics* 39(3):632-648. doi: 10.1148/rg.2019180091. Epub 2019 Mar 22. PMID: 30901284.
- [91] Rengier F, Delles M, Eichhorn J, Azad YJ, von Tengg-Kobligk H, Ley-Zaporozhan J, Dillmann R, Kauczor HU, Unterhinninghofen R, Ley S. (2014) “Noninvasive pressure difference mapping derived from 4D flow MRI in patients with unrepaired and repaired aortic coarctation.” *Cardiovasc Diagn Ther*. 4(2):97-103.
- [92] Pie Medical Imaging: User Manual Caas MRI 4D flow 2.0, Document control number PM1131 version 2.0, Netherlands 2017.
- [93] Højlund J, Sandmand M, Sonne M, Manton T, Jørgensen HL, Belhage B, van Lieshout JJ, Pott FC. (2012) “Effect of head rotation on cerebral blood velocity in the prone position.”

- Anesthesiol Res Pract.* 2012;647258. doi: 10.1155/2012/647258.
- [94] Watson GH.(1974) “Effect of head rotation on jugular vein blood flow. *Arch Dis Child.*”49(3):237-9. doi: 10.1136/adc.49.3.237.
- [95] Glor FP, Ariff B, Hughes AD, Verdonck PR, Barratt DC, Augst AD, Thom SA, Xu XY. (2004) “Influence of head position on carotid hemodynamics in young adults.” *Am J Physiol Heart Circ Physiol* 287(4):H1670-81.
- [96] Lorchrachoonkul T, Ti LK, Manohara S, Lye ST, Tan SA, Shen L, Kang DS. (2012) “Anatomical variations of the internal jugular vein: implications for successful cannulation and risk of carotid artery puncture.” *Singapore Med J.* 53(5):325-8.
- [97] Aristokleous N, Seimenis I, Georgiou GC, Nicolaidis A, Anayiotos AS. (2015) “The effect of head rotation on the geometry and hemodynamics of healthy vertebral arteries.” *Ann Biomed Eng.* 2015 Jun;43(6):1287-97. doi: 10.1007/s10439-015-1340-5.
- [98] Thomas LC, McLeodLR, Osmotherly PG, Rivett DA . (2014) “The effect of end-range cervical rotation on vertebral and internal carotid arterial blood flow and cerebral inflow: A sub analysis of an MRI study.” *Manual Therapy*, ISSN: 1356-689X, Vol: 20, Issue: 3, Page: 475-480.
- [99] Grover VK, Bala I, Bandi SS, et al. (2003)“Changes in Intracranial Pressure in Various Positions of the Head in Anaesthetised Patients.” *Bahrain Medical Bulletin*, Vol. 25, No. 4.
- [100] Hung OR, Hare GM, Brien S. (2000) “Head elevation reduces head-rotation associated increased ICP in patients with intracranial tumours.” *Can J Anaesth*, 47(5):415-20.
- [101] ]Grigoriev AI, Kotovskaya AR, Fomina GA (2011) The human cardiovascular system during space flight. *Acta Astronaut* 68:1495–1500.
- [102] Hargens AR, Vico L (2016)“Long-duration bed rest as an analog to microgravity.” *J Appl Physiol* 120:891-903.
- [103] Zhang LF, Hargens AR (2018)“Spaceflight induced intracranial hypertension and visual impairment: pathophysiology and countermeasures.” *Physiol Rev* 98:59–87.
- [104] Eklund A, Jóhannesson G, Johansson E et al (2016)“The pressure difference between

- eye and brain changes with posture.” *Ann Neurol* 80:269-276. doi:10.1002/ana.24713.
- [105] Lindén C, Qvarlander S, Jóhannesson G et al (2018) “Normal-tension glaucoma has normal intracranial pressure: a prospective study of intracranial pressure and intraocular pressure in different body positions.” *Ophthalmology* 125:361-368. doi:10.1016/j.ophtha.2017.09.022
- [106] Rangel-Castillo L, Gopinath S, Robertson CS (2008) “Management of intracranial hypertension.” *Neurol Clin* 26:521–541. doi:10.1016/j.ncl.2008.02.003.
- [107] Otsuka K, Cornelissen G, Furukawa S et al (2016)“Long-term exposure to space’s microgravity alters the time structure of heart rate variability of astronauts.” *Heliyon* 2:e00211. doi:10.1016/j.heliyon.2016.e00211.
- [108] Mekis D, Kamenik M (2010) “Influence of body position on hemodynamics in patients with ischemic heart disease undergoing cardiac surgery.” *Wien Klin Wochenschr* 122:59–62. doi:10.1007/s00508-010-1346-9.
- [109] Ciuti G, Righi D, Forzoni L, Fabbri A, Pignone AM (2013)“Differences between internal jugular vein and vertebral vein flow examined in real time with the use of multigate ultrasound color Doppler.” *AJNR Am J Neuroradiol* 34:2000–2004. doi:10.3174/ajnr.A3557.
- [110] Qvarlander S, Sundström N, Malm J, Eklund A (2013)“Postural effects on intracranial pressure: modeling and clinical evaluation.” *J Appl Physiol* 115:1474–1480. doi:10.1152/jappphysiol.00711.2013.
- [111] Holtackers RJ, Spronck B, Heusinkveld MH, Crombag G, Op t’Roodt J, Delhaas T, Kooi ME, Reesink KD, Hermeling E. (2016)“Head orientation should be considered in ultrasound studies on carotid artery distensibility.” *J Hypertens.* 34(8):1551-5.
- [112] Jayaraman MV, Boxerman JL, Davis LM, Haas RA, Rogg JM.(2012)“Incidence of extrinsic compression of the internal jugular vein in unselected patients undergoing CT angiography.” *AJNR Am J Neuroradiol.* 33(7):1247-50.
- [113] Shivanandan A. et al.(2018)“Effect of head pillow and shoulder roll on diameter of the right internal jugular vein.” *Indian Anaesth Forum* 52-18. DOI: 10.4103/TheIAForum.TheIAForum5218